UNIVERSITY OF CALIFORNIA

Santa Barbara

Understanding the Dielectric Constant in Organic Photovoltaic Materials

A dissertation submitted in partial satisfaction of the

requirements for the degree Doctor of Philosophy

in Chemistry

by

Michael Paul Hughes

Committee in charge:

Professor Thuc- Quyen Nguyen, Chair

Professor Martin Moskovits

Professor Rachel Segalman

Professor Mattanjah de Vries

June 2019

The dissertation of Michael P. Hughes is approved.

_____
Martin Moskovits

_____
Rachel Segalman

_____
Mattanjah de Vries

_____
Thuc- Quyen Nguyen, Committee Chair

May 2019

Understanding the Dielectric Constant in Organic Photovoltaic Materials

ACKNOWLEDGEMENTS

This work is dedicated to:

My parents, Nanette and Eric, for showing me the path to walk,

My family, giving strength to my legs,

To Prof. Martin Moskovits and Prof. Mattanjah de Vries, for never giving up on me,

To my beloved Katie, for walking this path with me,

And to Lily, for always lighting my way.

The author would also like to acknowledge the following funding sources:

Department of Chemistry and Biochemistry, UC Santa Barbara,

Department of the Navy, Office of Naval Research (Award No. N00014-14-1-0580).

Graduate Division, UC Santa Barbara, Graduate Opportunity Fellowship

VITA OF MICHAEL PAUL HUGHES
May 2019

EDUCATION

Bachelor of Science in Chemistry, Oregon State University, Corvallis, March 2014 (magna cum laude)
Doctor of Philosophy in Chemistry, University of California, Santa Barbara, May 2019 (expected)

PROFESSIONAL EMPLOYMENT

2014-2018: Teaching Assistant- General Chemistry, Department of Chemistry, University of California, Santa Barbara
2016-2018: Teaching Assistant- Advanced Analytical Techniques, Department of Chemistry, University of California, Santa Barbara
2017-2019: Program Assistant, Summer Sessions, Pre- College Program, University of California, Santa Barbara
2019: Instructor, Department of Chemistry, Santa Barbara City College

PUBLICATIONS

Ran, Niva; A. Love, John; Heiber, Michael; Jiao, Xuechen ; Hughes, Michael P.; Karki, Akchheta; Wang, Ming; Brus, V; Wang, Hengbin; Neher, Dieter; Ade, Harald; Bazan, Guillermo; Nguyen, Thuc-Quyen. 2018. Charge Generation and Recombination in an Organic Solar Cell with Low Energetic Offsets. Advanced Energy Materials. 8(5).

Hughes, Michael P.; Rosenthal, Katie D.; Ran, Niva A.; Seifrid, Martin; Bazan, Guillermo; Nguyen, Thuc-Quyen. 2018. Determining the Dielectric Constants of Organic Photovoltaic Materials Using Impedance Spectroscopy. Advanced Functional Materials. 28(32).

Hughes, Michael P.; Rosenthal, Katie D.; Dasari, R. R.; Luginbuhl, B. R.; Yurash, B.; Marder, S.; Moskovits, M.; Nguyen Q.; 2018. Charge Recombination Dynamics in Organic Photovoltaic Systems with Enhanced Dielectric Constant. Advanced Functional Materials. In press.

AWARDS

American Institute of Chemists Graduating Chemist Award, Oregon State University, 2014

Graduate Opportunity Fellowship, University of California, Santa Barbara, 2018

FIELDS OF STUDY

Major Field: Examination of the Dielectric Constant in Organic Photovoltaics with Prof. Thuc- Quyen Nguyen

Studies in Organic Photovoltaics Device Fabrication and Characterization with Dr. Jack Love and Dr. Niva Ran

Studies in X-Ray Photoelectron Spectroscopy, Theory and Application with Dr. Tom Mates

Studies in Cellulose Nano Crystals Fabrication and Application with Prof. John Simonsen

ABSTRACT

Understanding the Dielectric Constant in Organic Photovoltaic Materials

by

Michael Paul Hughes

The photovoltaic and electrical properties of organic semiconductors are characterized by their low dielectric constant, which leads to the formation of polarons and Frenkel excitons. These resulting excitons require careful engineering of complex devices to generate electricity using these materials. Furthermore, the low dielectric constant of organic semiconductors has been suggested to play a large role in geminate and bimolecular recombination losses to the performance of organic photovoltaics (OPV). However, despite the critical attention that the dielectric constant has received in discussions in the literature, there has not yet been a thorough study of the dielectric constant in common organic semiconductors and how it may change in the functional OPV device. In fact, there have been some inconsistent and contradictory reports on the trends of dielectric constants, making it difficult to identify trends. This work begins by providing a detailed explanation of the fabrication of organic photovoltaic devices, including fundamental problems encountered and how they relate to the dielectric constant. A specific methodology is then presented to determine the dielectric constant in OPV materials using impedance spectroscopy, including guidelines and illustrations of possible experimental pitfalls. This methodology is utilized to provide the

analysis for the dielectric constant of 20 common neat organic semiconductors. Additionally, the dielectric constant in blend systems is studied, and the relationship between the dielectric constant and blend morphology was determined. It is observed that the dielectric constant of a blend system can be very accurately predicted solely based on the dielectric constants of the neat materials, scaled by their respective weight ratios in the blend film. Increasing the dielectric constant of organic photovoltaic materials to reduce recombination rates has long been pursued, however, material modification often results in the modification of multiple device characteristics making system comparison difficult. Once establishing the viability of increased dielectric constant through chemical modification, a model system was developed to study recombination rate changes. A fullerene derivative with an increased dielectric constant by the addition of a triethylene glycol appendage to the fullerene (TEG-PCBM) was synthesized for examination. Devices were fabricated with TEG- PCBM blended with donors P3HT and PTB7-Th and found comparable performance to $PC_{60}BM$. This model system shows the rarely reported characteristic of an increase in the dielectric constant while leaving its other properties unaltered. Although observing a shift in recombination behavior, a reduction wasn't observed to increase device performance. Sensitivity of morphological conditions consistently prove too important when making such large chemical modifications and bimolecular recombination became trap-assisted monomolecular recombination. While triethlyene glycol appendages may prove to be ineffective in improving recombination through increased dielectric constant, provided is a robust methodology for studying recombination in future high dielectric systems.

TABLE OF CONTENTS

LIST OF FIGURES

I. *Introduction*

II. *Determining the Dielectric Constants of Organic Photovoltaic Materials Using Impedance Spectroscopy*

I. Introduction

It is my desire that this introduction serve two purposes: to firstly be an adequate background reading such that any interested party may understand my work and its motivations and secondly, as an introduction to the requirements for the study of organic photovoltaics. Fundamental study of this nature requires the fabrication of many different devices, all with unique architecture and processing conditions to master. Furthermore, all such considerations must be considered in relation to and their effect on the dielectric constant and thus a firm agreement on the basics is necessary.

A. Historical Context

It is the nature of science, that innovation does not belong to the individual but rather the community, as progress precipitates progress. With that said, it may occur that a singular discovery or inspiration may be so paradigm shifting, it is the genesis of new scientific thought. For that reason, it is necessary to understand such concepts as they are the source ideas from which a researcher's work expounds. There are two such innovations which sire my work and in the spirit of accessibility, I wish to briefly mention and explain their importance. The first such work is the paper[1], "Concerning an Heuristic Point of View Toward the Emission and Transformation of Light" one of the Annus Mirabilis papers by Albert Einstein for which he received the Nobel prize in physics in 1921[2]. It was in this paper which Einstein proposed the wave-particle duality nature of light. The relationship $hf=E$ describes a particle of light with a frequency, f, to behave as a quanta packet of energy, E, where h is the constant described by Plank[3]. This work builds on the efforts from scientists like Plank, Hertz[4], Maxwell[5] and others[6], however this paper bridged an important

knowledge void. This relationship describes the photoelectric effect, the phenomena in which photon energy exists as discrete packets able to interact with electrons existing in orbitals in discrete energetic levels. This effect is employed in bandgap engineered silicon based photovoltaic cells where visible photons of light are able to excite valence electrons into unoccupied states where they may be captured for the generation of electricity. It is with this understanding that we may tune molecular energy levels such that photons of visible light may excite valence electrons to unoccupied molecular orbitals.

The second such work "Synthesis of electrically conducting organic polymers: halogen derivatives of polyacetylene, $(CH)_x$" was published by Shirakawa, Louis, MacDiarmid, Chiang, and Heeger in 1977[7] and earned Shirakawa, MacDiarmid, and Heeger the Nobel Prize in 2000[8]. This cohort described a polymer with alternating single and double bonds, which allowed for delocalization and transport of an electron along the polymer backbone. Furthermore, they found that halogen doping of the material greatly increased conductivity. Such polymeric conjugation roots the field of organic photovoltaics as the primary charge transport method in a traditionally electrically insulating material and allows for charge extraction of photogenerated electrons. The singular caveat being the generally low dielectric constant of organic materials results in incomplete electron/hole separation upon photoexcitation, requiring careful device consideration and engineering which will be discussed in the following section.

B. Considerations for the Fabrication of Organic Photovoltaics

Before discussing different considerations for the fabrication of an optimized organic photovoltaic device and their potential impact on the measurement of the dielectric constant, it may be noted my failure to properly define the dielectric constant. This choice is because it

is not necessary to measure or quantify the dielectric constant to observe it's impact on the organic solar cell. The low dielectric constant was historically charged with the formation of the exciton, the bound electron/ hole pair, which requires a second material for complete charge separation[9]. Additionally, it is assumed that free charges may recombine when their separation distance falls below the capture radius described by Coulomb in **Equation 1**[10]**.**

$$r^2 = \frac{e^2}{4\pi\varepsilon kT} \quad (1)$$

This simple model expects two charged particles of the same mass will interact at a distance *r,* which is inversely proportional to the dielectric constant. The implication of this being the intrinsically low dielectric constant of organic materials results in not only the formation of excitons but also accounts for the high number of recombination events in even the highest performing devices[11]. However, for years the scientific community accepted these consequences and estimated the value of the dielectric constant in models to be three[12]. With the understanding that one doesn't require knowledge of the dielectric constant to understand the organic photovoltaic cell, I'll first address fabrication considerations as high-quality devices are required for measurement of the dielectric constant.

1. Material Choices

Of the two main classifications of materials used in organic photovoltaics, the electron donating materials have a larger catalog as synthetic chemists have long tuned the band gap and energy levels for increased efficiency, [13]. The electron accepting materials have been left behind partially due to the ubiquitous fullerene derivatives [6,6]-phenyl-C61-butyric acid methyl ester ($PC_{61}BM$) (first synthesized by Prof. Fred Wudl at the University of California at Santa Barbara[14]) and it's molecular relative, [6,6] phenyl-C71-butyric acid methyl ester ($PC_{71}BM$), who's high electron affinity, high electron mobility, the increased absorption range

when shifting to $PC_{71}BM$, left little reason to invest major efforts to new material designs[15]. It's for this reason that this work primarily focuses on solution processed electron donating materials with only several novel solution-processed non-fullerene acceptors being studied.

Conjugated polymers naturally have a bandgap due to the alternating bond lengths and localization of electron density[16]. Control of the bandgap size, the highest occupied molecular orbital (HOMO) level and lowest unoccupied molecular orbital (LUMO)'s level may be controlled by monomer selection and implemented during synthesis[17–21]. There exist two major methodologies to this end, homopolymers and donor/acceptor copolymers[22]. Simple early polymer donors such as poly[2-methoxy-5-(2-ethylhexyloxy)-1,4-phenylenevinylene] (MEH-PPV) and poly(3-hexylthiophene-2,5-diyl) (P3HT) utilized common regular monomers which functioned as adequate, low performance organic photovoltaics[9,13,23,24]. These materials have been extensively studied and function as well established control materials for fundamental studies[25,26]. Donor/acceptor copolymers employ alternating units of electron donating monomers and electron accepting monomers[27,28]. This modulation alters the bandgap and energy levels of the material for better hole extraction and exciton separation[29]. Furthermore, changes in structure will affect charge mobility, the absorption range, material phase assembly and size, and the performance figures of merit which will be discussed later[30–32]. This characteristic provides enormous utility to these materials as they can be constantly tuned and improved[33,34]. Additionally, there exists small molecule electron donating materials made of the same monomers and using

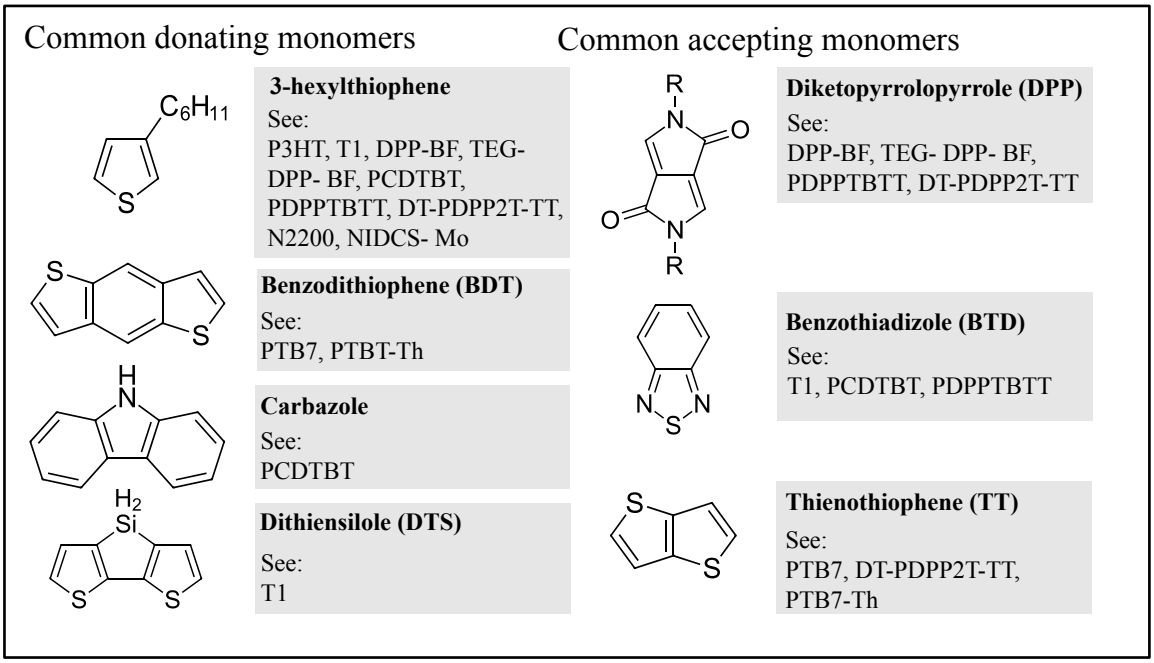

Figure 1. Common donor and acceptor units for organic photovoltaic materials

the same design principles[35]. Small molecules such as T1 share similar monomers as their polymeric counterparts as shown in **Figure 1**, yet these small molecule materials benefit from simpler synthesis and purification processes[36–38]. However, T1, like many other small molecule materials, suffer from inconsistent film morphology and delicate processing conditions which can limit consistent reproduction and overall performance. Lastly, there exists electron accepting materials which possess high electron affinity and may separate excitons which exist on donor materials when in correct proximity[39–43]. Synthetic emphasis has been on the development of unique electron donors as there exists the robust fullerene-based acceptors whose high electron mobility, large absorption range, and low energy levels which facilitate charge separation[43]. $PC_{61}BM$ and $PC_{71}BM$ and their derivatives have been so effective in organic photovoltaics, traditionally modifications are made around this cornerstone material[22,27,32]. Naturally, novel acceptor materials have always been synthesized

and studied, and more recently the development of high performing non-fullerene small molecule electron acceptors has shifted the synthetic paradigm[39,42,44–51].

The previous explanation of materials is a more simplistic description of the synthetic rational for the development of organic materials, of which has filled many dissertations. The purpose was to highlight several key aspects of material design which may impact my study on the dielectric constant in these materials. The first is the modular approach to organic photovoltaic material synthesis which may have two implications on this work[52–54]. Firstly, that it is possible that a single monomer may possess a high dielectric constant and isolating it may allow for the development of high dielectric materials. Secondly, implication of the modular nature of the synthesis is that repeated uses of monomers which are elementally very similar may limit the range of values as we test different materials. The next aspect of organic photovoltaic material design I want to highlight is that modulation to the monomer core is how the material energy levels change and what dictates the bandgap[55–57]. The consequence of this is any modification to these monomer core may change the dielectric constant in some unforeseen way, but it would also change every other aspect of the material making comparison irrelevant. To study the effect of the change in the dielectric constant has on recombination in OPV devices, the monomer's core and energy levels must be maintained. Finally, it should be mentioned that any synthetic change is likely to alter thin film morphology and eventual device phase separation[58–61]. With the effects that morphology has on the dielectric constant unknown, any synthetic change must be married to a firm understanding of morphological changes before any comparison may be allowed.

2. Device Architecture

While the effect of device architecture on the dielectric is not specifically studied here, the rational for the chosen structure should be understood. Organic photovoltaics employ the sandwich device structure, with a necessary transparent contact here being a conductive indium tin oxide (ITO) coated contact allowing photons thorough and a metallic cathode sandwiched on top, reflecting unabsorbed photons back into the device[62–64]. As stated before, the low dielectric constant in these materials requires the implementation of a second material for charge separation. Neat material diodes will have some performance as work function difference at the contacts will allow some charge separation, however long charge transport distance, surface area and energy alignment will always keep such performance minimal. For this reason, was developed the OPV bilayer device, in which electron donating and electron accepting materials are layered between the sandwich device[65,66]. Here, the energy levels may be appropriately aligned for optimal charge separation and layer thickness may be optimized for charge extraction considering individual mobilities[67,68]. Nevertheless, performance is limited by charge separation surface area and thickness constraints. Due to these limitations, the bulk heterojunction (BHJ) architecture was developed[69–72]. In this structure, the electron donating and electron accepting materials are homogeneously mixed in a common solvent, and spin-cast into a thin film onto the transparent ITO coated substrate. Extensive experimentation on material development and processing conditions during device fabrication afford specific material separation into pure nanometer-scale domains[60,73–79]. These domains range in size, purity, crystallinity, and mixing, all which impact device performance. Optimizing domain characteristics optimizes exciton separation, charge mobility and extraction in devices and is necessary for every developed system. The BHJ so

surpasses the bilayer architecture in its photovoltaic capacity that only the BHJ structure will be studied in this work[22,27,32]. The consequence of the BHJ architecture is the number of unknowns it presents to the understanding of the dielectric constant. How do the individual dielectric constant values compare to that of the blend, how does charge generation change in blended devices effect the dielectric constant, how do the unique processing conditions effect the dielectric constant are all questions raised by this complex device architecture.

3. Contacts

Device functionality requires contacts which possess work functions which energetically align for charge extraction[62,80,81]. Such alignment should match anode with the electron donor's HOMO level for hole extraction while cathode work function should encourage electron extraction as seen in **Figure 2**. Although charge extraction is possible through pristine metal contacts, OPV devices almost universally employ interfacial layers to improve charge extraction[82–86]. Interfacial layers serve several notable functions, firstly they help pin the Fermi level to reduce extraction barrier at the contacts which will lower V_{oc} and FF as such a barrier acts as a recombination center. While the metal work functions define the internal field which drives the device, the interfacial layer, such as MoO_x on the Ag contact shown in **Figure 2**, pins the electrode Fermi level to eliminate any barrier to charge extraction[87–89]. The second reason to utilize an interfacial layer is to increase improve material wetting between the organic active layer and metallic contact, this additionally helps remove any mechanical based extraction barrier[90]. Finally, these interfacial layers, have been shown to improve device stability and are a mainstay in the common OPV fabrication[91–93].

While the measurement of the dielectric constant should be independent from the contacts, what impact specific contacts and interfacial layers may have on this measurement are

unknown. As device contacts will be required for the impedance measurement to determine the dielectric constant, and examination of contact affects will also be required.

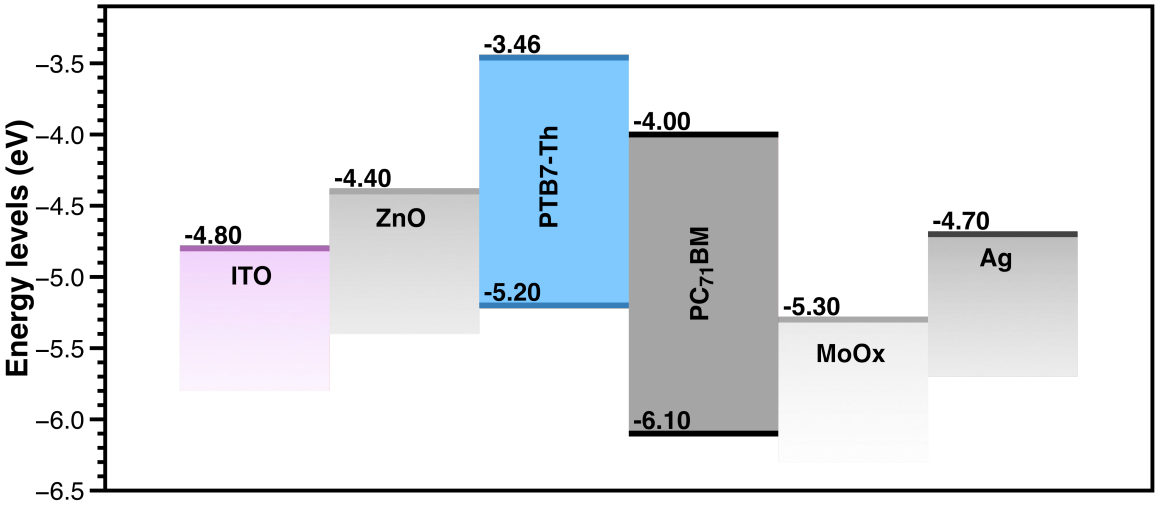

Figure 2. Energy levels for PTB7-Th:$PC_{71}BM$ photovoltaic cell showing contact work function alignment.

4. Morphology

Beyond material choice itself, the most important aspect of a functional OPV device may be the film morphology. The morphology of the thin film active layer has a direct impact on a device charge separation, charge mobility, and charge recombination[94–96]. Immediately upon spin casting, differences in solubility drive phase separation, which may nucleate pure crystal growth surrounded by heterojunctions[97–100]. The objective in thin film engineering is to optimize domain size and purity to maximize excitons reaching a heterojunction. Additionally, interfacial mixing at the heterojunction promotes exciton separation into free charges. Phase percolation must be sufficient for charge transportation and to promote high mobility and reduce recombination[101,102]. Moreover, film morphology plays a critical role at

the contact interfaces as it can promote either charge extraction or accumulation. This complexity necessitates each individual material system to have a unique optimized processing protocol.

The modular approach to material synthesis affords materials whose solubility parameters exist within a similar set of organic polar solvents[103,104]. For this reason, active layer engineering can operate mostly though solvent and processing changes instead of synthetic approaches. That's not implying that decisions in synthetic direction don't regularly have intended consequences to morphology[58,59,72,94,105–107]. The materials core structure will impact crystallization tendencies, packing distance and are regularly explored as new materials are produced. Additionally, modifications to the alkyl solubilizing chains, both in length and branching configuration, have a direct consequence to solubility and packing distance without changing energetic levels[108–111]. However, in general, material synthesis can focus on energetic changes to optimize performance, as there currently exists a plentitude of methods to control morphology in these structurally similar materials.

As mentioned before, self-assembly is rooted in solubility, so much of the device engineering exists in solvent and solvent additive control[74,76,79,112,113]. Furthermore, thermal annealing to promote controlled phase separation is regularly employed[114]. Techniques such as solvent annealing, substrate heating and modification, and nucleating materials have been used to control morphology of difficult systems[73,75,77,115]. For a system such as the small molecule donor T1 with the acceptor $PC_{61}BM$, morphology and the subsequent device performance are readily controlled through processing manipulation[116]. Simply casting the material from chlorobenzene creates a flat thin film with insufficient phase separation to generate high current. Throughout my research I worked often with this material, utilizing it's

adaptable morphology. During these studies I monitored morphology using atomic force microscopy (AFM), which images micro- scale surface topography, throughout these morphology studies. **Figure 3A,B** show the AFM images this as cast topography and phase respectively and have a root mean square (RMS) value of the topography, which may be considered the roughness, at 0.577 nm. That same film, when annealed at 140° C for 10 min shows larger structures in **Figure 3C,D** as the change in topography and phase is apparent and the RMS has increased to 6.7 nm. The published optimal conditions are achieved with the addition 0.4% v/v of diidooctane (DIO) and 70° C annealing. This film morphology presents smoother films with the topography and phase (**Figure 3E,F)** having a RMS value of 1.26 nm, however still possess pinholes which decrease the shunt resistance to a significant point. For this reason, 2.5% w/w high molecular weight polystyrene was added to increase the shunt resistance shown to have similar morphology (**Figure 3G,H**) and roughness as its optimal counterpart (RMS = 0.973 nm). This study, with several others, were conducted to assess the impact morphological changes have on the measured dielectric constant and will be discussed further in the next chapter. Beyond the application of atomic force microscopy for surface topography analysis, there exists a bevy of instruments which may further analyze morphology.[32,34,108,117] Grazing incident wide angle X-ray scattering (GI-WAXS) can inform with depth resolution, on molecular packing, ordering and crystal orientation in the film. Scanning electron microscope (SEM) can image phase separation and domain size near the surface, while tunneling electron microscopes (TEM) can image phase separation and domain size in the bulk. While I utilized existing morphology modification protocols from the literature and simply monitored correct changes using AFM and performance figures of merit, many additional instruments may be applied for analysis.

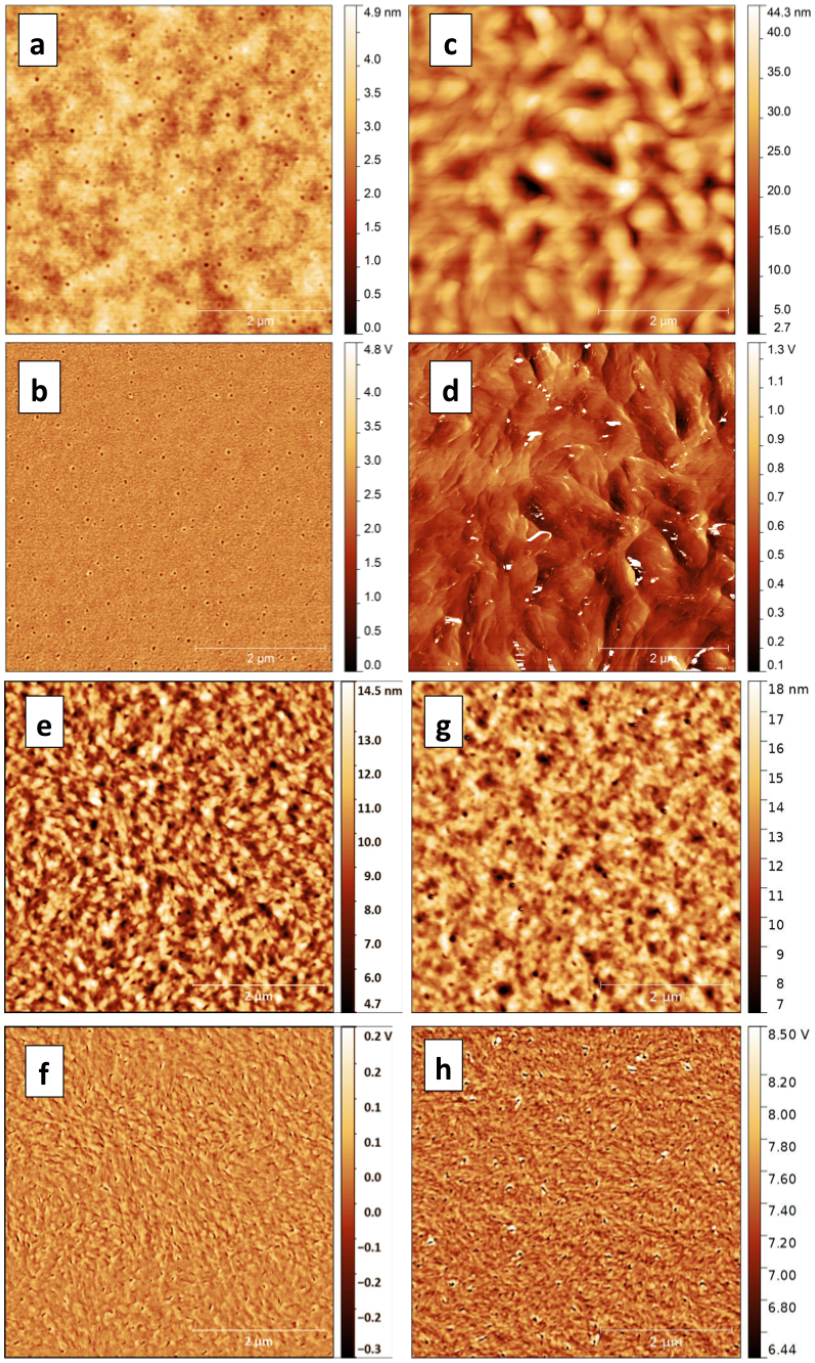

Figure 3. Atomic force microscopy images of T1:$PC_{60}BM$ system under different processing conditions. As cast topography (A) and phase (B), annealed at 140° C for 10 min topography (C) and phase (D), 0.4% DIO and annealed at 70° C for 10 min topography (E) and phase (F), 0.4% DIO and annealed at 70° C, 2.5% w/w high molecular weight polystyrene topography (G) and phase (H).

5. Charge Transport

Charge transport throughout the device can be characterized as a series of tunneling events or "hops" from organic molecule to molecule. While there are several models for considering charge transport in OPV's, we will consider the Marcus model in which hop rate, υ_{i-j}, from site *i* with energy E_i to site *j* with energy E_j may be described using **Equation 2**[27,34,40]**.**

$$\upsilon_{i-j} = \upsilon_0 exp\left\{-\frac{(E_j - E_i + E_r)^2}{4E_r kT}\right\} \quad (2)$$

This is when υ_0 is the hop attempt frequency, E_r is the re-organization energy and kT is the product of the temperature and the Boltzmann constant. These transport sites comprise a disordered density of states (DOS) in both the HOMO and LUMO which drive charge transport[118]. This disorder originates in organic photovoltaic materials from two places; energetic and material disorder. Energetic disorder stems from the degrees of freedom of the polymer or molecule which provide a multitude of unique energetic hopping destinations[119–121]. Material disorder relates more to the physical interaction between two organic molecules and their relation in space, and the effect it has on electronic coupling between molecules[122–125]. The presence of the re-organization energy in this model emphasizes the expected material polarization to accompany a hop[126–128]. As the charge moves from molecule to molecule, there exists a necessary electronic and atomic polarization and re-arrangement associated with a new energetic stability. For this work, it's important to consider the polarizations which are associated with every ionized molecule in the device, both as they move through to the contacts, as well as the opposing polarization on the part of the material which we will soon discuss.

To gauge overall performance a voltage is applied over a range of ± 1 V and the current is recorded, both in the dark and under solar simulated light, 100 mW cm^{-2} AM 1.5G[22,27,32].

Example sets of data can be found in **Appendix 1**. Electrical figures of merit include: the short circuit current, J_{sc}, which is the current produced at 0 V applied; the open circuit voltage, V_{oc}, which is the voltage at which no current is produced; and the fill factor, *FF*, which is the power produced between those points divided by the theoretical power which relates to the recombination in the device. We will discuss these more in the following chapters as well as their implications. Power conversion efficiency (PCE), η, is found through the product of these figures of merit, divided by the one sun power input, 100 mW cm^{-2} AM 1.5G as shown in **Equation 3**.

$$\eta = \frac{Voc*Jsc*FF}{100\ mW*cm^{-2}} \quad (3)$$

6. Recombination

Assuming morphology is correctly engineered, the greatest challenge to charge generation in OPV devices is recombination. The low dielectric constant of organic materials is the source of the high recombination behavior commonly observed[129–131]. For these studies, I've considered the three most common recombination processes: geminate, nongeminate, and trap assisted recombination. Geminate recombination, deriving from Gemini, the twin constellation, is the recombination of the original photo-induced electron/hole pair[10]. Due to the low dielectric constant of organic material, photo-excitation of an electron doesn't completely dissociate, instead forming an exciton. Excitons must migrate to a heterojunction of a material with appropriate energetic levels during their lifetime, otherwise will recombine geminately. High geminate recombination can occur with overlarge single-phase domains or from inability to dissociate at a heterojunction, originating from material or energetic level mismatch[132,133]. As recombination in this event occurs on a single molecule, geminate recombination is also referred to as monomolecular recombination. Another form of

monomolecular recombination is trap-assisted recombination otherwise known as Shokley-Read-Hall (SRH) recombination.[134–137] This occurs when energetic traps in the active layer capture free charges in an energetic well which they cannot escape, which in turn, acts as a recombination center for passing charges. The low dielectric constant of the material exacerbates the issue by allowing trapped charges to attract a recombination pair at great distance. These traps may occur from impurities in the material, born from synthesis, with energetic levels which may act as a trap for passing charges. We may also consider this process monomolecular as the recombination event, too, takes place on a single molecule. The bimolecular, also termed nongeminate, recombination occurs when two charges which originate from different excitons pass close enough to recombine.[138–141] The shortest distance of which two charges may safely pass in a given material was described earlier in the Coulomb capture radius in **Equation 1**[138,142]. This simple model expects that distance which charges may pass safely to exist with an inverse relationship with the dielectric constant. It is because of the low dielectric constant in these materials which keeps all recombination processes high, but bimolecular recombination has the greatest impact to overall performance in devices. It is for the relationship which the dielectric constant shares with recombination in OPV devices that motivates this thesis work. The overarching objective was to improve performance in organic photovoltaic devices resultant from decreased recombination due to increased dielectric constant. To achieve this, I began an immersive exploration into the dielectric constant, determining methodology for collecting the value, cataloging relevant values and considering how significant device fabrication decisions impact the measured result. The hope would be to discover the most effective method to improve the dielectric constant and report the results.

C. Introduction to the Dielectric Constant

The dielectric constant is a parameter that describes the permittivity of a material, or the response of a medium to an electric field. This response derives from molecular polarizations of different types and on different time scales. If an applied field exists for less time than the required polarization response, it will not affect the overall material capacitive response[143]. The capacitive response is the overall device polarization response to an applied electric field of a given frequency. The polarizations we will consider are: electronic, which occur from rearrangement of electrons in a bond (10^{15} Hz), atomic, from the modulation of atoms in molecules (10^{12} Hz), reorientation polarization from the molecular dipole alignment with the field (10^{9} Hz), and ionic, polarization from the movement of ions in a field (10^{3} Hz).[144] The resultant capacitance of these polarizations is cumulative, so as frequency decreases the measured capacitive response would possess all higher frequency polarizations. For this reason, any dielectric constant must be published with a measurement frequency. A material with a high dielectric constant will resist the electric field better than a material with a low dielectric constant. The dielectric constant is a dimensionless factor, often denoted as ε, which is always relative to vacuum permittivity, $\varepsilon_0 \approx 8.854 \times 10^{-12}$ F/m[145]. For comparison, silicon has a dielectric constant of 12.1 at 10^{6} Hz[118], while organic semiconductors often have dielectric constants around 2-5.[146–148] As discussed before, the result of a low dielectric constant is the Coulomb interaction between holes and electrons will be strong, thereby increasing effects of attraction and repulsion compared to a material with a high dielectric constant. As the dielectric constant is a frequency relevant parameter, it is necessary to discuss related timescales in organic photovoltaic devices. **Figure 4** shows the timescales of photoelectric species in devices on the lower independent axis with the corresponding

frequencies on the upper axis, while the dependent axis shows how each lifetime expiration affects overall species density. Primary excitations take place on the femto- to picosecond timescales with most geminate recombination occurring on the nanosecond timescale. The recombination of mobile carriers, or bimolecular recombination, takes place at the microsecond timescale and accounts for the largest reduction in species density[22]. Because bimolecular recombination is the largest loss mechanism, this work will specifically be interested in microsecond capacitive response, or the dielectric constant as measured at 10^6 Hz[10,138,142].

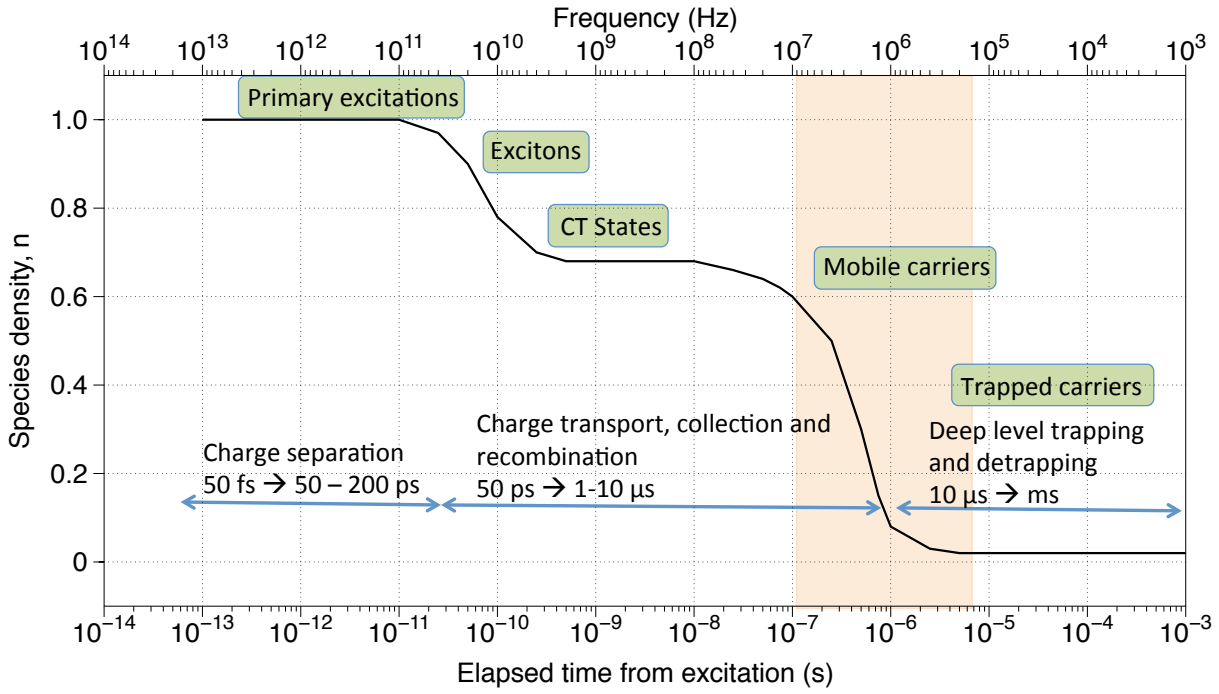

Figure 4. Relevant timescales for organic photovoltaic processes

II. Determining the Dielectric Constants of Organic Photovoltaic Materials Using Impedance Spectroscopy

A. Introduction

Photoexcitation of organic semiconductors leads to the formation of bound hole-electron pairs, termed Frenkel excitons.[149] This is in contrast to inorganic semiconductors, such as silicon, where photoexcitation leads to the formation of free charge carriers. The reason for this difference is the low dielectric constant of organic semiconductors. The low dielectric constant of organic semiconductors has been considered a main contributor to recombination-based losses in organic photovoltaics (OPV), including geminate and bimolecular recombination.[10,150] Geminate recombination, defined as the recombination of a hole and electron which originate from the same photon absorption event, is a result of the excitonic nature of organic semiconductors.[10,138,138,151] The exciton has a limited lifetime, and must be separated before the hole and electron recombine. The Coulomb capture radius described in **Equation 1** has an inverse relationship with the dielectric constant.

$$r^2 = \frac{e^2}{4\pi\varepsilon kT} \quad (1)$$

This highlights that increasing the dielectric constant should decrease the physical separation required to overcome this radius, resulting in an expected decrease in carrier recombination events. Indeed, this has been demonstrated in the literature. In a study by Collins et al. the dielectric constant of several materials was shown to have an inverse relationship to the voltage losses measured. The resulting devices showed an increase in the open-circuit voltage (V_{oc}), attributed to reduced charge-carrier recombination losses.[147] In work done by Ginger, et al. it was shown that by modifying the side chains of a

diketopyrrolopyrrole, DPP, based polymer donor, the dielectric constant was increased from 3.9 to 5, without changing the energetics of the polymer.[146] This improvement corresponded with an increase in device performance and specifically an increase in the free charge carrier lifetime and reduction in the charge recombination.

Despite the importance of the dielectric constant to the field of organic electronics, an in-depth study of dielectric constants has been absent from the literature. When necessary, most studies simplistically approximate the relative dielectric constant as $\varepsilon = 3$. In the rare event that the dielectric constant of an organic semiconductor is reported, it is most often determined using impedance spectroscopy. However, within the scarcity of dielectric constant values in OPV literature there is even less agreement on the optimal way for determining it. I've observed that the dielectric constant determined with impedance spectroscopy is highly dependent on experimental parameters such as the frequency of analysis, the magnitude of device leakage current, the applied DC bias, and the presence of light. Opinion differences exist throughout the field on the correct choice of frequency,[150,152,153] data presentation and analysis make it difficult to find agreeable values.[147,152] As a result, published dielectric constants for organic semiconductors span a range of 2 -16.7.[153] For reference, a dielectric constant of 16.7 is higher than the dielectric constant of silicon, and should therefore imply that free charge carriers can be formed within a single material upon photoexcitation. Additionally, work recently published indicates blend dielectric constants which are larger than either individual component.[154] This result stands in contrast to what has been repeatedly observed during this study and it is because of this discrepancy that I've explored how experimental parameters alter measured results.

In this chapter, I report a thorough investigation of the dielectric constant in organic semiconductors. This must begin by first discussing the challenges of determining the dielectric constant using impedance spectroscopy and highlight the possible reasons for error in the measurements. Following this I provide an analysis of the dielectric constant of seventeen OPV materials: seven polymer donors, three small molecule donors, one polymer acceptor, two fullerene-based acceptors and four non-fullerene small molecule acceptors (see Scheme 1 for the chemical structures). In the following chapter, additional materials will be studied, but this section regards neat materials which are optimized and analyzed separately. Among these neat materials is a case study in which modification of the side-chains of a small molecule donor molecule is used to understand the effect of chemical structure modifications to the dielectric constant. Having established the dielectric constant of the neat organic semiconductors, I naturally transition to the study of the dielectric constant of donor/acceptor blends as a function of blend ratios and processing conditions. It's repeatedly observed that the dielectric of donor/acceptor blend films can be predicted from the dielectric constant values of the neat materials, scaled by their weight ratio. This holds true irrespective of processing conditions and changes in morphology. This chapter's overall objective is to create a protocol for dielectric constant measurements without artifacts.

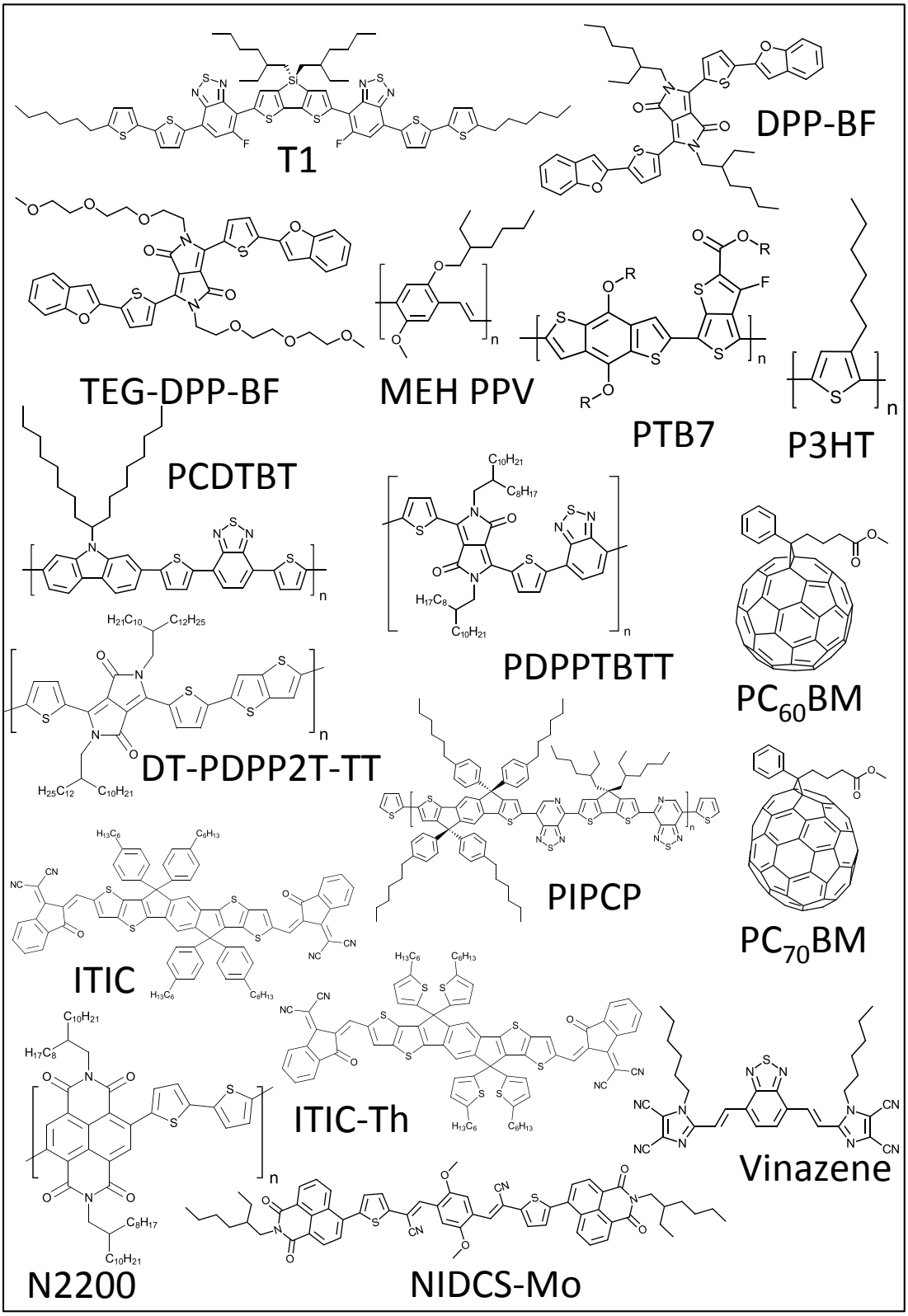

Scheme 1. Chemical structures of the semiconductors studied in this work.

B. Methodology to Determine the Dielectric Constant Using Impedance Spectroscopy

Impedance analyzers apply a direct current (DC) bias across a device, perturb the signal with a small alternating (AC) voltage, and monitor the resultant complex current.[143] The ratio of the complex AC voltage to the complex current is a complex number (with real and imaginary components), which describes the impedance, *Z*. The real part of *Z* is described as the resistance of the device, and the imaginary part describes the reactance of the device. Total impedance is the sum of these two values. The response of the sample to the AC perturbations is also dependent on the frequency of the AC bias, and an understanding of the frequency-dependence is critical to extracting information from impedance spectroscopy.

Traditionally, impedance data is described using the complex plane or Nyquist plots.[155–157] Both the low frequency (10^1-10^3 Hz) and high frequency regions (10^4-10^6 Hz) may have salient information, and careful analysis of both regions may provide insight into OPVs. Specifically, the small changes real impedance in the low frequency, which are associated with charge carriers, would otherwise be obscured in the Nyquist plots. Nyquist plots real and imaginary components together and yield important information about frequency and phase. For this reason, I use Bode analysis to describe the impedance data which separate the analysis of real and imaginary impedance; however, the Nyquist plots corresponding to **Figure 1** data are available in appendix 2 (**Figure A2.1**).

A frequency dependent capacitance spectrum can be calculated using the real and imaginary impedance values (Equation 2)[143].

$$C_{cor} = -\frac{1}{\omega}\left[\frac{Z'' - \omega L}{(Z' - R_S)^2 + (Z'' - \omega L)^2}\right] \tag{2}$$

Here *Z'* represents the real impedance, *Z''* represents the imaginary impedance, ω is the angular frequency ($\omega = 2\pi f$), *f* is linear frequency, *L* is inductance, and R_s is the AC series resistance. The series resistance affects the real impedance and can be extracted from the Bode plot where the real impedance saturates in the high frequency (**Figure 1A**). This saturation resistance originates from the total resistance of the system minus the resistance of the main polarization process. In the OPV devices this polarization process is attributed to the response of charge carriers in the device either photogenerated, thermogenerated, or defused from the contacts. Evidence for this is seen in the bias dependence of the low frequency where $R_{total} = R + R_s$, as further decreasing bias sweeps more charge carriers out of the device. The goal of these measurements must be to remove as many charge carriers from the device so the capacitance calculated in this regime is frequency independent. The dielectric constant should be evaluated at the material's geometric capacitance, which represents the capacitance measured when the capacitance derives from only the material itself- the electronic, atomic and ionic polarization. It's expected no obvious contributions from reorientation dipoles are observed in the solid matrix, however if present, would additionally contribute. For my work, I only consider materials with a depleted active layer and a frequency independent capacitance over the chosen frequency range as the reported dielectric constant. Measurements done with charge carriers present would calculate a dielectric permittivity. When the geometric capacitance is found, the value is calculated using the device thickness, *d* and area, *A* (Equation 3)[145].

$$\varepsilon = \frac{C_g d}{\varepsilon_0 A} \tag{3}$$

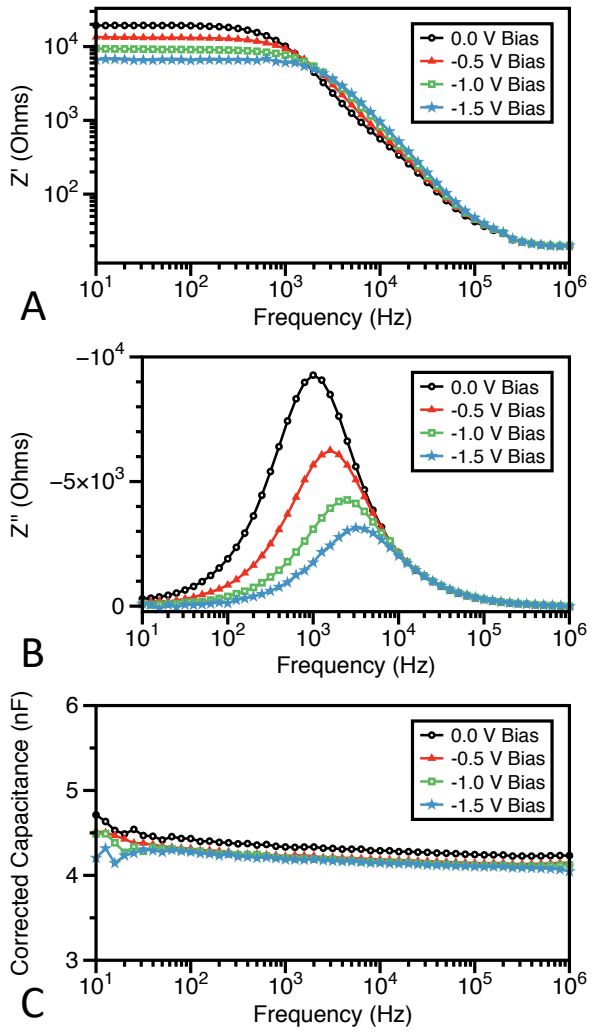

Figure 1. Example Bode plots of impedance data: (A) real impedance, (B) imaginary impedance, and (C) corrected capacitance

Frequency dependence on inductance influence results in a noticeable increase in capacitance at high frequency while the series resistance decreases capacitance in the same region[158]. For this work, the series resistance is extracted for every device using the real impedance spectra and used to correct the capacitance. The inductance is measured for the testing setup at 6 μH, however a ~ 1 μH variability may be observed as inductance varies between devices. Inductance, or the force that opposes the change of current flow, can derive from electrical channels within the device (self-inductance) and by nearby conductors (mutual

inductance)[158]. The inductive influence on impedance increases with frequency so deviations are observed in the high frequency regime[129]. Leakage current is the source of the self-inductance, as a result, devices with low leakage show much less deviation from the geometric capacitance in high frequency.

When the capacitance does not have a strong frequency dependence, a geometric capacitance, C_g, is collected at 1 MHz (**Figure 1C**). This frequency is chosen as it corresponds to the timescale of nongeminate recombination[159,160] (1 μs) in organic solar cell devices which is the main loss mechanism I expect to reduce with higher dielectric values[138].

Next, I needed to systematically demonstrate experimental details that may convolute the impedance spectra. In the following section I explore the significance and effects of: AC frequency, DC bias, illumination, choice of contacts, and device quality (shunt resistance).

1. The Importance of AC Frequency

Impedance spectroscopy is a sensitive bulk measurement that can capture multiple processes, which can be difficult to deconvolute.[14] The response of the sample to the AC field of varying frequencies is cumulative: at low frequencies the impedance analyzer measures all species which are able to contribute to the signal[144]. As the frequency is increased, certain contributing species will not be able to respond fast enough to the changes in field, in essence freezing their response, and their contribution will be silenced. In order to arrive at the true dielectric constant of a material, it is necessary to understand the polarizations that contribute to the overall capacitance and 'silence' undesirable polarizations.

At a given frequency, impedance spectroscopy will measure everything within the sample that is able to respond to the AC bias. Ions, for example, which are relatively large species that have to migrate within the sample in order to respond to the field, will tend to have a

relatively slow response to the field, and can be detected at a frequency range of 10-10^3 Hz.[161,162] Charge carriers such as holes and electrons tend to have a higher mobility than ions, and can be detected at frequencies in the range of 10^3-10^4 Hz.[10,138,162] It is critical to emphasize here that the response of species such as ions and charge carriers to the AC field does not describe the intrinsic response of the material to the field, or in other words, the dielectric constant which is relevant to describing recombination and charge separation in OPV. For this reason, determination of the dielectric constant of organic materials is done at high frequencies, in the range of 10^5-10^6 Hz, and with great efforts to remove charge carriers present. It may be observed in **Figure 1A** and **1B** that both the real and imaginary impedance contributions are low in this frequency range indicating minimal resistance from the dominate contributor. In this range the only contribution to the resistance of the field in the material itself and contacts, with contact resistance being accounted for separately in **Equation 2**.

2. The Effect of DC Bias

Impedance measurements of OPV materials can be highly sensitive to the DC bias, and the DC bias must therefore be considered for each experiment. If a semiconductor film has Ohmic contacts, the DC bias across this film can have a significant effect on the charge carrier density in the film[80]. As the bias across the electrodes becomes increasingly positive, more charge carriers may diffuse from the contacts into the film, until the contacts biased for charge injection (forward bias), when charge carrier density in the film will be highest[10,163]. The charge carriers from the contacts will complicate the characteristics measured by impedance spectroscopy and may skew the determination of the relative permittivity. To determine the dielectric constant, the DC bias should be used to reduce charge carriers in the device. To that end, each sample is scanned with increasing reverse biases to ensure depletion of the active

layer of charge carries. Even in the dark, charge carriers can diffuse into the film from the contacts.[164,165] **Figure 1A** shows the reduction of the real impedance in the low frequency region, as a result of charge depletion from the active layer. Charge carriers do not respond in the high frequency region and the bias-independent low impedance saturation results from the AC contact resistance. **Figure 1B** shows the effect of bias on the imaginary impedance both reducing the magnitude and pushing the characteristic frequency higher as the system loses more low frequency contribution to the overall impedance. Although the effect of depleting the active layer appears insignificant in **Figure 1C**, magnification shows a reduction in capacitance as you deplete the region. An example of this effect is shown in the SI **Figure S2**.

3. The Effects of Illumination

Photoexcitation can lead to charge carrier generation, especially in the case of high performance donor:acceptor blends. For this reason, the presence of light may introduce additional capacitance in the impedance measurements, skewing the results. To eliminate light contamination, special care should be taken to ensure these measurements are done in the dark. I've used films of P3HT:$PC_{61}BM$ and neat P3HT to illustrate the effects of stray illumination on the capacitance spectra. Experiments examining capacitive contributions from light were done and the results are shown in **Figure 2**.

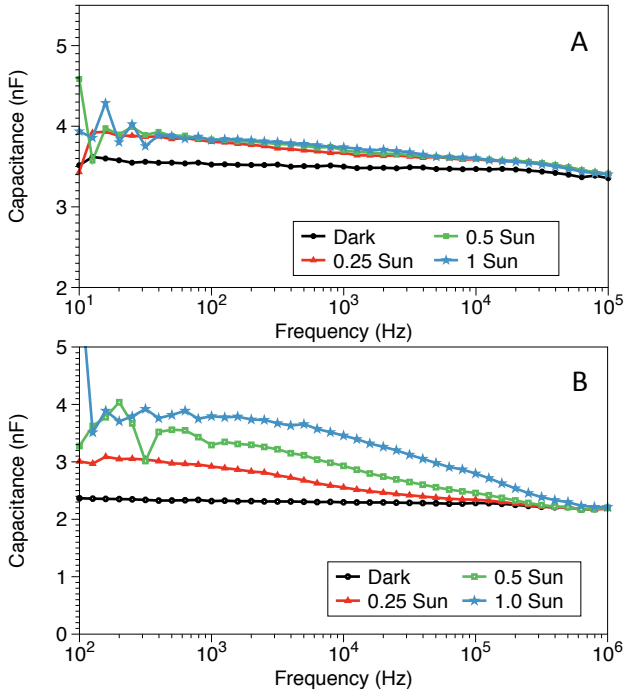

Figure 2. Influence of light on capacitance on (A) pristine P3HT and (B) P3HT:$PC_{61}BM$ blend

The results indicate that in blend systems such as P3HT:$PC_{61}BM$, the capacitance will increase by 64% at 1 kHz with one sun illumination and by 26% with 0.25 sun illumination. This effect is reduced in pristine materials, most likely as a result of reduced free charge generation efficiency. In pristine P3HT films the capacitance increased by 7% and 5% at 1 kHz under one sun and 0.25% sun illumination respectively. In both films the capacitance gain is limited to the low frequency regime, with all light intensities converging to the geometric capacitance around 1 MHz.

4. Choice of Contacts

Contacts can also influence low frequency impedance. The material choice for the contacts may have added characteristics in the measured impedance. To illustrate this effect, I

fabricated devices using the architectures *ITO/active layer/Al*, *ITO/active layer/Ca/Al*, and *ITO/active layer/LiF/Al*. Measurements with LiF hole blocking layer on the cathode show a sharp decrease in capacitance in the low frequency region while applying negative DC bias. Data in the appendix 2 (**Figure A2.3**) shows a decrease in the low frequency capacitance in devices with LiF, while devices with Ca/Al or just Al contacts are free of this deviation. While the mechanism for this reduction is not fully known, it may be that the introduction of ions at the contacts influences the capacitance in the low frequency regime. It is worth noting that no deviance is observed with 0 V DC bias applied to the LiF device, indicating this effect is only present at stronger DC fields.

5. Contribution of Shunt Resistance

The most common contributing factor to artificial capacitance in OPV devices is also the most challenging to eliminate. Leakage current, which results from charges leaking from the electrodes into the active layer, can produce noise in the low frequency regime and deviations of capacitance further into the high frequency regime. This behavior had been observed in several blend systems, one example is PTB7:PCBM (**Figure A,B**). To more systematically examine how leakage changes the capacitance spectra, a series of T1:PCBM devices were prepared with thickness ranging from 280 nm to 70 nm by varying spin speed from 500 RPM to 4000 RPM respectively. An example of the dark J-V scans of a thick, low-leakage device and a thin, high-leakage device from this set is shown in **Figure 3C**. When comparing the different capacitance spectra, according to Equation 2, the capacitance is expected to have an inverse relationship with thickness when all other variables are unchanged. This is the observed behavior in the low frequency regime, but devices with higher leakage (dotted lines) show deviation from this trend in the high frequency region (>10kHz) (**Figure 3D)**. When the

capacitance is corrected by thickness and area to describe a dielectric constant spectrum (appendix 2, **Figure A2.4**), the thicker, low-leakage devices show good agreement on the dielectric constant at 1 MHz. The thinner, high-leakage devices, however, differ on the dielectric constant, giving lower than expected values. For this reason, it is critical that low-leakage devices which show a frequency independent geometric capacitance are used for the determination of the dielectric constant.

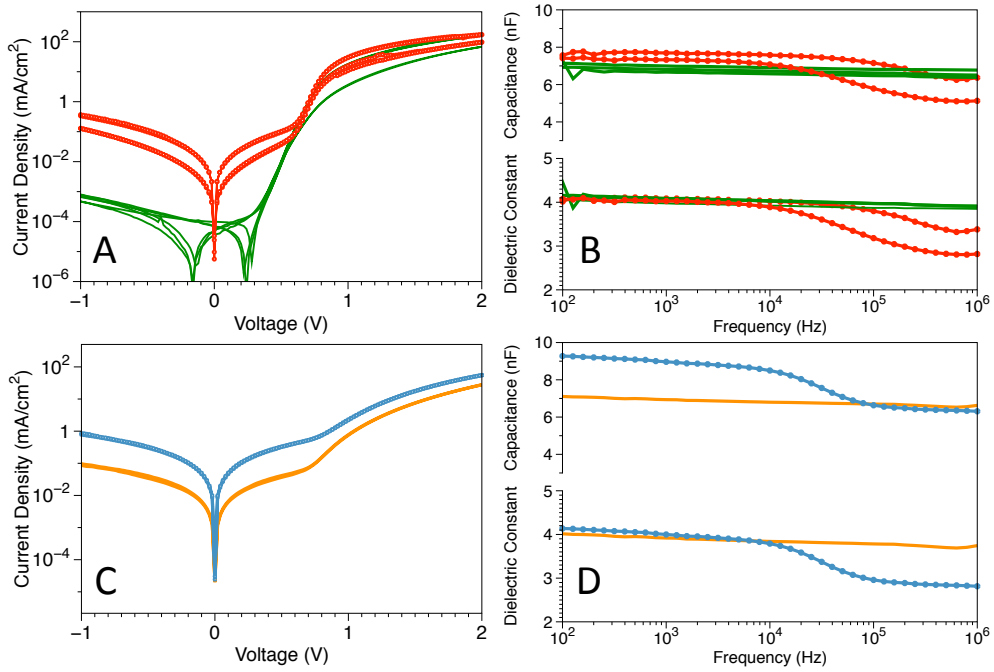

Figure 3. Impact of high leakage (dotted lines) versus low leakage (smooth lines) devices on the frequency dependence of the capacitance and resulting dielectric constant for PTB7:PCBM (A,B) and T1:PCBM (C,D). Multiple traces of high and low leakage devices are shown for the PTB7:PCBM system to show the reproducibility of this behavior.

C. The Dielectric Constant of Organic Semiconductors

Having established the correct protocol to determine the capacitance value that is relevant for describing the relative permittivity in OPV materials, I catalog values by measuring the

relative permittivity for a range of neat materials, blends, and the effect of processing conditions (morphology).

1. Neat Organic Semiconductors: Molecular Structure and the Dielectric Constant

Characterized are of seventeen organic semiconductors used in OPV devices. The semiconductors can be divided into four major groups. Polymer donor materials: *regioregular Poly(3-hexylthiophene-2,5-diyl)* (**P3HT**), *Poly[[4,8-bis[(2-ethylhexyl)oxy]benzo[1,2-b:4,5-b']dithiophene-2,6-diyl][3-fluoro-2-[(2-ethylhexyl)carbonyl]thieno[3,4-b]thiophenediyl]]* (**PTB7**), *Poly[2-methoxy-5-(2-ethylhexyloxy)-1,4-phenylenevinylene]* (**MEH PPV**), *Poly[2,5-bis(2-octyldodecyl)-3,6-bis(thien-2-yl)pyrrolo[3,4-c]pyrrole-1,4-dione-5',5''- diyl-benzo-2,1,3-thiadiazol-4,7-diyl]* (**PDPPTBTT**)[166],*(IUPAC name unavailable)* (**DT-PDPP2T-TT**)[167], *Poly[N-9'-heptadecanyl-2,7-carbazole-alt-5,5-(4',7'-di-2-thienyl-2',1',3'-benzothiadiazole)]* (**PCDTBT**), *Poly[(4-(6-([1,2,5]thiadiazolo[3,4-c]pyridin-4-yl)-4,4-di(heptan-3-yl)-4H-cyclopenta[2,1-b:3,4-b']dithiophen-2-yl)-7-(4,4,9,9-tetrakis(4-hexylphenyl)-4,9-dihydro-s-indaceno[1,2-b:5,6-b']dithiophen-2-yl)-[1,2,5]thiadiazolo[3,4-c]pyridine)]* (**PIPCP**)[168]; small molecule electron donating materials: *7,7'-(4,4-bis(2-ethylhexyl)-4H-silolo[3,2-b:4,5-b']dithiophene-2,6-diyl)bis(6-fluoro-4-(5'-hexyl-[2,2'-bithiophen]-5-yl)benzo[c][1,2,5]thiadiazole)* (**T1**)[169], *3,6-bis[5-(benzofuran-2-yl)thiophen-2-yl]-2,5-bis(2-ethylhexyl)pyrrolo[3,4-c]pyrrole-1,4-dione* (**DPP-BF**), and a derivative of DPP-BF with triethylene glycol side chains *3,6-bis(5-(benzofuran-2-yl)thiophen-2-yl)-2,5-bis(2-(2-(2-methoxyethoxy)ethoxy)ethyl)pyrrolo[3,4-c]pyrrole-1,4-dione* (**TEG-DPP-BF**); polymer acceptor material: *poly[[N,N-bis(2-octyldodecyl)-napthalene-1,4,5,8-bis(dicarboximide)-2,6-diyl]-alt-5, 5'-(2,2'-bithiophene)]* (**N2200**)[44]; small molecule electron accepting materials: *[6,6]-Phenyl-C61-butyric*

acid methyl ester (**$PC_{60}BM$**), *[6,6]-Phenyl-C71-butyric acid methyl ester* (**$PC_{70}BM$**), *4,7-bis[2-(1-hexyl- 4,5-dicyano-imidazol-2-yl)vinyl]benzo[c][1,2,5]-thiadiazole* (**Vinazene**)[45], *2E,2'E)-3,3'-(2,5-dimethoxy-1,4-phenylene)bis(2-(5-(4-(N-(2-ethylhexyl)-1,8-naphthalimide)yl) thiophen 2-yl)acrylonitrile* (**NIDCS-MO**)[46,170], *3,9-bis(2-methylene-(3-(1,1-dicyanomethylene)-indanone))-5,5,11,11-tetrakis(4-hexylphenyl)-dithieno[2,3-d:2',3'-d']-s-indaceno[1,2-b:5,6-b']dithiophene* (**ITIC**)[47], *(IUPAC name unavailable)* (**ITIC-Th**)[48]. These materials structures can be viewed in Scheme 1 for comparison. Average relative permittivity values and standard deviation from a minimum of eight samples are summarized in **Table 1**.

Name	Avg. ε	Std. Dev. (±)	Name	Avg. ε	Std. Dev. (±)
PIPCP	2.65	0.14	PCDTBT	3.6	0.22
N2200	2.73	0.1	MEH PPV	3.26	0.15
P3HT	2.9	0.19	NIDCS-Mo	3.62	0.1
DT-PDPP2T-TT	2.95	0.3	T1	3.72	0.09
DPP-BF	3	0.16	TEG-DPP-BF	3.84	0.13
PDPPTBTT	3	0.19	Vinazene	4.56	0.25
ITIC	3.04	0.09	$PC_{60}BM$	4.61	0.07
PTB7	3.23	0.13	$PC_{70}BM$	4.75	0.15
ITIC-Th	3.24	0.08			

Table 1. List of dielectric constants of pristine OPV materials and standard deviations.

The neat semiconductors have dielectric constant values in the range from 2-5. In general, polymer donors have lower dielectric constants than the small molecule donors: polymers have a dielectric constant of about 3, while small molecules have a dielectric constant of 3-3.5 (**Figure 4**). Furthermore, within the small molecules, the acceptors $PC_{60}BM$, $PC_{70}BM$, and vinazene have the highest dielectric constant values. Crystallinity, polymer length, density and other factors can impact the dielectric constant of polymers and organic molecules[171,172]. Work has shown that bringing a solution cast film from the melt increases crystallinity and dielectric constant by way of decreased porosity and increased molecular dipoles per volume[173]. Additionally, it may be assumed that increased dipole alignment in a crystalline film may increase dipoles interacting with the field. An increase to the dielectric constant can be observed from addition of more polar groups, as seen with ITIC and ITIC-Th. Unfortunately, simply counting polar groups will not predict the value. This is why PCDTBT has a higher dielectric constant that the other polymers measured despite having less polar groups. The reasoning for this lack of predictability comes from the impact of orientation of dipoles in the crystallites and the crystallite orientation within the film, which is unknown. But from these results, it appears that the impact of film structure may overwhelm the impact of polar groups, which makes prediction from the molecular structure difficult. When making systematic changes on a molecule which has little impact on the morphology, I was able to observe the change this makes to the dielectric constant.

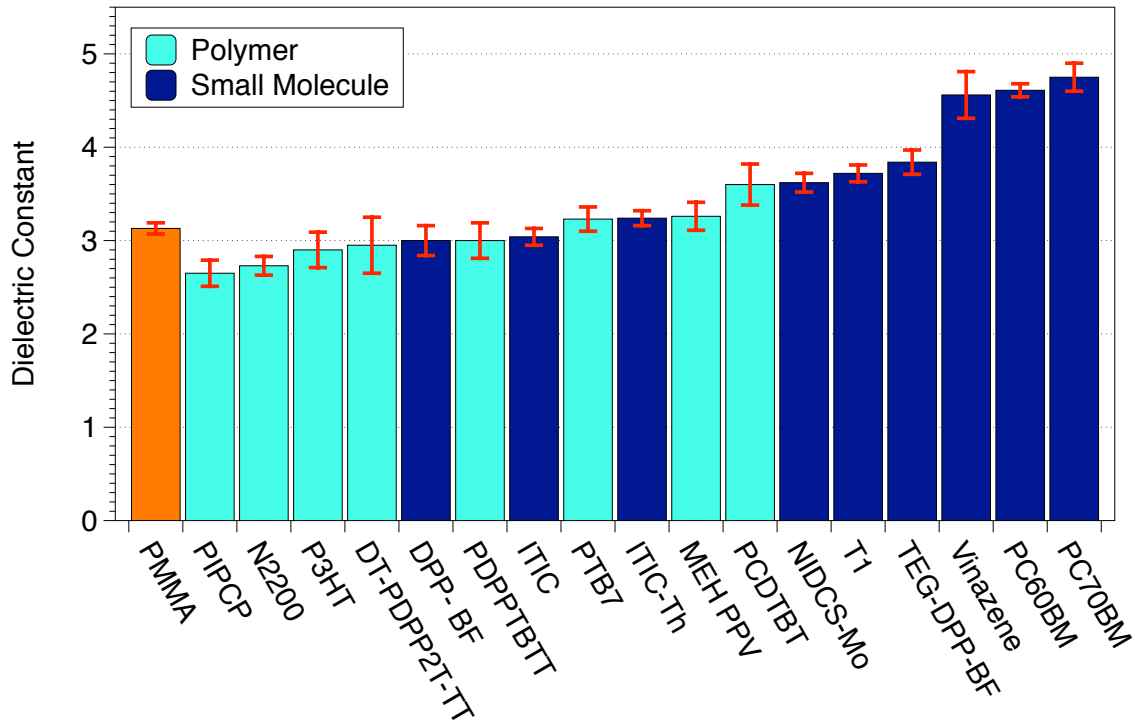

Figure 4. Dielectric constants of a reference polymer, PMMA, and pristine organic semiconductor materials.

Among the neat materials studied, DPP-BF and TEG-DPP-BF provide an interesting comparison. Considering the limited range of these values, I explored the possibility of increasing the relative permittivity through molecular design. Collaborating with an organic chemist I had the diethylhexyl solubilizing chains on DPP-BF ($\varepsilon = 3.00 \pm 0.16$) replaced with triethylene glycol (TEG) chains to create TEG-DPP-BF. Polyethylene glycol is known to have a high dielectric constant ($\varepsilon \approx 12$) due to the rapid polarization of dipoles throughout the chain. I observed a 28% increase in the relative permittivity, with $\varepsilon = 3.84 \pm 0.13$ for TEG-DPP-BF. These results are in agreement with previous reports that have shown that replacement of solubilizing chains can increase the dielectric constant.[146,174] However, work done examining the effect of the increase of the dielectric constant via solubilizing chain modifications have

shown that increase in performance only corresponds to changes in morphology, not the increased dielectric constant.[175,176] The synthesis of TEG-DPP-BF is reported in the experimental section of this chapter.

Its important to highlight a surprising result from the literature which was published during my studies, as it comprised much of my time and energy to disprove and explain. The paper in question reported a polymer donor material with a measured dielectric constant of ε= 16.7. A relative permittivity of 16.7 is very high, especially when compared to the relative permittivity of Si (ε=12.1) or Ge (ε=16.0)[118]; these materials are able to generate free carriers directly from photoexcitation without the need for an acceptor material to provide a driving force for charge generation. Furthermore, when PDPPTBTT was blended with $PC_{60}BM$, Zhang *et al.* reported that the dielectric constant of the blend was significantly lower, ε= 6.8. However, following the procedure describe above, the relative permittivity I've found for PDPPTBTT was only ε= 2.95 ± 0.30. However, the authors show a $1/C^2$ vs voltage plot, which was able to be reproduced as well (**Figure 5A**). From this plot, it is possible to extract ε=17, but does little to describe the behavior of the capacitor. During the testing of this material when holding frequency at 1 kHz and sweeping voltage, there is a spike of capacitance which peaks at a level corresponding with a dielectric constant of 17 (**Figure 5B**). The bias associated with this spike is the diffusion regime of the forward bias (**Figure 5C**). At this bias, the device is flooding with injected charge carriers[163] and a resultant double layer capacitance at the device interface associated with this temporary high value. However, the results also show a very steady lower capacitance in the reverse bias, even at the frequency of 1 kHz, which saturates to a value related to a dielectric constant of around 3. This further illustrates

the wide range of control that one needs to consider when measuring the dielectric constant of organic solar cell materials.

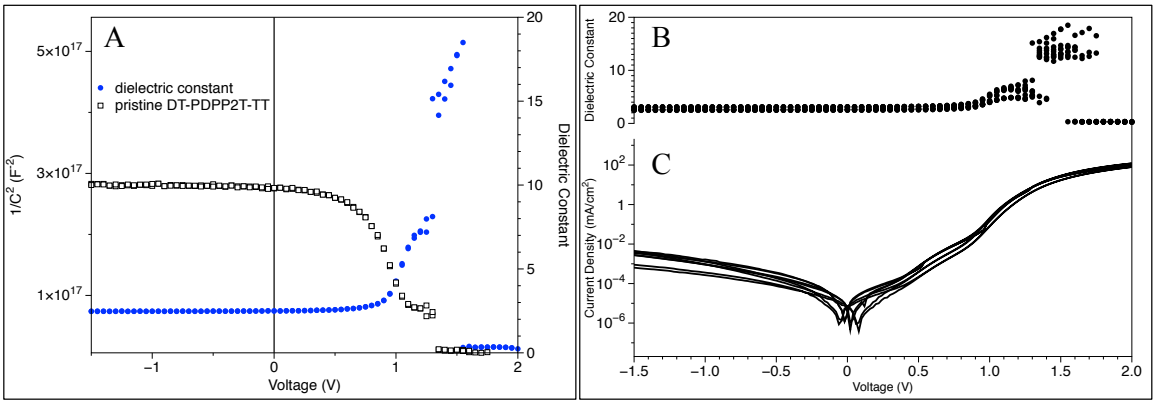

Figure 5. An overlay (A) of the recreated DT-PDPP2T-TT $1/C^2$ versus voltage graph (white boxes) with the resultant dielectric constant for perspective (blue circles). This data is replicated for 6 devices (B) and shown to have a predictable spike in capacitance, which corresponds to the diffusion/injection regime of the dark JV graphs (C).

2. Bulk Heterojunction Blends: The Effect of Blend Ratios and Morphology on the Blend Dielectric Constant

Bulk heterojunction (BHJ) solar cells involve the mixing of a donor and an acceptor to achieve charge separation and extraction. Therefore, understanding how the dielectric constant of a blend system relates to the values of the pristine materials is especially significant. To gain a more general view of the dielectric constant in blend systems relevant to OPVs, I blended several common systems and determined their respective dielectric constants.

As shown in Table 2, I discovered that the dielectric constant of the blends could be closely estimated through the weighted average of the pristine values. This trend held for all the systems tested indicating that it may be possible to use the rule of mixtures to closely estimate the dielectric constant of blends.

The materials rule of mixtures states that certain properties of a composite can be estimated through the weighted mean of the components[177], which can describe elasticity, thermal and electrical conductivity. This estimation is described between two bounds, which represent the parallel and perpendicular effects of the specific property[178]. This result indicates that the dielectric constant, when measured under the discussed constraints, can be viewed as a material value. Using this model, the dielectric constant may be predicted within error using a simple expression (**Equation 4**) where *f* is the volume fraction of donor and acceptor materials.

Material (D/A)	Blend Ratio (D:A)	Donor ε	Acceptor ε	Measured blend ε	Calculated blend ε	% Difference
P3HT: $PC_{60}BM$	50:50	2.90	4.61	3.82± 0.07	3.76	1.57%
P3HT: $PC_{70}BM$	50:50	2.90	4.75	3.99± 0.14	3.83	4.01%
T1: $PC_{60}BM$	60:40	3.72	4.61	4.04 ± 0.2	4.08	0.99%
PIPCP: $PC_{60}BM$	50:50	2.65	4.61	3.73 ± 0.1	3.63	2.68%

Table 2. List of dielectric constants of blend OPV materials and those calculated using the rule of mixtures.

$$\left(\frac{f}{\varepsilon_D}+\frac{1-f}{\varepsilon_A}\right)^{-1} \le \varepsilon_B \le f\varepsilon_D + (1-f)\varepsilon_A \tag{4}$$

Optimizing the performance of BHJ solar cells most often requires optimization of the nanoscale morphology[179–181]. To this end, different processing conditions such as thermal annealing, solvent annealing, and solvent additives are often employed to influence

morphology. These processes have been shown to affect material mixing, crystallinity, domain size, which may also affect the relative permittivity. Its widely understood that crystallinity has a direct effect on the dielectric constant.[173] However, even when the crystallinity of OPV materials is increased, the crystallites are randomly orientated through the film and often a large volume fraction of the film remains amorphous. Therefore, it is not currently widely understood how the dielectric constant of OPV films may change with processing conditions.

For this study, I examined two common donors; the polymer P3HT and small molecule T1 blended with $PC_{60}BM$ under different processing conditions. These conditions were chosen from the literature both as examples of optimal and suboptimal material morphology for comparison. Changes in surface morphology were tracked using atomic force microscopy and reported in appendix 2 (**Figure A2.5**). The processing conditions for the T1:$PC_{60}BM$ system are as follows: "as cast" involving no special treatment after spin casting from chlorobenzene; "0.4% DIO" in which 0.4% v/v of diiodooctane is added to the chlorobenzene prior to spin casting, followed by thermal annealing at 70° C for 10 min; and "annealed" in which the BHJ films are annealed on a hot plate at 150° C for 10 minutes. These conditions should correspond to a fully mixed morphology with no crystallites (as cast); crystallites of T1 of optimum of around 30-40 nm, optimum for OPV applications (0.4% v/v DIO); large T1 crystallites on the order of 100 nm (annealed at 150° C for 10 minutes).[182]. The aforementioned processing conditions are tested for T1 blended 60:40 with $PC_{60}BM$ with the addition of another, "2.5% PS." This label corresponds to the addition of 2.5% w/w high molecular weight (900,000 da) polystyrene to 0.4% v/v DIO in chlorobenzene and annealed at 70° C for 10 min. This has been shown in the literature to improve performance and thicken

films[73,74]. Similarly examined were P3HT: $PC_{60}BM$ blends under the following processing conditions: “as cast” in which no processing after casting takes place, “annealed” in which the BHJ films are annealed on a hot plate at 140° C for 10 min[183], and “3.0% DIO” in which 3.0% v/v of diiodooctane is added to the chlorobenzene prior to spin casting. As in the case of the T1:$PC_{60}BM$ blends, these conditions correspond to a range of donor:acceptor mixing and degrees of crystallinity. [184,185]

The resultant impedance data shows a 1 MHz dielectric constant, which is independent of processing conditions (see **Figure 6**). Despite the varied morphologies achieved with processing conditions, the results indicate that the dielectric constant of BHJ blend films are still best described by the rule of mixtures. In other words, my results suggest that overall, the dielectric constant of a BHJ blend can be predicted solely based on the neat material dielectric constant values, scaled by the weight ratios in the BHJ blend. There may be changes in crystallinity and therefore density and alignment, however results thus far indicate no change to the dielectric constant. The important take home message from these results is that in order to increase the dielectric constant in OPV devices chemists must develop neat organic semiconductors with high relative permittivity.

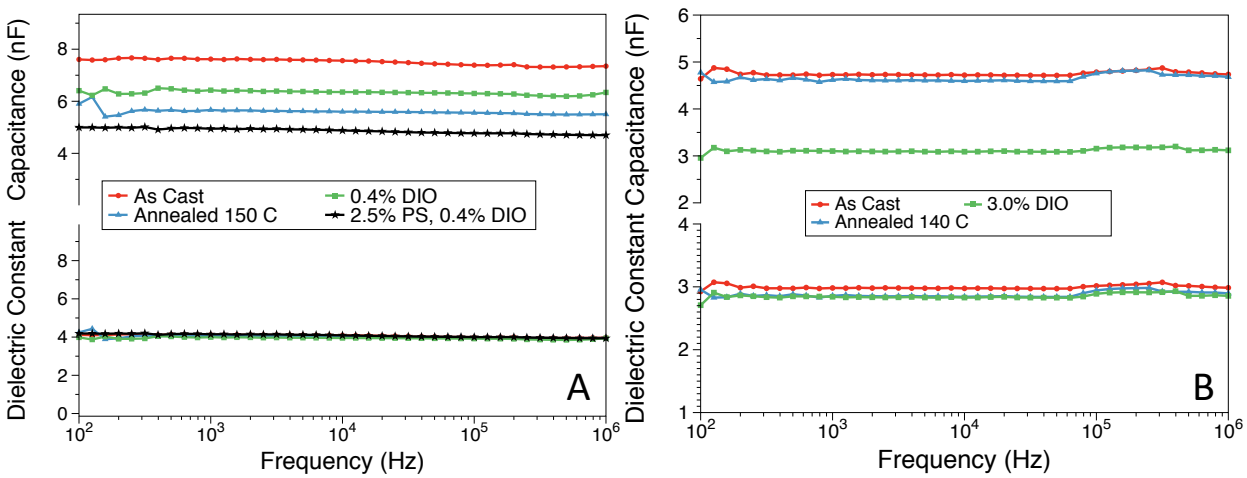

Figure 6. Capacitance (upper) and dielectric constant (lower) of T1:$PC_{60}BM$ (A) and P3HT:$PC_{60}BM$ (B) systems under different processing conditions.

In light of these results, it's necessary to address another study that was published during my time at UCSB and required me to address the conflict of results directly to the authors.[186] In this study, the researchers found that the dielectric constant of a BHJ blend composed of PTB7:$PC_{70}BM$ and PCDTBT:$PC_{70}BM$ was higher than the dielectric constant of either pristine donor or acceptor, implying that polymer-fullerene intermixing produces interfacial dipoles which significantly increase device capacitance. The authors found that the PTB7:$PC_{70}BM$ and PCDTBT:$PC_{70}BM$ blends have dielectric constants of 4.6 and 6.3 respectively, while the reported relative values of PTB7, PCDTBT and $PC_{70}BM$ were 3.1, 3.0 and 3.9, respectively. This result seemingly contradicts the trend I have observed thus far, whereby the dielectric constant of a BHJ blend is a linear combination of the dielectric constant values of the neat materials. Therefore, I needed to study the materials reported in the study by Constantinou et al[186]., and tried to reproduce the reported value following the conditions used in their study. However, after careful trials, I find that the BHJ of PTB7:$PC_{70}BM$ does in fact follow the rule of mixtures with a dielectric constant of 3.93 ±

0.05, a value which can be closely predicted from the weighted average of the neat material dielectric constant values. To illustrate, using **Equation 4** with a 40:60 weight ratio of PTB7:$PC_{70}BM$ (dielectric constants of 3.23 ± 0.13 and 4.75 ± 0.1 for the neat materials, respectively) gives an expected dielectric constant between 4.0 and 4.12. The value is slightly below this estimation but within error of the pristine materials. My hypothesis is that the authors may have measured the reported dielectric constant without completely depleting the active layer. By repeating impedance measurements under these conditions, I was able to reproduce a capacitance that would fit their reported value (**Figure 7**). Impedance spectroscopy was carried out at the frequencies shown, and with bias ranging from -1.5 V to 1.0 V and light intensities of 1.0, 0.5, 0.1 and 0.01 sun. The resultant capacitances were converted to "dielectric constant" and plotted semi-transparent to observe point overlap. Here, I must stress once more that under these conditions the measured capacitance is not the relevant capacitance to describe the dielectric constant of the blend. The high capacitance may be explained by the presence of photo-generated charge carriers or by the diffused charges from insufficient reverse voltages, neither of which contribute to the true geometric capacitance of a blend. This is expected as I have already shown that blend films have a large increase in capacitance under a given illumination condition than compared with the pristine materials alone.

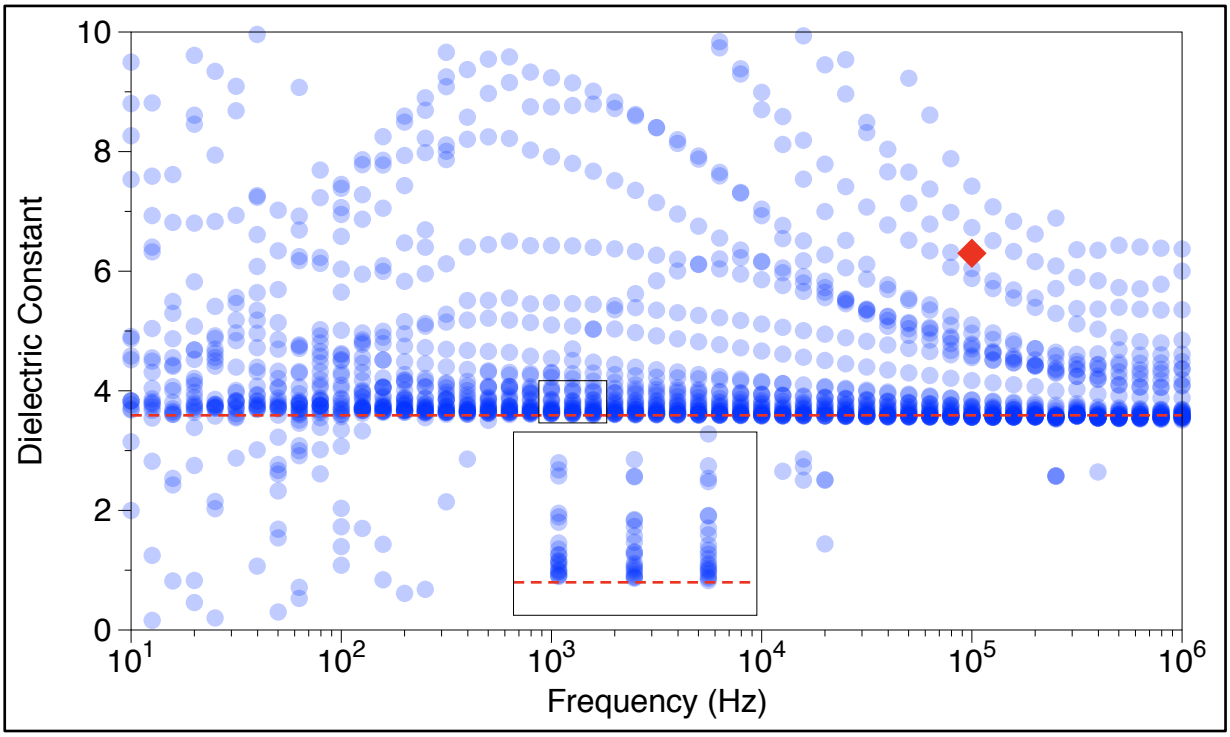

Figure 7. An illustration of the possible dielectric constants measurable from a single PCDTBT:PCBM solar cell as described in the literature. A saturation of dielectric constants represents the saturation to the geometric capacitance as active layer is appropriately depleted (inset). Red point depicts previously published value for the system. Points below C_g are present due to artifacts caused by high E fields.

I conclude this results from the presence of the donor:acceptor interface creating a population of free charge carriers not afforded in the pristine film. This implies that the requirement for active layer depletion may change in the blend film, and without careful consideration a dielectric constant convoluted with the capacitance of charge carriers may be measured. A complete understanding of this specific variance would require publishing of the voltage, frequency and leakage properties of the devices studied. Furthermore, the authors used LiF/Al contacts in their measurement, which I have shown can distort the measured

dielectric constant. This example illustrates the care that must be taken when using impedance spectroscopy to extract the relative permittivity values of semiconductors and BHJ blends, in particular.

D. Conclusion

In summary, this chapter is a comprehensive overview of the methodology and potential complications for determining the dielectric constant in organic semiconductors especially in the blend, using impedance spectroscopy. Impedance spectroscopy can provide information about a range of processes in the organic semiconductor, and care must be taken to ensure that the conclusions from the measurements represent the questions at hand. In general, to extract the dielectric constant relevant for OPV, impedance spectroscopy must be done on good quality diodes with high shunt resistance. In addition, if the sample can generate charge carriers from photoexcitation (an OPV device, for example), the measurements should be done in the dark. To deplete the sample from generated free charge carriers generated or charge carriers diffused from the contacts, it may be necessary to apply a reverse DC bias. Finally, if the above conditions have been met, the capacitance of sample should not be dependent on the frequency. However, if the capacitance does have some frequency-dependence, the best results would be obtained from the capacitance the high frequency regime (10^6 Hz). While these are general guidelines, there may be exceptions, and the impedance spectra each material system must be scrutinized to gain an understanding of the experimental conditions that may give erroneous results, and those that are relevant.

From this study of the dielectric constant of organic semiconductors, my goal was to make clear some misconceptions about collecting and interpreting this value. Importantly, blends of donor:acceptor materials have a dielectric constant that can be predicted based on the weight

ratio of the neat materials and their respective dielectric constants. I've found a model common to polymer mixtures[187] to predict the dielectric constants of the blends, within a small percent error from the dielectric constant measured using impedance spectroscopy. In addition, this study implies that processing conditions and morphology do not influence the dielectric constant of the blend. I have shown that due to the complex nature of impedance spectroscopy it is possible to misinterpret the results and report miscellaneous values for the dielectric constant, both for the neat materials and blend films. Overall, the dielectric constant of a blend film can be predicted solely based on the dielectric constant values of its neat components, scaled for their weight ratios. My hope that this study will shed light on the range of values reported in the literature, and that it may act as a future guideline for researchers in the field.

D. Experimental Section

Unless otherwise specified in the body of text, all devices were fabricated and characterized via the following procedure. Care was taken to assure these experimental conditions remained consistent.

Device Fabrication: (Materials purchased and where vs. synthesized here) ITO coated glass substrates were thoroughly cleaned by scrubbing with soapy water, then sonicating in soapy water, ultra-pure water, acetone and IPA, sequentially. Immediately before fabrication the devices were O_2 plasma cleaned (Plasmaflo DDC-FMG). Following the cleaning procedure, a 30 nm layer of PEDOT:PSS was spin cast onto the substrate at 2500 rpm for 40 seconds (PWMSO Series Photo Resist Spinner) then dried at 140 °C for 20 minutes. The active layer of study was then spin cast atop the PEDOT:PSS in an inert N_2 environment. All

active layer thermal annealing was performed with the substrates directly on the hotplate, glass-side down. Finally, the metal cathode was thermally evaporated on top of the active layer (Angstrom Engineering Series EQ Thermal Evaporator).

All solutions were prepared previously and stirred on a hot plate overnight before spin casting in the nitrogen atmosphere.

Device Characterization: The solar cell characteristics of these devices were measured in a nitrogen-purged glovebox. The device J-V characteristics were measured (Keithley 2602) in the dark and under simulated 1 sun (100 mW cm^{-2} AM 1.5G) irradiation to assess the leakage and performance parameters of each device.

Impedance analysis: IS was performed on these devices (Solartron SI 1260) and analyzed with Zplot measurement software. These measurements were taken from zero to increasing negative bias across several orders of magnitude of frequencies (10^{1}-10^{6} Hz), additional details are thouroughly discussed in the body of this work. Thickness and device area measurements were determined using a profilometer (Ambios XP-100).

Synthesis of TEG-DPP-BFu

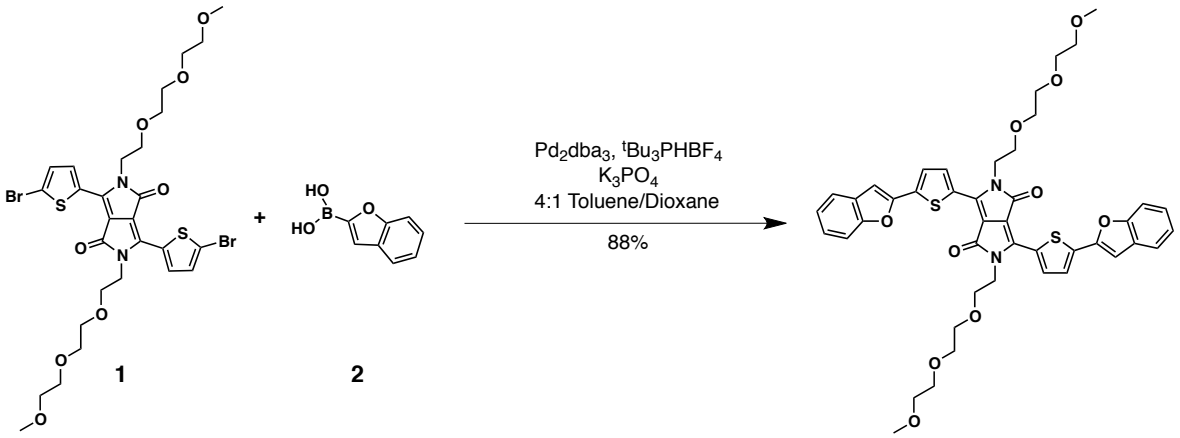

Scheme 2. Synthetic route for the preparation of TEG-DPP-BFu.

Compound **1** was synthesized according to previously reported methods. Compound **2** was purchased from TCI and used without further purification.

3,6-bis(5-(benzofuran-2-yl)thiophen-2-yl)-2,5-bis(2-(2-(2-methoxyethoxy)ethoxy)ethyl)pyrrolo[3,4-c]pyrrole-1,4-dione (TEG-DPP-BFu): Under N_2 atmosphere, 3,6-bis-(5-bromo-thiophen-2-yl)-2,5-bis(2-(2-(2-methoxyethoxy)ethoxy)ethyl)pyrrolo[3,4-c]pyrrole-1,4-dione (1 eq, 0.134 g, 0.18 mmol), benzofuran-2-boronic acid (3.25 eq, 0.084 g, 0.52 mmol), tris(dibenzylideneacetone)dipalladium(0) (3 mol%, 6 mg, .0066 mmol) and tri-tert-butylphosphonium tetrafluoroborate (15 mol%, 8 mg, 0.028 mmol) was mixed with 2.3 mL of anhydrous toluene in a microwave vial and sealed with a Teflon cap. 0.7 mL of degassed dioxane and 1.8 mL (20 eq) of degassed 2.0 M potassium phosphate were transferred to the vial by syringe. The reaction mixture was stirred and heated to 90 ºC under N_2 for 48 hours. The reaction mixture was allowed to cool down to room temperature, after which it was poured into 30 mL of methanol and then stirred for 30 minutes. The precipitated solid was then collected by vacuum filtration and washed with several portions of distilled water,

methanol, isopropanol, and hexanes. The solid was dried *in vacuo* to obtain a pure product. 3,6-bis(5-(benzofuran-2-yl)thiophen-2-yl)- 2,5-bis(2-(2-(2-methoxyethoxy)ethoxy)ethyl)pyrrolo[3,4-c]pyrrole-1,4-dione is formed as a shiny, dark-green powder (yield: 88 %) with mp 233 ºC. ^{1}H NMR (500 MHz, CD_2Cl_2, ppm) = 8.89 (d, *J* = 4.2 Hz, 2H), 7.63 (dd, *J* = 7.9, 5.8 Hz, 4H), 7.54 (d, *J* = 8.2 Hz, 2H), 7.40 – 7.32 (m, 2H), 7.27 (t, *J* = 7.4 Hz, 2H), 7.13 (s, 2H), 4.33 (t, *J* = 6.2 Hz, 4H), 3.82 (t, *J* = 6.1 Hz, 4H), 3.64 (dd, *J* = 5.9, 3.5 Hz, 4H), 3.56 (dd, *J* = 5.8, 3.5 Hz, 4H), 3.52 (dd, *J* = 5.8, 3.6 Hz, 4H), 3.42 (dd, *J* = 5.7, 3.6 Hz, 4H), 3.26 (s, 6H). ^{13}C NMR (CD_2Cl_2): 161.6, 155.4, 150.5, 139.8, 138.3, 136.3, 130.1, 129.3, 125.8, 125.8, 123.9, 121.6, 111.6, 109.1, 104.1, 72.3, 71.3, 70.9, 69.5, 59.0, 42.5. MS (FD-TOF) m/z: [M^+] calculated for $C_{44}H_{44}N_2O_{10}S_2$: 824.24, found 824.18.

III. Charge Recombination Dynamics in Organic Photovoltaic Systems with Enhanced Dielectric Constant

A. Introduction

An important aspect of organic materials that enables organic photovoltaics (OPV) to continually improve is the tunability of their morphological and electrical properties.[16,35] This can be particularly advantageous in OPV cells whose high recombination rates are significant due to the low dielectric constants of organic materials,[189] which leads to the formation of bound electron-hole pairs, termed excitons, that require a two-material donor/acceptor system for charge separation to occur. [132,133] Consequently, the development of the optimal bulk heterojunction (BHJ) solar cell still demands extensive research and device optimization. Accordingly, two longstanding questions remain in my effort to understand the factors which limit OPV device efficiency: can effective chemical modification strategies be developed for increasing the dielectric constants of OPV materials; and, will that, in turn, result in decreased charge recombination in the resulting device.[146,175,176,190] If past is prologue, material modifications that have increased the dielectric constant of the OPV blend bring undesirable morphological[173,175] and energetic changes[174,186,190] along with this positive result. Thus, the final goal of my work is to develop a strategy and materials that increases the dielectric constant without simultaneously vitiating other beneficial attributes of the OPV system's performance.

Modifying the dielectric constant through the addition of polar groups[144] on the material core has been reported,[190] however, to be accompanied by impact on the material's energetic levels, which may produce a larger undesirable impact on their properties than the

benefits bestowed by the increased dielectric constant. For this reason, the incorporation of polar groups on side chains away from the molecular orbitals tends to be the more common approach for changing dielectric constant.[171,174,175] Several attempts, including my own, have been made on increasing the dielectric constant through chemical modifications. In chapter 2, I discussed the synthesized triethylene glycol (TEG) modified benzofuran-based donor which increased the dielectric constant from a value of 3.00 to 3.84.[189] However, some of the modified materials properties, such as its morphology and phase separation behavior were adversely affected, so that a functional device could not be processed. Others have succeeded in increasing dielectric constants through the addition of a TEG chain, as shown by Torabi et. al.[130] in which solubility and mobility were maintained. But those authors did not provide device performance data. Cho et. al.[146] have seen an improved dielectric constant of ~1 through the addition of a cyano moiety which resulted in improved device performance; however, neither device achieved more than 1.5% power conversion efficiency. Zhang et. al.[176] successfully modified $PC_{60}BM$ with various length cyano-capped chains, all of which increased the material dielectric constant by ~1 without changing the relevant electron orbital energetic levels. While this resulted in improved performance from one tested system, it was observed that the device performance was dielectric constant independent and was ascribed to a morphology change resulting from side chain length changes.

While work has been carried out to show that the dielectric constant can be increased considerably, to date, no material has been found that increases the dielectric constant without causing alterations of other significant device properties, making system comparisons difficult. This study is an opportunity to report a departure from this commonly-encountered undesirable combination. Using a TEG-modified, fullerene-based electron acceptor I found a

material that consistently behaves as its non-modified counterpart in all other pertinent respects thereby allowing the exploration of how the increased dielectric constant alone changes the system's recombination dynamics.

B. Materials for a Model System

A $PC_{60}BM$ derivative with triethylene glycol side chains (TEG-PCBM) was synthesized *via* trans-esterification method from $PC_{60}BM$ and triethylene glycol monomethyl ether as per the modified literature procedure in 74% yield.[191,192] It is this electron accepting material and its $PC_{60}BM$ counterpart which are utilized with two electron donating materials as shown in **Scheme 1.** The traditional donor poly(3-hexylthiophene-2,5-diyl) (P3HT) and a

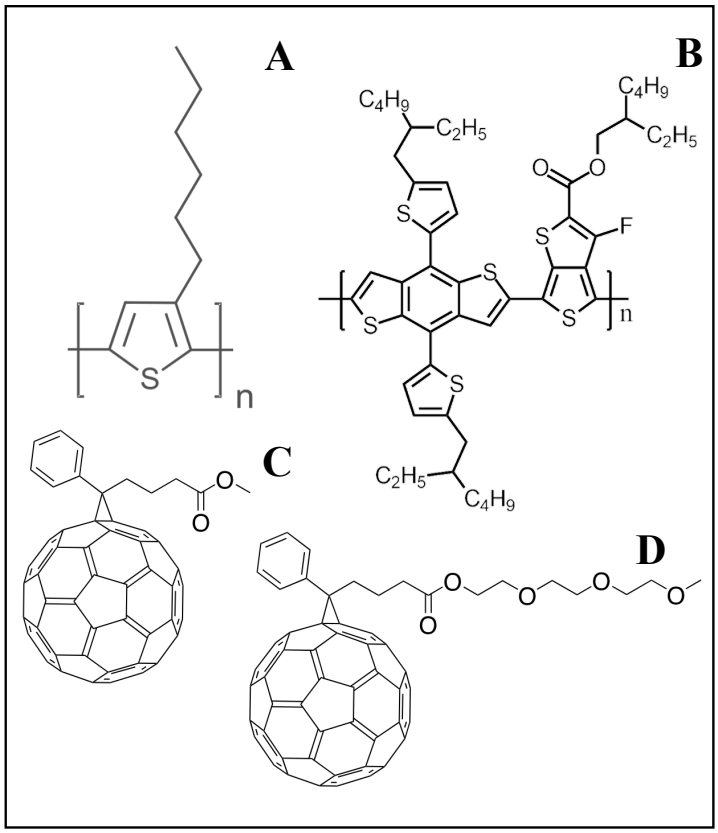

Scheme 1. Chemical structures for experimental materials; the donors P3HT (A) and PTB7-Th (B); and the acceptors $PC_{60}BM$ (C) and TEG-$PC_{60}BM$ (D)

well-characterized high-performing donor, poly([2,6′-4,8-di(5-ethylhexylthienyl)benzo[1,2-b;3,3-b]dithiophene]3-fluoro-2[(2-ethylhexyl)carbonylthieno[3,4-b]thiophenediyl}) (PTB7-Th), were chosen, retaining each donor's optimum blend ratio and processing conditions when blended with each acceptor.

C. Dielectric Constant and Permanent Dipoles

Understanding how molecular polarity affects charge-carrier recombination rates requires examination of both permanent and induced dipoles. Although permanent dipoles do not contribute significantly to the dielectric constant in a solid matrix, the reorientation of permanent dipoles may contribute. A large change in the permanent molecular dipole could also have a large effect on morphology and molecular packing.[58,193] Measuring the dielectric constant provides a measure of the magnitude to the transient dipoles, that would tend to reorient in response to an applied electric field.

1. Dielectric Constant

The dielectric constant was measured using the methodology described in chapter 2. Impedance analysis was employed by applying an AC electric field with varying frequencies to the device to determine the resistance, i.e. the real part of the impedance, *Z'*, and the reactance, the imaginary part of the impedance *Z''*.[129] Correcting for both series resistance R_s which is measured for each device (~10 Ω) and the inductance L of the system which was measured to be ~ 6 μH, the capacitance of the system can be calculated from the measured the impedance spectra using **Equation 1**.[142]

$$C_{cor} = -\frac{1}{\omega}\left[\frac{Z'' - \omega L}{(Z' - R_S)^2 + (Z'' - \omega L)^2}\right] \quad (1)$$

Here ω is the angular frequency ($\omega = 2\pi f$), and f is the frequency. The frequency-independent geometric capacitance is determined by carrying out impedance measurements in the dark, at large reverse bias (-1.5 V), and in diodes which demonstrate high shunt resistances.[158,189] Corrected capacitance spectra as a function of frequency and applied bias for several light intensities are reported in appendix 3. I observed the required frequency independent impedance values throughout the testing range of 10^1-10^6 Hz and therefore chose to carry out measurements of C_g at 10^6 Hz, which represents a timescale relevant to free charge carrier lifetime,[10,138] as a function of other pertinent variables. This value, along with thickness d, area A, and the permittivity of free space ε_0 were used to determine the dielectric constant using **Equation 2**.[143,145] The values are listed for the systems in **Table 1,** and

$$\varepsilon = \frac{C_g d}{\varepsilon_0 A} \quad (2)$$

as expected, showed an increase in the dielectric constant of ~1. I have previously shown,[189] as have others,[130,175] that the TEG side chain raises the dielectric constant of OPV materials in this manner. I would expect the increase of the dielectric constant at 1 MHz to result in an increased shielding of charges on a timescale relevant to bimolecular recombination,[10,16] decreasing its magnitude.

2. Permanent Dipoles

Density functional theory (DFT) calculations with the B3LYP functional and 6-31G(d,p) basis set, were employed to estimate the magnitude and direction of changes to the permanent dipole upon the addition of the TEG side chain. The results, shown in **Figure A3.3** in appendix 3, show a small directional shift and only a 1.5% change in magnitude. So small a change in dipole is expected to leave the molecular packing and arrangement unchanged,[193,194] while the polarizability[130,144] increases.

D. Device Performance

J-V measurements were carried out under simulated 1 sun (100 mW cm^{-2} AM 1.5G) conditions. The power conversion efficiency (PCE), voltage at open-circuit conditions (V_{OC}), current at short-circuit conditions (J_{SC}), and fill factor (*FF*) are reported in **Table 1**. *J-V* graphs of each system for varying light intensities are provided in appendix 3, **Figure A3.4**. Similar performance was observed when comparing each donor material with the modified and unmodified acceptors. It should be noted that the *FF*, which is determined in part by recombination behavior,[16,131,139] is maintained for each acceptor, even slightly improved from 49% to 51% and 49.5% to 54% in the P3HT and PTB7-Th systems respectively. The two donors trade off J_{sc} improvement for V_{oc} improvement with no major differences for the various acceptors. The P3HT system was able to gain current from a J_{sc} of -7.8 mA/cm^2 to -9.54 mA/cm^2 while losing operating potential as the V_{oc} dropped from 0.62V to 0.56V with the addition of the TEG chain. The PTB7-Th lost current as the J_{sc} dropped from -19.3 mA/cm^2 to -15.8 mA/cm^2, however, the V_{oc} increased from 0.83 V to 0.85 V when blended with the modified acceptor. In total, the performance is quite similar, far closer than what was reported for other TEG-modified systems.[130,175,189] The recombination current was also calculated and found to be comparable in each system. The recombination current graphs for each system are listed in appendix 3.

Material (D/A)	ε	J_{sc} (mA/cm^2)	V_{oc} (V)	FF (%)	PCE (%)
P3HT: $PC_{60}BM$	2.99	-7.8	0.62	49.0	2.4
P3HT: TEG-PCBM	3.95	-9.54	0.56	51.0	2.7
PTB7-Th: $PC_{60}BM$	2.68	-19.3	0.83	49.5	7.9
PTB7-Th: TEG-PCBM	3.58	-15.8	0.85	54.3	7.3

Table 1. Dielectric constant and performance data for several blend systems

E. Dissociation Efficiency

According to the theory of monomolecular recombination developed by Onsager,[195] and later improved by Braun[196] to include the finite exciton lifetime, the thermally and electric field dependent free charge generation rate, *G(T,E)*, can be expressed as a product of the maximum generation rate of the system and the probability of exciton separation, *P(T,E)*, as follows:[133]

$$G(T,E) = G_{max}P(T,E) \quad (3)$$

Braun postulated the more complete model of exciton separation given by **Equation 4**,[131,133]

$$P(T,E) = \frac{k_D(E)}{k_D(E)+k_F} \quad (4)$$

which includes the rate of exciton decay to the ground state, k_F, along with the rate of exciton dissociation k_D to free charge carriers. The rate of exciton dissociation may be expressed by **Equation 5**[133]

$$k_D = k_R \frac{3}{4\pi a^3} e^{-E_b/kT}\left[1 + b + \frac{b^2}{3} + \frac{b^3}{18} + \frac{b^4}{180} + \cdots\right] \quad (5)$$

which depends on the rate of free charges re-entering the bound exciton state, k_R, initial charge separation distance, a, and exciton binding energy, E_b. Additionally, the term $b = e^3E/8\pi\varepsilon k^2T^2$ expresses the inverse relationship between the dielectric constant ε and dissociation rate, which implies an improved dissociation rate for increased values of the dielectric constant.

The field dependence of charge separation can usually be observed under small electric fields where the field V_{OC}-V < 0.1 V.[131,133] In this region charge diffusion contributes largely to the photocurrent (J_{ph}) as demonstrated by the measured field dependence in this range. At larger applied fields where V_{OC}-V > 0.1 V the photocurrent saturates as drift behavior

dominates, so that charge separation becomes field independent. For this study I calculate the photocurrent using $J_{ph} = J_L - J_D$ in which the light current (J_L) and dark current (J_D) are measured at each light intensity. When blended with $PC_{60}BM$, the P3HT system shows the expected field dependence at low fields and saturates above V_{OC}-V = 0.1 V as shown in **Figure 1A**. The TEG counterpart appears to have reduced dissociation efficiency at all applied fields contrary to expectation. **Equation 5** suggests an improved dissociation efficiency with increased dielectric constant. As carrier density is decreased by reducing light intensity, this difference is accentuated (**Figure 1B, C**). A finite number of traps may cause this behavior as an increased carrier density would dilute the overall reduction of the separation efficiency. In **Figure 2A, B** it may be observed that the dissociation efficiency for the PTB7-Th donor systems behave similarly. It is only at low carrier density of 2.0 optical density (OD) (produced by illuminating with 0.01 sun) that one may observe the TEG modified acceptors

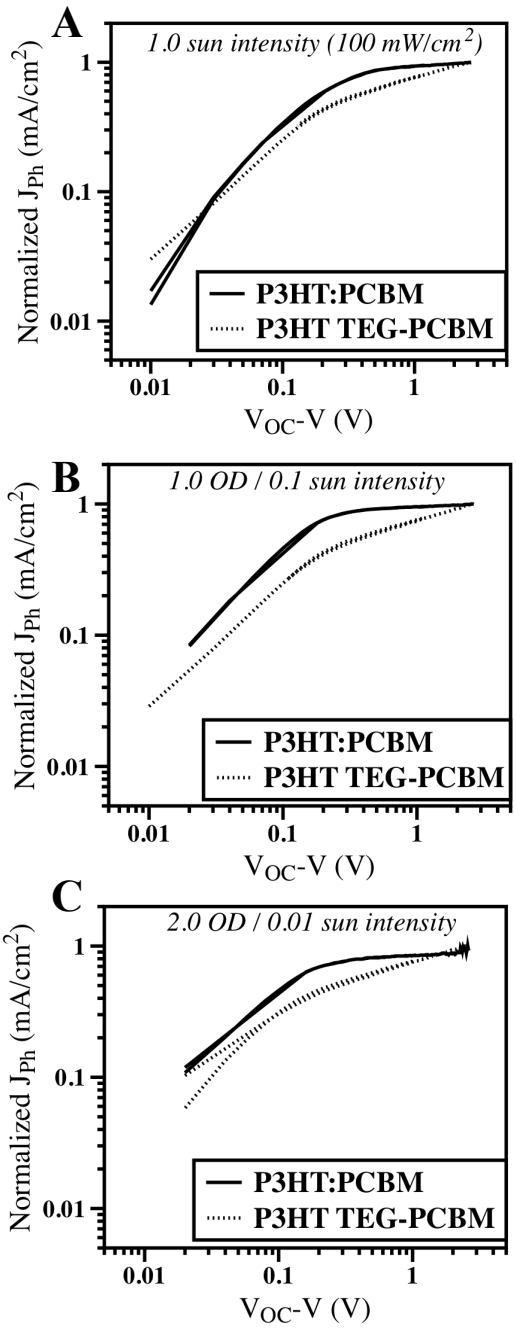

Figure 1. Normalized photocurrent as a function of applied internal field (V_{oc}-V) for P3HT systems

dissociation efficiency reduced to the level observed for the P3HT based systems. The PTB7-Th blend exhibits a higher charge density system as seen in the *J-V* curves, further

evidence that this behavior is observed more clearly at lower carrier densities. Nevertheless, the increased dielectric constant of the TEG modified $PC_{60}BM$ does not seem to improve dissociation efficiency, in fact, it worsens it.

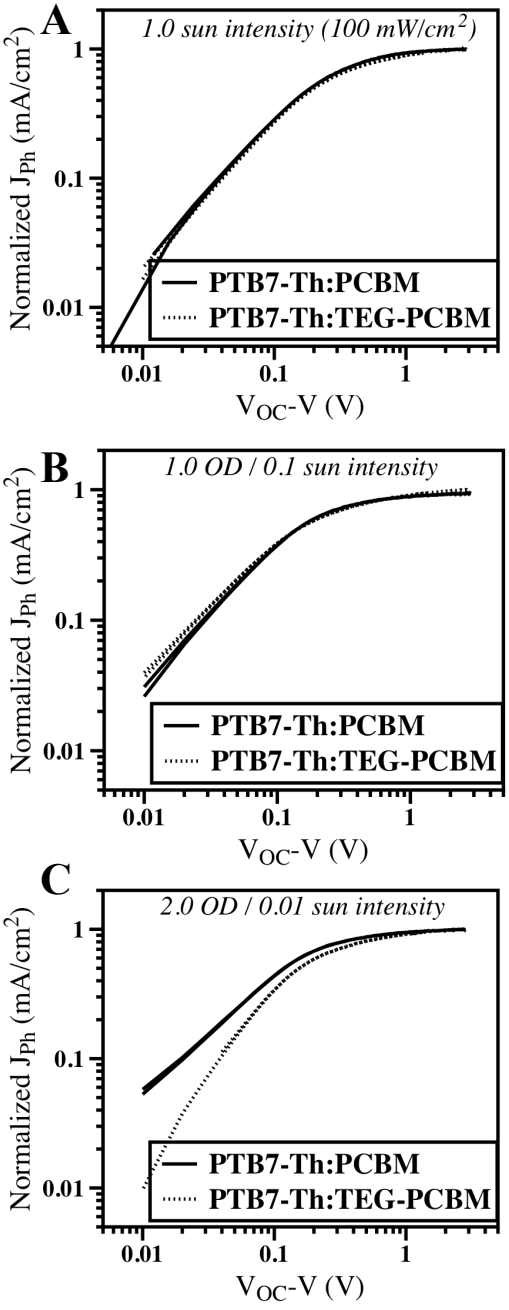

Figure 2. Normalized photocurrent as a function of applied internal field (V_{oc}-V) for PTB7-Th systems

F. Recombination Dynamics

Much can be understood about the nature of a system's recombination by examining how the *JV* figures-of-merit respond to varying light intensity.[142] Because mono- and bimolecular recombination respond differently to light intensity,[197] this provides a simple methodology for understanding how structure changes affect recombination behavior.

1. Log[Jsc] vs. Log[intensity]

The light intensity dependence of the J_{sc} shows the importance of recombination under short circuit conditions when the internal field is high. Deviations from a linear correlation indicate significant contributions from recombination at short circuit conditions.*[131,132,142]* **Figure 3A, B** indicate that all four systems fail to achieve a slope of unity, however, none deviate significantly, indicating only a small impact from the effect recombination. The PTB7-Th systems show more similar behavior although they deviate more greatly from unity. This possibly indicates closer morphological and charge transport properties, although deviating from ideality.

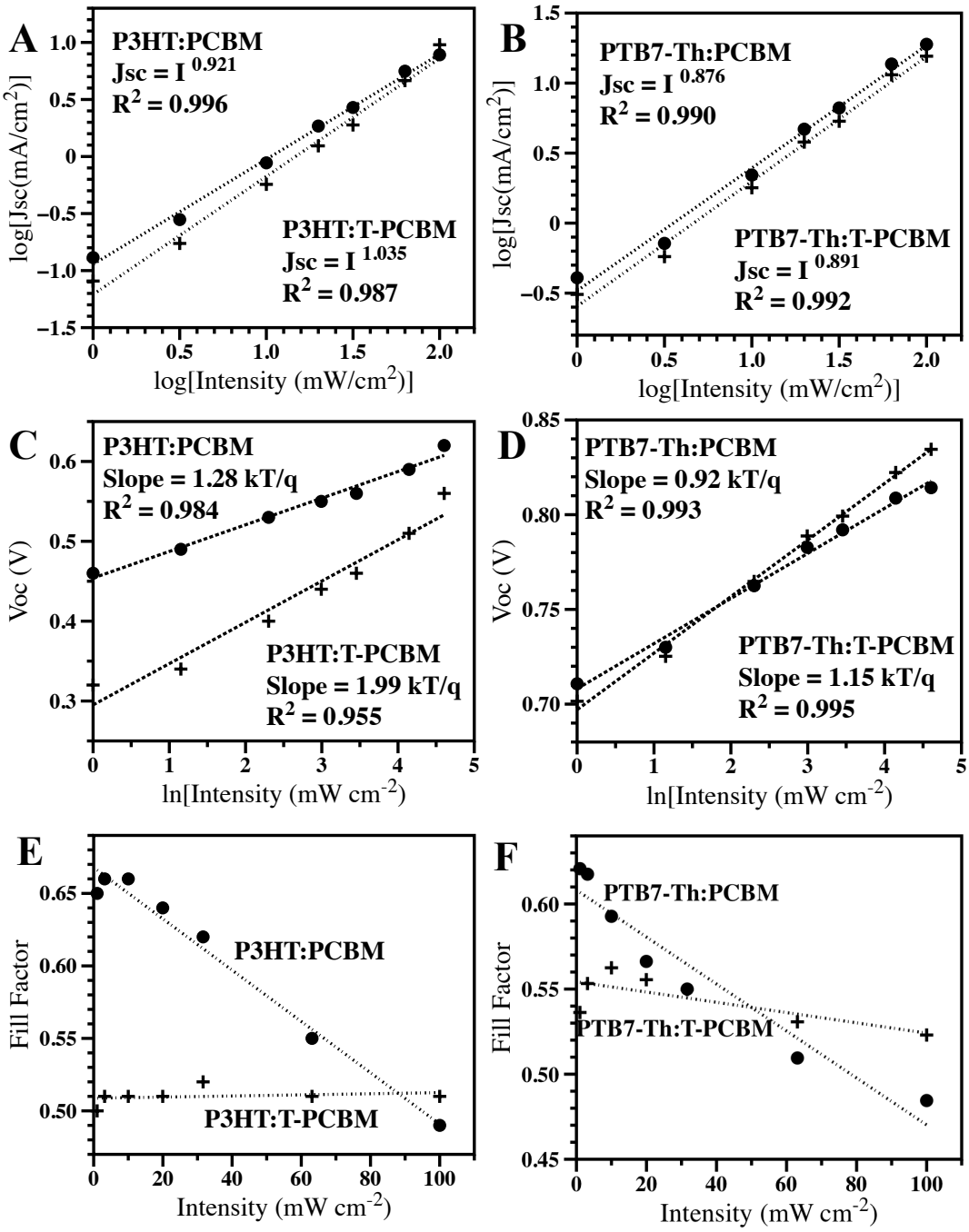

Figure 3. Recombination data for P3HT and PCBM (circles) and TEG- PCBM (crosses); the short circuit current vs. the light intensity dependence for P3HT (A) and PTB7-Th (B) systems; the Voc vs. the light intensity dependence for P3HT (C) and PTB7-Th (D) systems; and the FF vs. light intensity dependence for P3HT (E) and PTB7-Th (F) systems

2. Voc vs. ln[intensity]

Under open-circuit conditions no charges are swept out of the device, therefore, all charges recombine.[197] It is for this reason examination of the light intensity dependence on V_{oc} can provide information on recombination dynamics. The open circuit recombination rate, *R,* is equal to the generation rate *G* which is equal to the sum of two terms as shown in **Equation 6**,[132,197]

$$R(V_{OC}) = G = \frac{n_{OC}}{\tau_r} + \gamma n_{OC}^2 \quad (6)$$

where n_{oc} is the charge (either electron or hole) density at open circuit, τ_r the monomolecular recombination lifetime, and γ the bimolecular recombination coefficient. In the Langevin model[16] $\gamma = e\mu/\varepsilon_0\varepsilon_r$, showing an inverse relationship of the dielectric constant on bimolecular recombination, although most systems require a prefactor when describing the observed behavior with the Langevin coefficient, $\gamma = \xi\gamma_L$.[140,151,198]

The voltage at open-circuit can be calculated using the two terms in **Equation 7**.[132] At T = 0 K the V_{oc} is comprised only of the first term, which describes the V_{oc} as the energy gap between the acceptor's lowest unoccupied molecular orbital (LUMO) and the donor's highest occupied molecular orbital (HOMO) with a reduction Δ, which is attributed to molecular disorder originating from solution-cast films phase-separated ordering.[199] This Δ value is often measured to lie in the range 0.2 – 0.3 eV and is regularly given an estimated constant value of 0.3 eV.[133]

$$V_{OC} = \frac{1}{e}\left(E_{LUMO}^{Fullerene} - E_{HOMO}^{Polymer} - \Delta\right) - \frac{kT}{e} ln\left(\frac{n_e n_h}{N_C^2}\right) \quad (7)$$

The second term describes the temperature dependent filling of available conductive states, where n_e and n_h are electron and hole density, respectively, and N_c is the available

conductive states in the donor and acceptor, here assumed to be equal. The density of thermalized carriers results from the kinetic equilibrium between photogeneration and recombination. Altering the recombination behavior will, therefore, result in a variation in the carrier density dependence on V_{oc}. In systems in which bimolecular recombination is dominant, one can assume $\gamma > 1/(n_{OC}\tau_r)$ and $n_e n_h = (n_{OC})^2 = G/\gamma$. Substituting these conditions into **Equation 7** produces the following simplified equation that relates the change in V_{oc} to the incident light intensity I: $\delta V_{OC} = (k_B T/e)\, ln(I) + constant$. In systems in which monomolecular recombination is dominant, both n_e and n_h are intensity dependent at open circuit conditions and therefore the slope of the equation of V_{oc} as a function of ln(I) will be $2(k_BT/e)$. In fact, **Figure 3C** shows that for the P3HT system the above-mentioned slope goes from a slope value of 1.28 k_BT/e in the $PC_{60}BM$ device to a value of 1.99 k_BT/e for the TEG modified system. This clearly indicates that the presence of the TEG chain shifted the dominant recombination process from bimolecular to monomolecular at open circuit voltage. **Figure 3D** shows a similar behavior for the PTB7-Th systems, where there is an increase in the slope with the TEG modified acceptor, however this change is smaller, with its value changing from 0.92 k_BT/e to 1.15 k_BT/e. Again, the PTB7-Th donor appears to have a more consistent recombination behavior with the modified acceptor than the P3HT, but both show signs of increased deep trap-based Shockley-Read-Hall (SRH) monomolecular recombination.

3. FF vs. Intensity

The *FF* is a metric that convolutes many aspects of the solar cell that relate to the photogenerated excitons becoming extracted charges.[139,200] Properties such as mobility, material domain size, donor/acceptor interface and contact/device interface properties can

influence the *FF*. In fact, it may be considered to be a measure of the degree of recombination in the device.[201] Devices which experience bimolecular dominant recombination should have *FF* that show light intensity dependence, because a decrease in the number of charge carriers result in decreased recombination and an increased *FF*.[142] In contrast, systems in which recombination is primarily monomolecular are light intensity independent and should show a constant *FF* with changing carrier density, as observed in **Figure 3E** which shows that the *FF* of P3HT shifts from light intensity dependent to almost completely intensity-independent behavior when changing the acceptor from $PC_{60}BM$ to TEG-$PC_{60}BM$. This shows a move from bimolecular dominated recombination to monomolecular recombination. Because the values of *FF* measured with 1.0 sun illumination are almost equal, it seems unlikely that the bimolecular recombination was simply reduced by increasing the dielectric constant; it is more likely that SRH dominant monomolecular recombination was increased.[141] Additionally, the observed behavior is consistent with the data shown in **Figure 3F,** which shows a more intensity-independent behavior from the TEG modified acceptor when blended with PTB7-Th, but less than for the P3HT systems. Again, PTB7-Th shows more consistent recombination behavior with both acceptors however a clear shift to more monomolecular dominant recombination behavior.

G. Conclusion

In summary, this study examined a functional fullerene-based electron accepting material with improved dielectric constant by the addition of a triethylene glycol side chain with little consequence to the permanent dipole. I found that when blended with the electron donors, P3HT and PTB7-Th, both materials responded comparably with the modified acceptor and

the $PC_{60}BM$ control. It's also observed that dissociation efficiency worsened with the addition of the TEG chain, an effect which is amplified by the decreased carrier density. One proposal is that finite traps may explain this behavior; at higher carrier densities the dissociation behavior becomes comparable in both systems. Recombination does not appear to strongly affect the current at short circuit conditions but does have a large effect at open circuit voltage. With P3HT the recombination at V_{OC} changes from primarily bimolecular dominant recombination to monomolecular dominant, indicating a shift to Shockley-Read-Hall trap-based recombination. PTB7-Th behaves similarly but to a less pronounced extent. The shift from light dependent to light independent fill factors in both donor systems further indicates a move to monomolecular recombination, however the fill factor value remains low suggesting that the overall recombination is not reduced.

Reducing recombination is paramount to the goal of bringing organic photovoltaics to market. The low dielectric constant of these materials has long been known to be at the core of many of the issues plaguing the photon to extracted electron/hole process. This material found a way to include a polarizing dipole in the system without producing major changes to device behavior which allowed us to examine recombination dynamics in a device with an increased dielectric constant. However, it appears that the additional TEG-chain introduced SRH traps into the system, and while the dielectric constant did indeed increase, this did not reduce bimolecular recombination or improve dissociation efficiency. I conclude that small dielectric constant increases do not significantly reduce the magnitude of trapping sites or other pertinent processes that might lead to the improved performance of organic photovoltaics.

H. Experimental Section

TEG-PCBM Synthesis: As per the modified reported procedure[191], 6,6]-phenyl-C_{60}-butyric acid methyl ester (1.0 g, 1.1 mmol) was dissolved in 1,2-dichlorobenzene (50 mL) in a multi-neck round bottom flask. Dibutyltin(IV) oxide (0.06 g, 0.22 mmol), triethylene glycol monomethyl ether (18.0 g, 109.7 mmol) was added to the solution and the reaction mixture was stirred at 170 ^{o}C for 48 h. The solvent was removed under reduced pressure and the crude product was purified through column chromatography (silica, 20:80 v/v EtOAc/toluene) to afford TEG-PCBM as a brown solid. Yield: 0.84 g, 74%. ^{1}H and ^{13}C NMR data is in agreement with that reported in the literature[191,192,202]. HRMS (MALDI) calculated for $C_{78}H_{26}O_5$ (M^+), 1042.1780; found 1042.1785. Anal Calcd. For $C_{78}H_{26}O_5$: C, 89.82; H, 2.51. Found: C, 89.49; H, 2.84.

Device Fabrication: ITO coated glass substrates were thoroughly cleaned by scrubbing with soapy water, then sonicating in soapy water, ultra-pure water, acetone and IPA, sequentially. Immediately before fabrication the devices were O_2 plasma cleaned (Plasmaflo DDC-FMG). Following the cleaning procedure, a 20 nm layer of ZnO was prepared by mixing one-part diethyl zinc solution (15% w/w in toluene, Sigma-Aldrich) with two parts tetrahydrofuran (Sigma-Aldrich), mixing and filtering to 0.45 μm. The solution was then spin-cast at 4000 RPM for 1 minute (PWMSO Series Photo Resist Spinner) then dried at 110 °C for 15 minutes. The active layer of study was then spin cast atop the ZnO in an inert N_2 environment. P3HT:PCBM/TEG-PCBM active layer solution is prepared at a 1.2:1 ratio in chlorobenzene (Sigma-Aldrich) to a solids concentration 27 mg/mL. Solution is then spin-cast at 1750 RPM for one minute and annealed for 120°C for 10 minutes.[183] All active layer thermal annealing is performed with the substrates directly on the hotplate, glass-side down.

PTB7-Th:PCBM/TEG-PCBM active layer solution is prepared at a 1:1.5 ratio in chlorobenzene with 2% v/v diphenyl ether (Sigma-Aldrich) to a solids concentration 30 mg/mL.[203] Solution was then spin-cast at 1500 RPM for one minute and never annealed. Finally, 7 nm of MoO_x was thermally evaporated on top of the active layer followed by 100 nm of Ag. (Angstrom Engineering Series EQ Thermal Evaporator).

All solutions were prepared previously and stirred on a hot plate overnight before spin casting in the nitrogen atmosphere.

Device Characterization: The solar cell characteristics of these devices were measured in a nitrogen-purged glovebox. The device *J-V* characteristics were measured (Keithley 2602) in the dark and under simulated 1 sun (100 mW cm^{-2} AM 1.5G) irradiation to assess the leakage and performance parameters of each device. To simulate other illumination intensities, a neutral density optical filter (Newport 5215) was placed between the lamp and sample and calibrated using a NREL certified silicon diode.

Impedance analysis: IS was performed on these devices (Solartron SI 1260) and analyzed with Zplot measurement software. These measurements were taken with a perturbation of 20 mV, from zero to increasing negative bias across several orders of magnitude of frequencies (10^1-10^6 Hz), and with varying degrees of illumination. Thickness and device area measurements were determined using a profilometer (Ambios XP-100).

DFT Calculations: Dipole moments for PCBM and TEG-PCBM were determined by density functional theory calculations.[204] Values were obtained from the gas-phase optimized geometries using the B3LYP functional and 6-31G(d,p) basis set.

IV. Conclusion

A. Impedance Spectroscopy

This work relied heavily on use of impedance spectroscopy as the source methodology for determining the dielectric constant. As such, much of my experience has been in understanding the benefits and limitations of using this instrument. For determining the dielectric constant, it's a robust system contingent on several assumptions. The impedance analyzer applies a field to a device and perturbs that field from mHz to GHz range and measures the current response on the electrodes. Physically, this is precisely the process I wish to probe which reduces additional experimental variables to consider. This, however, is because the greatest recombination losses occur at the timescales relevant to a frequency near 1 MHz. If we wished to observe the dielectric response on a timescale closer to excitonic material response or geminate losses, we would need to measure capacitance at frequencies approaching visible light. Theoretically under these experimental parameters, this frequency blind spot should not change the measured dielectric constant. The geometrical capacitance measured should be devoid of all external polarizations and derive from the material only. At this frequency range, and assuming the absence of ions or molecular rearrangement, the polarization response should result from electronic and atomic polarizations only. The onset of atomic polarization may be expected at 10^{12} Hz to deconvolute from the electronic polarization with an onset of 10^{15} Hz. Because these polarizations are constant through the OPV relevant timescales, the geometric capacitance and resultant dielectric constant should additionally remain unchanged. Regardless of the high-frequency behavior, I chose to concern myself with material behavior demonstrating frequency independent capacitance at 1 MHz as relevant to non-geminate recombination.

Additionally, it should be noted about impedance spectroscopy that there exist certain considerations for device fabrication. Much can be said of the importance of device consistency during testing, a fact which doesn't lend well to the inconsistency of self-assembled thin films. Considering devices first which present clear and accurate results, an assumption must be made on consistent film thickness and density. This is challenging to prove and almost impossible to confirm on every device of hundreds. Thickness and area measurements must be accurate to the nm scale for thickness and μm scale for area, when determining the dielectric constant from impedance produced geometric capacitance. The error in these measurements has the largest effect on value error after impedance data has been collected, and it took years to optimize these measurement techniques to reduce error. When considering the device for testing using impedance analysis, several things must be considered before approving data for analysis. Firstly, large surface area electrodes are necessary in the sandwich configuration which make good wetted contact with the active layer. Due to the inconsistent nature of self-assembly, good collection statistics are necessary as device to device variation cannot be easily quantified. Finally, as current on the electrodes is ultimately being measured, any current inducing artifacts must be adequately understood and controlled. Artifacts like leakage current, photo current and injected current can all appear to be unexpected capacitance.

Ultimately, impedance spectroscopy is a robust methodology for measuring geometric capacitance of organic thin films over the necessary frequency range. It's an important note that such is a static measurement, a value relating to the response of the material only. Impedance spectroscopy may also be employed as a useful instrument in exploring the dynamic processes of charge accumulation and recombination dynamics. It's an important to

understand, this measurement is a convolution of photo-induced charge and capacitive-induced image charge and as such, appropriate deconvolution and modeling are necessary.

B. The Dielectric Constant of Neat Materials and Blends

In cataloging dielectric constant of organic photovoltaic materials over years, I was able to accumulate a broad knowledge of the range and outliers expected in these materials. The range of dielectric constant consistently exist within the narrow range of 2-5 for a simple reason, the material structure and behavior similarities. Elementally and structurally these materials are all very similar, sharing conjugated carbon backbones as a material core. Beyond that cyano and halogen insertion for electron density, there is little elemental diversity. Additionally, we expect formation of crystallites with order surrounded by heterojunction boundaries in no particular orientation. The resultant dielectric constant is mostly devoid of specific crystal effects as they don't share a common orientation direction, the capacitance generates from the atomic and electronic polarizations. So, the common elemental makeup yields very similar values when measured correctly. It's from this understanding which encouraged validation studies of organic materials with published dielectric constants beyond this range, all of which proved published in error.

Unfortunately, no specific monomers appear to raise the dielectric constant when searching for synthetic trends. Fullerene balls have high dielectric constant as they have a large delocalization of electron density with is evenly polarizable in this three-dimensional material. Further, it proves impossible to deconvolute any benefit from small increases in the dielectric constant between separate materials and any resultant behavior as many other variables must also change.

The unremarkable genesis of the dielectric constant provides an accessible hold for predicting blend values. Through several studies, the blend dielectric constant can be readily predicted by the weighted average of the neat materials value through the rule of mixtures. This stands to reason as this value should relate to the material devoid of any photo-induced, leaked or diffused charge. When the measurement is done appropriately, the dielectric constant of any OPV device should exist between the bounds of the values of the neat materials. This, as well, stands in conflict with some literature reports and required collaborative debate and consideration. The published theory is the excess polarization exists as response to intramolecular coupling between donor and acceptor. However, without generated charge in the CT state, there should exist no new polarizable bonds, and when the active layer is appropriately depleted, no such value is observed. It necessitates an appreciation that this value is a material value, not one which describes any dynamic external processes. As discussed before, impedance spectroscopy may be employed to observe charge dynamics however no such information should be described in the published dielectric constant value.

C. Altering the Dielectric Constant to Improve Device Performance

There have been several successful attempts in the literature to improve the dielectric constant of organic photovoltaic materials, of which we've discussed many in previous chapters. In this work, I was able to observe two such materials which both improved their dielectric constant through the modification of solubilizing alkyl chains with polarizable triethylene glycol chains. Generally speaking, it is possible to increase the dielectric constant of organic photovoltaic materials by the addition of polar heteroatomic moieties which are highly polarizable to the solubilizing chains such as the aforementioned TEG chains, cyano

groups and halogens. As mentioned in the introduction, modification to the core may change the dielectric constant but subsequent alteration to energy levels makes comparison impossible. Even more than that, almost any structural modification to these materials should impact film morphology as self-assembly is extremely sensitive to solvent and molecular packing changes. The result is, most material modifications never occur without changes to the fabricated device. More importantly, is the realization that improvements to this value rarely improve it beyond our expected range of 2-5. Years of material testing bares out the truth that the material dielectric constant of iso-oriented crystallites of the same elemental makeup and composition will yield very similar values. Furthermore, advancement in material design for the improved absorption range, mobility, self-assembly and morphology afford much improved recombination behavior with no measured improvement to the dielectric constant. In that, performance gains in the past decade have made considerable strides without the material dielectric constants improving slightly. While the dielectric constant may always be the cause of high recombination in organic photovoltaic materials, it appears to be an intrinsic property, confined in range by the composition and application. Fortunately, recombination improvements abound, meaning we can always expect improved performance in these systems, while accepting the permanence of the low dielectric constant and all of its consequences.

References

[1] A. Einstein, *Ann. Phys.* **1905**, *322*, 132.

[2] "The Nobel Prize in Physics 1921," can be found under https://www.nobelprize.org/prizes/physics/1921/summary/

[3] M. Planck, *Ann Phys.* **1901**, *4*.

[4] H. Hertz, *Ann. Phys.* **1887**, *267*, 983.

[5] J. C. M. F.R.S, *Lond. Edinb. Dublin Philos. Mag. J. Sci.* **1862**, *23*, 85.

[6] *The Theory of Electromagnetism*, Elsevier, **1964**.

[7] H. Shirakawa, E. J. Louis, A. G. MacDiarmid, C. K. Chiang, A. J. Heeger, *J. Chem. Soc. Chem. Commun.* **1977**, 578.

[8] "The Nobel Prize in Chemistry 2000," can be found under https://www.nobelprize.org/prizes/chemistry/2000/summary/

[9] G. Yu, J. Gao, J. C. Hummelen, F. Wudl, A. J. Heeger, *Science* **1995**, *270*, 1789.

[10] C. M. Proctor, M. Kuik, T.-Q. Nguyen, *Prog. Polym. Sci.* **2013**, *38*, 1941.

[11] B. Bernardo, D. Cheyns, B. Verreet, R. D. Schaller, B. P. Rand, N. C. Giebink, *Nat. Commun.* **2014**, *5*, 3245.

[12] A. Pivrikas, N. S. Sariciftci, G. Juška, R. Österbacka, *Prog. Photovolt. Res. Appl.* **2007**, *15*, 677.

[13] F. G. Brunetti, R. Kumar, F. Wudl, *J. Mater. Chem.* **2010**, *20*, 2934.

[14] M. Eiermann, F. Wudl, M. Prato, M. Maggini, **1994**, *116*, 8364.

[15] J. Luis Delgado, P.-A. Bouit, S. Filippone, M. Ángeles Herranz, N. Martín, *Chem. Commun.* **2010**, *46*, 4853.

[16] Rand, B. (Ed.), Richter, H. (Ed.). (2014). *Organic Solar Cells.* New York: Pan Stanford, https://doi.org/10.1201/b17301

[17] S. Qu, H. Tian, *Chem. Commun.* **2012**, *48*, 3039.

[18] B.-G. Kim, X. Ma, C. Chen, Y. Ie, E. W. Coir, H. Hashemi, Y. Aso, P. F. Green, J. Kieffer, J. Kim, *Adv. Funct. Mater.* **2013**, *23*, 439.

[19] B. Carsten, J. M. Szarko, L. Lu, H. J. Son, F. He, Y. Y. Botros, L. X. Chen, L. Yu, *Macromolecules* **2012**, *45*, 6390.

[20] G. Li, R. Zhu, Y. Yang, *Nat. Photonics* **2012**, *6*, 153.

[21] J. Mei, K. R. Graham, R. Stalder, J. R. Reynolds, *Org. Lett.* **2010**, *12*, 660.

[22] Rand, B. (Ed.), Richter, H. (Ed.). (2014). *Organic Solar Cells Fundamentals, Devices, and Upscaling.*. New York: Pan Stanford, https://doi.org/10.1201/b17301

[23] P. Vanlaeke, A. Swinnen, I. Haeldermans, G. Vanhoyland, T. Aernouts, D. Cheyns, C. Deibel, J. D'Haen, P. Heremans, J. Poortmans, J. V. Manca, *Sol. Energy Mater. Sol. Cells* **2006**, *90*, 2150.

[24] N. S. Sariciftci, D. Braun, C. Zhang, V. I. Srdanov, A. J. Heeger, G. Stucky, F. Wudl, *Appl. Phys. Lett.* **1993**, *62*, 585.

[25] G. Garcia-Belmonte, P. P. Boix, J. Bisquert, M. Sessolo, H. J. Bolink, *Sol. Energy Mater. Sol. Cells* **2010**, *94*, 366.

[26] V. Shrotriya, G. Li, Y. Yao, T. Moriarty, K. Emery, Y. Yang, *Adv. Funct. Mater.* **2006**, *16*, 2016.

[27] C. Brabec, U. Scherf, V. Dyakonov, *Organic Photovoltaics: Materials, Device Physics, and Manufacturing Technologies*, John Wiley & Sons, **2011**.

[28] L. Pandey, C. Risko, J. E. Norton, J.-L. Brédas, *Macromolecules* **2012**, *45*, 6405.

[29] S.-S. Sun, C. Zhang, A. Ledbetter, S. Choi, K. Seo, C. E. Bonner, M. Drees, N. S. Sariciftci, *Appl. Phys. Lett.* **2007**, *90*, 043117.

[30] J. Roncali, P. Leriche, P. Blanchard, *Adv. Mater.* **2014**, *26*, 3821.

[31] J. Hou, H.-Y. Chen, S. Zhang, G. Li, Y. Yang, *J. Am. Chem. Soc.* **2008**, *130*, 16144.

[32] W. C. H. Choy, *Organic Solar Cells: Materials and Device Physics*, Springer Science & Business Media, **2012**.

[33] S. Logothetidis, *Mater. Sci. Eng. B* **2008**, *152*, 96.

[34] A. Facchetti, T. Marks, *Transparent Electronics: From Synthesis to Applications*, John Wiley & Sons, **2010**.

[35] S. D. Collins, N. A. Ran, M. C. Heiber, T.-Q. Nguyen, *Adv. Energy Mater.* **2017**, *7*, 1602242.

[36] P. Zalar, M. Kuik, N. A. Ran, J. A. Love, T.-Q. Nguyen, *Adv. Energy Mater.* **2014**, *4*, 1400438.

[37] L. A. Perez, K. W. Chou, J. A. Love, T. S. van der Poll, D.-M. Smilgies, T.-Q. Nguyen, E. J. Kramer, A. Amassian, G. C. Bazan, *Adv. Mater.* **2013**, *25*, 6305.

[38] L. A. Perez, K. W. Chou, J. A. Love, T. S. van der Poll, D.-M. Smilgies, T.-Q. Nguyen, E. J. Kramer, A. Amassian, G. C. Bazan, *Adv. Mater.* **2013**, *25*, 6380.

[39] C. B. Nielsen, S. Holliday, H.-Y. Chen, S. J. Cryer, I. McCulloch, *Acc. Chem. Res.* **2015**, *48*, 2803.

[40] B. Kippelen, J.-L. Brédas, *Energy Environ. Sci.* **2009**, *2*, 251.

[41] J. Yu, Y. Zheng, J. Huang, *Polymers* **2014**, *6*, 2473.

[42] D. Meng, D. Sun, C. Zhong, T. Liu, B. Fan, L. Huo, Y. Li, W. Jiang, H. Choi, T. Kim, J. Y. Kim, Y. Sun, Z. Wang, A. J. Heeger, *J. Am. Chem. Soc.* **2016**, *138*, 375.

[43] C.-Z. Li, H.-L. Yip, A. K.-Y. Jen, *J. Mater. Chem.* **2012**, *22*, 4161.

[44] H. Yan, Z. Chen, Y. Zheng, C. Newman, J. R. Quinn, F. Dötz, M. Kastler, A. Facchetti, *Nature* **2009**, *457*, 679.

[45] R. Y. C. Shin, P. Sonar, P. S. Siew, Z.-K. Chen, A. Sellinger, *J. Org. Chem.* **2009**, *74*, 3293.

[46] O. K. Kwon, J.-H. Park, D. W. Kim, S. K. Park, S. Y. Park, *Adv. Mater.* **2015**, *27*, 1951.

[47] Y. Lin, J. Wang, Z.-G. Zhang, H. Bai, Y. Li, D. Zhu, X. Zhan, *Adv. Mater.* **2015**, *27*, 1170.

[48] Y. Lin, F. Zhao, Q. He, L. Huo, Y. Wu, T. C. Parker, W. Ma, Y. Sun, C. Wang, D. Zhu, A. J. Heeger, S. R. Marder, X. Zhan, *J. Am. Chem. Soc.* **2016**, *138*, 4955.

[49] Y. Lin, Y. Li, X. Zhan, *Adv. Energy Mater.* **2013**, *3*, 724.

[50] J. Zhao, Y. Li, H. Lin, Y. Liu, K. Jiang, C. Mu, T. Ma, J. Y. Lin Lai, H. Hu, D. Yu, H. Yan, *Energy Env. Sci* **2015**, *8*, 520.

[51] L. Gao, Z.-G. Zhang, H. Bin, L. Xue, Y. Yang, C. Wang, F. Liu, T. P. Russell, Y. Li, *Adv. Mater.* **2016**, *28*, 8288

[52] L. Ilies, H. Tsuji, Y. Sato, E. Nakamura, *J. Am. Chem. Soc.* **2008**, *130*, 4240.

[53] Q. Guo, J. Dong, D. Wan, D. Wu, J. You, *Macromol. Rapid Commun.* **2013**, *34*, 522.

[54] L. J. Lindgren, F. Zhang, M. Andersson, S. Barrau, S. Hellström, W. Mammo, E. Perzon, O. Inganäs, M. R. Andersson, *Chem. Mater.* **2009**, *21*, 3491.

[55] C. Piliego, T. W. Holcombe, J. D. Douglas, C. H. Woo, P. M. Beaujuge, J. M. J. Fréchet, *J. Am. Chem. Soc.* **2010**, *132*, 7595.

[56] J. Hou, H.-Y. Chen, S. Zhang, R. I. Chen, Y. Yang, Y. Wu, G. Li, *J. Am. Chem. Soc.* **2009**, *131*, 15586.

[57] J. E. Coughlin, Z. B. Henson, G. C. Welch, G. C. Bazan, *Acc. Chem. Res.* **2014**, *47*, 257.

[58] U. Vongsaysy, D. M. Bassani, L. Servant, B. Pavageau, G. Wantz, H. Aziz, *J. Photonics Energy* **2014**, *4*, 040998.

[59] H. Kast, A. Mishra, G. L. Schulz, M. Urdanpilleta, E. Mena-Osteritz, P. Bäuerle, *Adv. Funct. Mater.* **2015**, *25*, 3414.

[60] S. Mukherjee, C. M. Proctor, G. C. Bazan, T.-Q. Nguyen, H. Ade, *Adv. Energy Mater.* **2015**, *5*, n/a.

[61] J.-L. Wang, F. Xiao, J. Yan, Z. Wu, K.-K. Liu, Z.-F. Chang, R.-B. Zhang, H. Chen, H.-B. Wu, Y. Cao, *Adv. Funct. Mater.* **2016**, *26*, 1803.

[62] H. Ishii, K. Sugiyama, E. Ito, K. Seki, *Adv. Mater.* **1999**, *11*, 605.

[63] S. Antohe, *Phys. Status Solidi A* **1993**, *136*, 401.

[64] C. Goh, R. J. Kline, M. D. McGehee, E. N. Kadnikova, J. M. J. Fréchet, *Appl. Phys. Lett.* **2005**, *86*, 122110.

[65] K. H. Lee, P. E. Schwenn, A. R. G. Smith, H. Cavaye, P. E. Shaw, M. James, K. B. Krueger, I. R. Gentle, P. Meredith, P. L. Burn, *Adv. Mater.* **2011**, *23*, 766.

[66] H. Gommans, T. Aernouts, B. Verreet, P. Heremans, A. Medina, C. G. Claessens, T. Torres, *Adv. Funct. Mater.* **2009**, *19*, 3435.

[67] A. Tada, Y. Geng, Q. Wei, K. Hashimoto, K. Tajima, *Nat. Mater.* **2011**, *10*, 450.

[68] B. Yang, Y. Yuan, P. Sharma, S. Poddar, R. Korlacki, S. Ducharme, A. Gruverman, R. Saraf, J. Huang, *Adv. Mater.* **2012**, *24*, 1455.

[69] P. Peumans, S. Uchida, S. R. Forrest, in *Mater. Sustain. Energy*, Co-Published With Macmillan Publishers Ltd, UK, **2010**, pp. 94–98.

[70] F. Yang, M. Shtein, S. R. Forrest, *Nat. Mater.* **2005**, *4*, 37.

[71] M. Li, F. Liu, X. Wan, W. Ni, B. Kan, H. Feng, Q. Zhang, X. Yang, Y. Wang, Y. Zhang, Y. Shen, T. P. Russell, Y. Chen, *Adv. Mater.* **2015**, *27*, 6296.

[72] W. Shin, T. Yasuda, G. Watanabe, Y. S. Yang, C. Adachi, *Chem. Mater.* **2013**, *25*, 2549.

[73] Y. Huang, W. Wen, S. Mukherjee, H. Ade, E. J. Kramer, G. C. Bazan, *Adv. Mater.* **2014**, *26*, 4168.

[74] C. McDowell, M. Abdelsamie, K. Zhao, D.-M. Smilgies, G. C. Bazan, A. Amassian, *Adv. Energy Mater.* **2015**, *5*, 1501121.

[75] C. Lindqvist, J. Bergqvist, C.-C. Feng, S. Gustafsson, O. Bäcke, N. D. Treat, C. Bounioux, P. Henriksson, R. Kroon, E. Wang, A. Sanz-Velasco, P. M. Kristiansen, N. Stingelin, E. Olsson, O. Inganäs, M. R. Andersson, C. Müller, *Adv. Energy Mater.* **2014**, *4*, 1301437.

[76] P. Zalar, M. Kuik, N. A. Ran, J. A. Love, T.-Q. Nguyen, *Adv. Energy Mater.* **2014**, *4*, 1400438.

[77] J. D. Zimmerman, B. E. Lassiter, X. Xiao, K. Sun, A. Dolocan, R. Gearba, D. A. Vanden Bout, K. J. Stevenson, P. Wickramasinghe, M. E. Thompson, S. R. Forrest, *ACS Nano* **2013**, *7*, 9268.

[78] K. R. Graham, P. M. Wieruszewski, R. Stalder, M. J. Hartel, J. Mei, F. So, J. R. Reynolds, *Adv. Funct. Mater.* **2012**, *22*, 4801.

[79] H.-C. Liao, C.-C. Ho, C.-Y. Chang, M.-H. Jao, S. B. Darling, W.-F. Su, *Mater. Today* **2013**, *16*, 326.

[80] V. D. Mihailetchi, P. W. M. Blom, J. C. Hummelen, M. T. Rispens, *J. Appl. Phys.* **2003**, *94*, 6849.

[81] G. Zhang, S. A. Hawks, C. Ngo, L. T. Schelhas, D. T. Scholes, H. Kang, J. C. Aguirre, S. H. Tolbert, B. J. Schwartz, *ACS Appl. Mater. Interfaces* **2015**, *7*, 25247.

[82] R. Steim, S. A. Choulis, P. Schilinsky, C. J. Brabec, *Appl. Phys. Lett.* **2008**, *92*, 093303.

[83] H. Spanggaard, F. C. Krebs, *Sol. Energy Mater. Sol. Cells* **2004**, *83*, 125.

[84] M. S. White, D. C. Olson, S. E. Shaheen, N. Kopidakis, D. S. Ginley, *Appl. Phys. Lett.* **2006**, *89*, 143517.

[85] Q. Wei, T. Nishizawa, K. Tajima, K. Hashimoto, *Adv. Mater.* **2008**, *20*, 2211.

[86] M. D. Irwin, D. B. Buchholz, A. W. Hains, R. P. H. Chang, T. J. Marks, *Proc. Natl. Acad. Sci.* **2008**, *105*, 2783.

[87] M. T. Greiner, M. G. Helander, W.-M. Tang, Z.-B. Wang, J. Qiu, Z.-H. Lu, *Nat. Mater.* **2012**, *11*, 76.

[88] H. Ishii, N. Hayashi, E. Ito, Y. Washizu, K. Sugi, Y. Kimura, M. Niwano, Y. Ouchi, K. Seki, *Phys. Status Solidi A* **2004**, *201*, 1075.

[89] R. J. Davis, M. T. Lloyd, S. R. Ferreira, M. J. Bruzek, S. E. Watkins, L. Lindell, P. Sehati, M. Fahlman, J. E. Anthony, J. W. P. Hsu, *J. Mater. Chem.* **2011**, *21*, 1721.

[90] S. R. Cowan, P. Schulz, A. J. Giordano, A. Garcia, B. A. MacLeod, S. R. Marder, A. Kahn, D. S. Ginley, E. L. Ratcliff, D. C. Olson, *Adv. Funct. Mater.* **2014**, *24*, 4671.

[91] Y. Sun, C. J. Takacs, S. R. Cowan, J. H. Seo, X. Gong, A. Roy, A. J. Heeger, *Adv. Mater.* **2011**, *23*, 2226.

[92] C.-H. M. Chuang, P. R. Brown, V. Bulović, M. G. Bawendi, *Nat. Mater.* **2014**, *13*, 796.

[93] M. C. Scharber, N. S. Sariciftci, *Prog. Polym. Sci.* **2013**, *38*, 1929.

[94] R. Fitzner, E. Mena-Osteritz, A. Mishra, G. Schulz, E. Reinold, M. Weil, C. Körner, H. Ziehlke, C. Elschner, K. Leo, M. Riede, M. Pfeiffer, C. Uhrich, P. Bäuerle, *J. Am. Chem. Soc.* **2012**, *134*, 11064.

[95] T. L. Benanti, D. Venkataraman, *Photosynth. Res.* **2006**, *87*, 73.

[96] G. J. Hedley, A. J. Ward, A. Alekseev, C. T. Howells, E. R. Martins, L. A. Serrano, G. Cooke, A. Ruseckas, I. D. W. Samuel, *Nat. Commun.* **2013**, *4*, 2867.

[97] L. Schmidt-Mende, A. Fechtenkötter, K. Müllen, E. Moons, R. H. Friend, J. D. MacKenzie, *Science* **2001**, *293*, 1119.

[98] B. Walker, A. B. Tamayo, X.-D. Dang, P. Zalar, J. H. Seo, A. Garcia, M. Tantiwiwat, T.-Q. Nguyen, *Adv. Funct. Mater.* **2009**, *19*, 3063.

[99] M. Granström, K. Petritsch, A. C. Arias, A. Lux, M. R. Andersson, R. H. Friend, *Nature* **1998**, *395*, 257.

[100] M. A. Ruderer, S. Guo, R. Meier, H.-Y. Chiang, V. Körstgens, J. Wiedersich, J. Perlich, S. V. Roth, P. Müller-Buschbaum, *Adv. Funct. Mater.* **2011**, *21*, 3382.

[101] J. Weickert, R. B. Dunbar, H. C. Hesse, W. Wiedemann, L. Schmidt-Mende, *Adv. Mater.* **2011**, *23*, 1810.

[102] J. L. Li, M. Kastler, W. Pisula, J. W. F. Robertson, D. Wasserfallen, A. C. Grimsdale, J. S. Wu, K. Müllen, *Adv. Funct. Mater.* **2007**, *17*, 2528.

[103] M. T. Lloyd, J. E. Anthony, G. G. Malliaras, *Mater. Today* **2007**, *10*, 34.

[104] P. A. Troshin, H. Hoppe, J. Renz, M. Egginger, J. Y. Mayorova, A. E. Goryachev, A. S. Peregudov, R. N. Lyubovskaya, G. Gobsch, N. S. Sariciftci, V. F. Razumov, *Adv. Funct. Mater.* **2009**, *19*, 779.

[105] Y. Liu, C. Mu, K. Jiang, J. Zhao, Y. Li, L. Zhang, Z. Li, J. Y. L. Lai, H. Hu, T. Ma, R. Hu, D. Yu, X. Huang, B. Z. Tang, H. Yan, *Adv. Mater.* **2015**, *27*, 1015.

[106] Y. Lin, P. Cheng, Y. Li, X. Zhan, *Chem. Commun.* **2012**, *48*, 4773.

[107] J. D. Zimmerman, X. Xiao, C. K. Renshaw, S. Wang, V. V. Diev, M. E. Thompson, S. R. Forrest, *Nano Lett.* **2012**, *12*, 4366.

[108] J. Mei, D. H. Kim, A. L. Ayzner, M. F. Toney, Z. Bao, *J. Am. Chem. Soc.* **2011**, *133*, 20130.

[109] T. Lei, J.-Y. Wang, J. Pei, *Chem. Mater.* **2014**, *26*, 594.

[110] R. Fitzner, C. Elschner, M. Weil, C. Uhrich, C. Körner, M. Riede, K. Leo, M. Pfeiffer, E. Reinold, E. Mena-Osteritz, P. Bäuerle, *Adv. Mater.* **2012**, *24*, 675.

[111] A. T. Yiu, P. M. Beaujuge, O. P. Lee, C. H. Woo, M. F. Toney, J. M. J. Fréchet, *J. Am. Chem. Soc.* **2012**, *134*, 2180.

[112] A. K. K. Kyaw, D. H. Wang, C. Luo, Y. Cao, T.-Q. Nguyen, G. C. Bazan, A. J. Heeger, *Adv. Energy Mater.* **2014**, *4*, 1301469.

[113] J. K. Lee, W. L. Ma, C. J. Brabec, J. Yuen, J. S. Moon, J. Y. Kim, K. Lee, G. C. Bazan, A. J. Heeger, *J. Am. Chem. Soc.* **2008**, *130*, 3619.

[114] O. Synooka, K.-R. Eberhardt, C. R. Singh, F. Hermann, G. Ecke, B. Ecker, E. von Hauff, G. Gobsch, H. Hoppe, *Adv. Energy Mater.* **2014**, *4*, n/a.

[115] A. Sharenko, N. D. Treat, J. A. Love, M. F. Toney, N. Stingelin, T.-Q. Nguyen, *J Mater Chem A* **2014**, *2*, 15717.

[116] L. A. Perez, K. W. Chou, J. A. Love, T. S. van der Poll, D.-M. Smilgies, T.-Q. Nguyen, E. J. Kramer, A. Amassian, G. C. Bazan, *Adv. Mater.* **2013**, *25*, 6305.

[117] Synooka, O., Eberhardt, Kai-Rudi, Singh, C. R., Hermann, F., Ecke, G., Ecker, B., von Hauff, E., Gobsch, G., Hoppe, H. *Adv. Energy Mater.* **2014**, *4*, 1300981

[118] William M. Haynes. *CRC Handbook of Chemistry and Physics*, *97th Edition*, CRC Press, **2016,** *97*, 2652.

[119] J. M. Frost, M. A. Faist, J. Nelson, *Adv. Mater.* **2010**, *22*, 4881.

[120] F. Gao, S. Himmelberger, M. Andersson, D. Hanifi, Y. Xia, S. Zhang, J. Wang, J. Hou, A. Salleo, O. Inganäs, *Adv. Mater.* **2015**, *27*, 3868.

[121] C. Zheng, A. R. Penmetcha, B. Cona, S. D. Spencer, B. Zhu, P. Heaphy, J. A. Cody, C. J. Collison, *Langmuir* **2015**, *31*, 7717.

[122] P. K. Nayak, G. Garcia-Belmonte, A. Kahn, J. Bisquert, D. Cahen, *Energy Environ. Sci.* **2012**, *5*, 6022.

[123] R. G. E. Kimber, E. N. Wright, S. E. J. O'Kane, A. B. Walker, J. C. Blakesley, *Phys. Rev. B* **2012**, *86*, 235206.

[124] R. Noriega, J. Rivnay, K. Vandewal, F. P. V. Koch, N. Stingelin, P. Smith, M. F. Toney, A. Salleo, *Nat. Mater.* **2013**, *12*, 1038.

[125] T. Heumueller, T. M. Burke, W. R. Mateker, I. T. Sachs-Quintana, K. Vandewal, C. J. Brabec, M. D. McGehee, *Adv. Energy Mater.* **2015**, *5*, 1500111.

[126] K. Feron, W. J. Belcher, C. J. Fell, P. C. Dastoor, *Int. J. Mol. Sci.* **2012**, *13*, 17019.

[127] D. P. Hoffman, S. Y. Leblebici, A. M. Schwartzberg, R. A. Mathies, *J. Phys. Chem. Lett.* **2015**, *6*, 2919.

[128] G. Li, N. Govind, M. A. Ratner, C. J. Cramer, L. Gagliardi, *J. Phys. Chem. Lett.* **2015**, *6*, 4889.

[129] H. Cesiulis, N. Tsyntsaru, A. Ramanavicius, G. Ragoisha, in *Nanostructures Thin Films Multifunct. Appl.* (Eds.: I. Tiginyanu, P. Topala, V. Ursaki), Springer International Publishing, **2016**, pp. 3–42.

[130] S. Torabi, F. Jahani, I. V. Severen, Catherine Kanimozhi, S. Patil, R. W. A. Havenith, R. C. Chiechi, L. Lutsen, D. J. M. Vanderzande, T. J. Cleij, J. C. Hummelen, L. J. A. Koster, *Adv. Funct. Mater.* **2015**, *25*, 150.

[131] M. M. Mandoc, W. Veurman, L. J. A. Koster, B. de Boer, P. W. M. Blom, *Adv. Funct. Mater.* **2007**, *17*, 2167.

[132] S. R. Cowan, A. Roy, A. J. Heeger, *Phys. Rev. B* **2010**, *82*, 245207.

[133] P. W. M. Blom, V. D. Mihailetchi, L. J. A. Koster, D. E. Markov, *Adv. Mater.* **2007**, *19*, 1551.

[134] G.-J. A. H. Wetzelaer, M. Scheepers, A. M. Sempere, C. Momblona, J. Ávila, H. J. Bolink, *Adv. Mater.* **2015**, *27*, 1837.

[135] M. Kuik, L. J. A. Koster, G. A. H. Wetzelaer, P. W. M. Blom, *Phys. Rev. Lett.* **2011**, *107*, 256805.

[136] M. M. Mandoc, F. B. Kooistra, J. C. Hummelen, B. de Boer, P. W. M. Blom, *Appl. Phys. Lett.* **2007**, *91*, 263505.

[137] S. R. Cowan, W. L. Leong, N. Banerji, G. Dennler, A. J. Heeger, *Adv. Funct. Mater.* **2011**, *21*, 3083.

[138] C. M. Proctor, C. Kim, D. Neher, T.-Q. Nguyen, *Adv. Funct. Mater.* **2013**, *23*, 3584.

[139] R. Mauer, I. A. Howard, F. Laquai, *J. Phys. Chem. Lett.* **2010**, *1*, 3500.

[140] A. Pivrikas, G. Juška, A. J. Mozer, M. Scharber, K. Arlauskas, N. S. Sariciftci, H. Stubb, R. Österbacka, *Phys. Rev. Lett.* **2005**, *94*, 176806.

[141] A. Moliton, J.-M. Nunzi, *Polym. Int.* **2006**, *55*, 583.

[142] V. V. Brus, C. M. Proctor, N. A. Ran, T.-Q. Nguyen, *Adv. Energy Mater.* **2016**, *6*, 1400438.

[143] M. E. Orazem, B. Tribollet, *Electrochemical Impedance Spectroscopy*, John Wiley & Sons, **2011**.

[144] C. J. F. Böttcher, O. C. van Belle, P. Bordewijk, A. Rip, *Theory of Electric Polarization*, Elsevier Scientific Pub. Co., **1978**.

[145] H. D. Young, R. A. Freedman, *University Physics with Modern Physics*, Pearson, Boston, **2015**.

[146] N. Cho, C. W. Schlenker, K. M. Knesting, P. Koelsch, H.-L. Yip, D. S. Ginger, A. K.-Y. Jen, *Adv. Energy Mater.* **2014**, *4*, 20527–20535.

[147] S. D. Collins, C. M. Proctor, N. A. Ran, T.-Q. Nguyen, *Adv. Energy Mater.* **2015**.

[148] V. V. Brus, C. M. Proctor, N. A. Ran, T.-Q. Nguyen, *Adv. Energy Mater.* **2016**, *6*, 1502250.

[149] J. Frenkel, *Phys. Rev.* **1931**, *37*, 17.

[150] S. Chen, S.-W. Tsang, T.-H. Lai, J. R. Reynolds, F. So, *Adv. Mater.* **2014**, *26*, 6125.

[151] S. D. Collins, N. A. Ran, M. C. Heiber, T.-Q. Nguyen, *Adv. Energy Mater.* **2017**, *7*, 1602242.

[152] V. V. Brus, *Semicond. Sci. Technol.* **2012**, *27*, 035024.

[153] G. Zhang, T. M. Clarke, A. J. Mozer, *J. Phys. Chem. C* **2016**, DOI 10.1021/acs.jpcc.6b01169.

[154] I. Constantinou, X. Yi, N. T. Shewmon, E. D. Klump, C. Peng, S. Garakyaraghi, C. K. Lo, J. R. Reynolds, F. N. Castellano, F. So, *Adv. Energy Mater.* **2017**, *7*, 1601947.

[155] G. Perrier, R. de Bettignies, S. Berson, N. Lemaître, S. Guillerez, *Sol. Energy Mater. Sol. Cells* **2012**, *101*, 210.

[156] B. Arredondo, B. Romero, G. Del Pozo, M. Sessler, C. Veit, U. Würfel, *Sol. Energy Mater. Sol. Cells* **2014**, *128*, 351.

[157] T. Kuwabara, C. Iwata, T. Yamaguchi, K. Takahashi, *ACS Appl. Mater. Interfaces* **2010**, *2*, 2254.

[158] B. W. Veal, P. M. Baldo, A. P. Paulikas, J. A. Eastman, *J. Electrochem. Soc.* **2015**, *162*, H47.

[159] C. Vijila, S. P. Singh, E. Williams, P. Sonar, A. Pivrikas, B. Philippa, R. White, E. N. Kumar, S. G. Sandhya, S. Gorelik, J. Hobley, A. Furube, H. Matsuzaki, R. Katoh, *J. Appl. Phys.* **2013**, *114*, 184503.

[160] C. Deibel, D. Rauh, A. Foertig, *Appl. Phys. Lett.* **2013**, *103*, 043307.

[161] S. D. Collins, O. V. Mikhnenko, T. L. Nguyen, Z. D. Rengert, G. C. Bazan, H. Y. Woo, T.-Q. Nguyen, *Adv. Electron. Mater.* **2017**, *3*, 1700005.

[162] E. M. Walker, M. C. Lonergan, *Appl. Phys. Lett.* **2016**, *108*, 213301.

[163] C. G. Shuttle, R. Hamilton, B. C. O'Regan, J. Nelson, J. R. Durrant, *Proc. Natl. Acad. Sci.* **2010**, *107*, 16448.

[164] J. Fischer, W. Tress, H. Kleemann, J. Widmer, K. Leo, M. Riede, *Org. Electron.* **2014**, *15*, 2428.

[165] G.-J. A. H. Wetzelaer, P. W. M. Blom, *NPG Asia Mater.* **2014**, *6*, e110.

[166] Q. Guo, J. Dong, D. Wan, D. Wu, J. You, *Macromol. Rapid Commun.* **2013**, *34*, 522.

[167] W. Li, K. H. Hendriks, W. S. C. Roelofs, Y. Kim, M. M. Wienk, R. A. J. Janssen, *Adv. Mater.* **2013**, *25*, 3182.

[168] M. Wang, H. Wang, T. Yokoyama, X. Liu, Y. Huang, Y. Zhang, T.-Q. Nguyen, S. Aramaki, G. C. Bazan, *J. Am. Chem. Soc.* **2014**, *136*, 12576.

[169] T. S. van der Poll, J. A. Love, T.-Q. Nguyen, G. C. Bazan, *Adv. Mater.* **2012**, *24*, 3646.

[170] O. K. Kwon, J.-H. Park, S. K. Park, S. Y. Park, *Adv. Energy Mater.* **2015**, *5*, 1400929.

[171] J. Kesters, S. Govaerts, G. Pirotte, J. Drijkoningen, M. Chevrier, N. Van den Brande, X. Liu, M. Fahlman, B. Van Mele, L. Lutsen, D. Vanderzande, J. Manca, S. Clément, E. Von Hauff, W. Maes, *ACS Appl. Mater. Interfaces* **2016**, *8*, 6309.

[172] C. Lungenschmied, S. Bauer, R. Schwödiauer, S. Rodman, D. Fournier, G. Dennler, C. J. Brabec, *J. Appl. Phys.* **2011**, *109*, 044503.

[173] R. Gregorio, E. M. Ueno, *J. Mater. Sci.* **1999**, *34*, 4489.

[174] M. Breselge, I. Van Severen, L. Lutsen, P. Adriaensens, J. Manca, D. Vanderzande, T. Cleij, *Thin Solid Films* **2006**, *511–512*, 328.

[175] Chen Xingxing, Zhang Zijian, Ding Zicheng, Liu Jun, Wang Lixiang, *Angew. Chem. Int. Ed.* **2016**, *55*, 10376.

[176] Zhang Sheng, Zhang Zijian, Liu Jun, Wang Lixiang, *Adv. Funct. Mater.* **2016**, *26*, 6107.

[177] Y. Prawoto, J. R. P. Djuansjah, N. B. Shaffiar, *Comput. Mater. Sci.* **2012**, *65*, 528.

[178] W. Soboyejo, *Mechanical Properties of Engineered Materials*, CRC Press, **2002**.

[179] A. K. K. Kyaw, D. H. Wang, C. Luo, Y. Cao, T.-Q. Nguyen, G. C. Bazan, A. J. Heeger, *Adv. Energy Mater.* **2014**, *4*, 1301469.

[180] K. R. Graham, P. M. Wieruszewski, R. Stalder, M. J. Hartel, J. Mei, F. So, J. R. Reynolds, *Adv. Funct. Mater.* **2012**, *22*, 4801.

[181] G. Long, B. Wu, A. Solanki, X. Yang, B. Kan, X. Liu, D. Wu, Z. Xu, W.-R. Wu, U.-S. Jeng, J. Lin, M. Li, Y. Wang, X. Wan, T. C. Sum, Y. Chen, *Adv. Energy Mater.* **2016**, 1600961.

[182] J. A. Love, C. M. Proctor, J. Liu, C. J. Takacs, A. Sharenko, T. S. van der Poll, A. J. Heeger, G. C. Bazan, T.-Q. Nguyen, *Adv. Funct. Mater.* **2013**, *23*, 5019.

[183] Y.-C. Huang, Y.-C. Liao, S.-S. Li, M.-C. Wu, C.-W. Chen, W.-F. Su, *Sol. Energy Mater. Sol. Cells* **2009**, *93*, 888.

[184] X. Guo, C. Cui, M. Zhang, L. Huo, Y. Huang, J. Hou, Y. Li, *Energy Environ. Sci.* **2012**, *5*, 7943.

[185] J. T. Rogers, K. Schmidt, M. F. Toney, E. J. Kramer, G. C. Bazan, *Adv. Mater.* **2011**, *23*, 2284.

[186] I. Constantinou, X. Yi, N. T. Shewmon, E. D. Klump, C. Peng, S. Garakyaraghi, C. K. Lo, J. R. Reynolds, F. N. Castellano, F. So, *Adv. Energy Mater.* **2017**, *7*, 1601947.

[187] M. S. M. Alger, *Polymer Science Dictionary*, **1997**.

[188] J. Mei, K. R. Graham, R. Stalder, S. P. Tiwari, H. Cheun, J. Shim, M. Yoshio, C. Nuckolls, B. Kippelen, R. K. Castellano, J. R. Reynolds, *Chem. Mater.* **2011**, *23*, 2285.

[189] M. P. Hughes, K. D. Rosenthal, N. A. Ran, M. Seifrid, G. C. Bazan, T.-Q. Nguyen, *Adv. Funct. Mater.* **2018**, *28*, 1801542.

[190] Y. Lu, Z. Xiao, Y. Yuan, H. Wu, Z. An, Y. Hou, C. Gao, J. Huang, *J Mater Chem C* **2013**, *1*, 630.

[191] J. Bullock, B. Worfolk, *Process of Manufacturing an Electron Transport Material*, **2017**, US20170098772A1.

[192] R. Søndergaard, M. Helgesen, M. Jørgensen, F. C. Krebs, *Adv. Energy Mater.* **2011**, *1*, 68.

[193] H.-C. Liao, C.-C. Ho, C.-Y. Chang, M.-H. Jao, S. B. Darling, W.-F. Su, *Mater. Today* **2013**, *16*, 326.

[194] Y.-T. Fu, D. A. da Silva Filho, G. Sini, A. M. Asiri, S. G. Aziz, C. Risko, J.-L. Brédas, *Adv. Funct. Mater.* **2014**, *24*, 3790.

[195] L. Onsager, *Phys. Rev.* **1938**, *54*, 554.

[196] C. L. Braun, *J. Chem. Phys.* **1984**, *80*, 4157.

[197] L. J. A. Koster, V. D. Mihailetchi, R. Ramaker, P. W. M. Blom, *Appl. Phys. Lett.* **2005**, *86*, 123509.

[198] J. Szmytkowski, *Chem. Phys. Lett.* **2009**, *470*, 123.

[199] G. Garcia-Belmonte, J. Bisquert, *Appl. Phys. Lett.* **2010**, *96*, 113301.

[200] B. Kippelen, J.-L. Brédas, *Energy Environ. Sci.* **2009**, *2*, 251.

[201] B. Qi, J. Wang, *Phys. Chem. Chem. Phys.* **2013**, *15*, 8972.

[202] L. Chen, S. Tian, Y. Chen, *Polym. Chem.* **2014**, *5*, 4480.

[203] S. Hong, H. Kang, G. Kim, S. Lee, S. Kim, J.-H. Lee, J. Lee, M. Yi, J. Kim, H. Back, J.-R. Kim, K. Lee, *Nat. Commun.* **2016**, *7*, 10279.

[204] M. J. Frisch, G. W. Trucks, H. B. Schlegel, G. E. Scuseria, M. A. Robb, J. R. Cheeseman, G. Scalmani, V. Barone, G. A. Petersson, H. Nakatsuji, X. Li, M. Caricato, A. Marenich, J. Bloino, B. G. Janesko, R. Gomperts, B. Mennucci, H. P. Hratchian, J. V. Ortiz, A. F. Izmaylov, J. L. Sonnenberg, D. Williams-Young, F. Ding, F. Lipparini, F. Egidi, J. Goings, B. Peng, A. Petrone, T. Henderson, D. Ranasinghe, V. G. Zakrzewski, J. Gao, N. Rega, G. Zheng, W. Liang, M. Hada, M. Ehara, K. Toyota, R. Fukuda, J. Hasegawa, M. Ishida, T. Nakajima, Y. Honda, O. Kitao, H. Nakai, T. Vreven, K. Throssell, J. A. Montgomery, Jr., J. E. Peralta, F. Ogliaro, M. Bearpark, J. J. Heyd, E. Brothers, K. N. Kudin, V. N. Staroverov, T. Keith, R. Kobayashi, J. Normand, K. Raghavachari, A. Rendell, J. C. Burant, S. S. Iyengar, J. Tomasi, M. Cossi, J. M. Millam, M. Klene, C. Adamo, R. Cammi, J. W. Ochterski, R. L. Martin, K. Morokuma, O. Farkas, J. B. Foresman, and D. J. Fox, *Gaussian 09*, Gaussian, Inc., Wallingford CT, **2016**.

Appendix 1

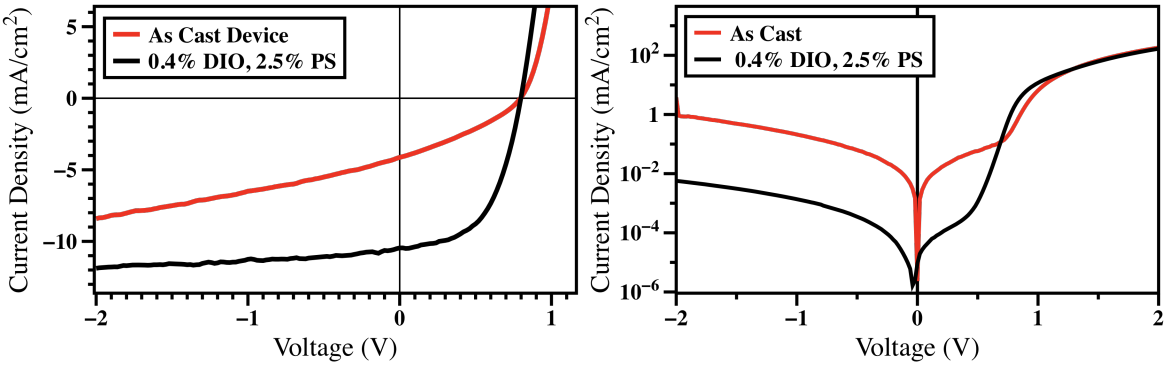

Figure A1.2. Example *JV* data. On the left is traditional current/voltage graph with the red trace being a poor-functioning device with low *FF* and underperforming J_{sc}. On the right is a traditional logarithmic current/voltage graph showing the red trace being again poor performing with high leakage. This is shown by the high current density in the reverse bias and diffusion regime in the low forward biases. Conversely, the black trace, made by the addition of certain processing conditions shows a better performing device with improved J_{sc} and *FF* without changing V_{oc}. Additionally the right graph shows leakage current orders of magnitude lower than the as cast device. This would be an appropriate device for impedance testing.

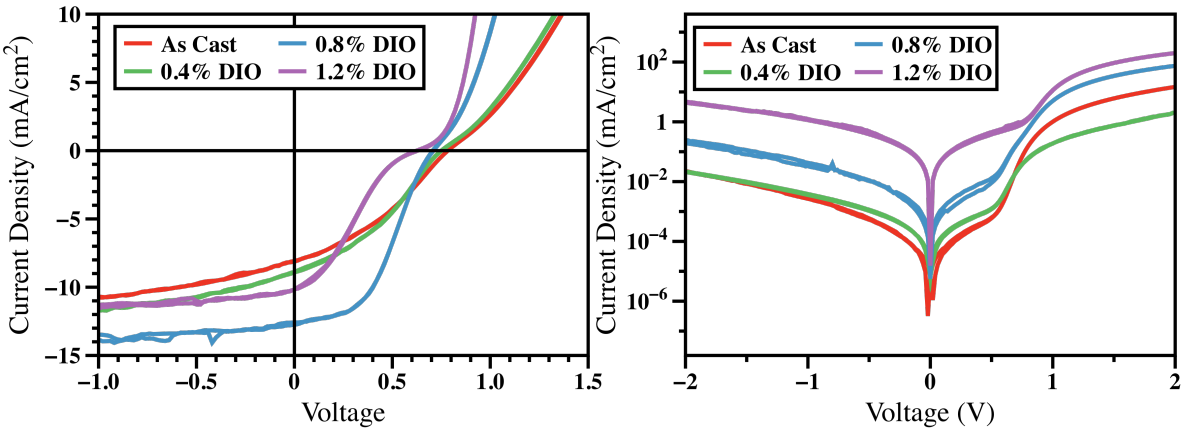

Figure A1.2. Example data of a series of devices (T1:$PC_{61}BM$) with varying amount of the solvent additive diidooctane (DIO) which is known to increase domain size of T1 crystals in this system. Excess DIO makes domains too large and interferes with charge transport. As shown here, the addition of DIO shows the growth of the "S" shape curve (left) in the current/voltage graph indicative of charge extraction problems. The logarithmic current/ voltage graph (right) shows the increase in leakage current (decreased shunt resistance) with the increase of DIO and increased crystal grain boundaries. Any JV graph with "S" shaped curve must reassess the device contacts.

Appendix 2

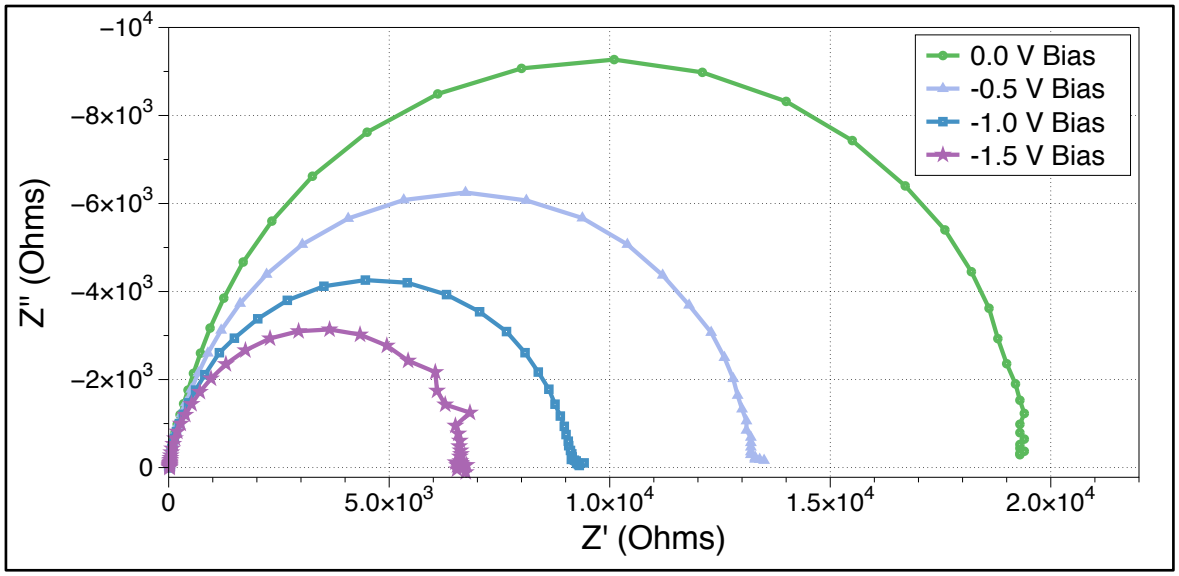

Figure A2.1. Nyquist plots of example data from Figure 1.

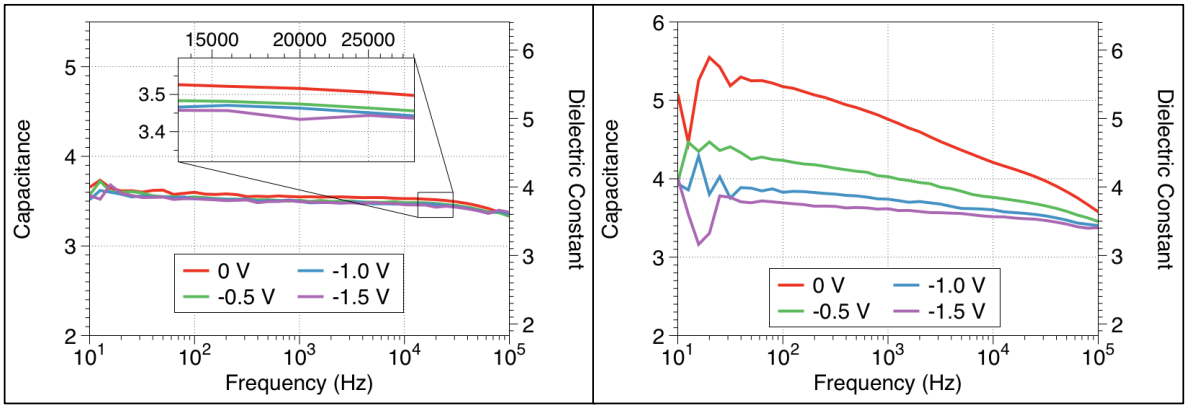

Figure A2.2. Example of the importance of active layer depletion relating to Figure 1. The left plot is the film measured in the dark at furthering reverse bias. It's visible in the magnification insert that the capacitance decreases slightly at reverse biases but that decrease seems to saturate at -1.5 V. The right plot shows active layer depletion at one sun illumination. This greatly increases charge carrier concentration, which extenuates the depleting behavior.

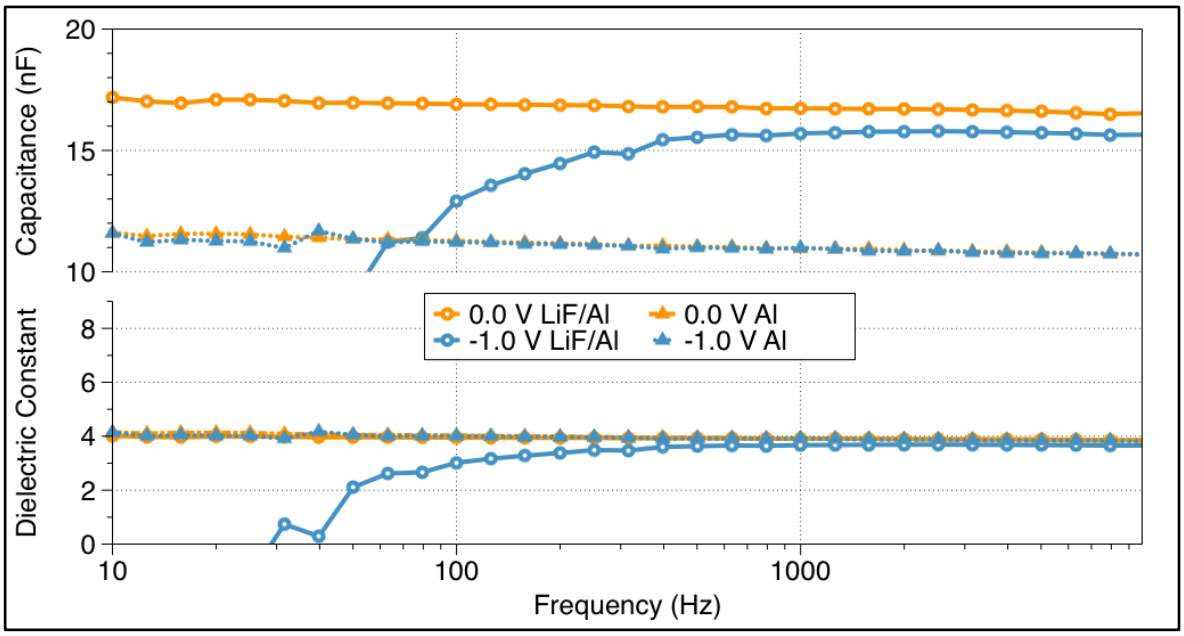

Figure A2.3. T1: $PC_{60}BM$ solar cells with and without LiF hole blocking layer. Variance in capacitance is result of thickness differences.

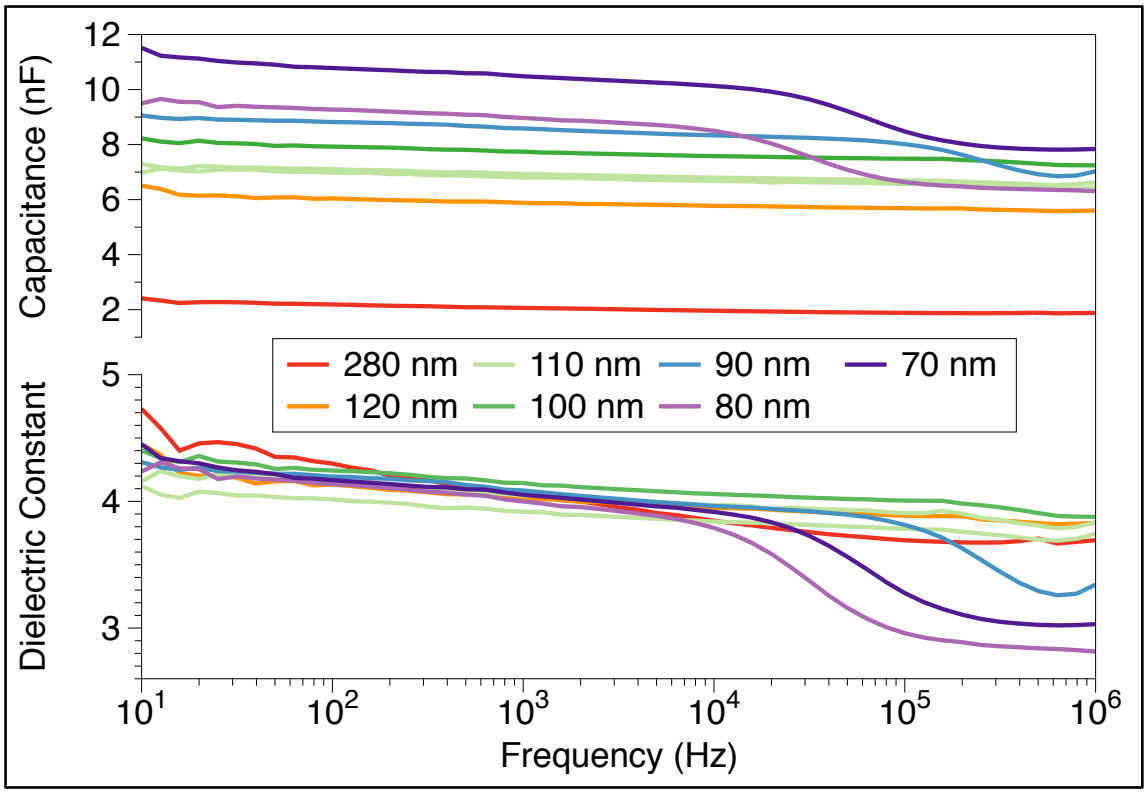

Figure A2.4. T1:$PC_{60}BM$ devices with variable thickness and increasing leakage (decreasing shunt resistance) and the resultant capacitance and dielectric constant plots showing deviation in thinner devices.

Appendix 3

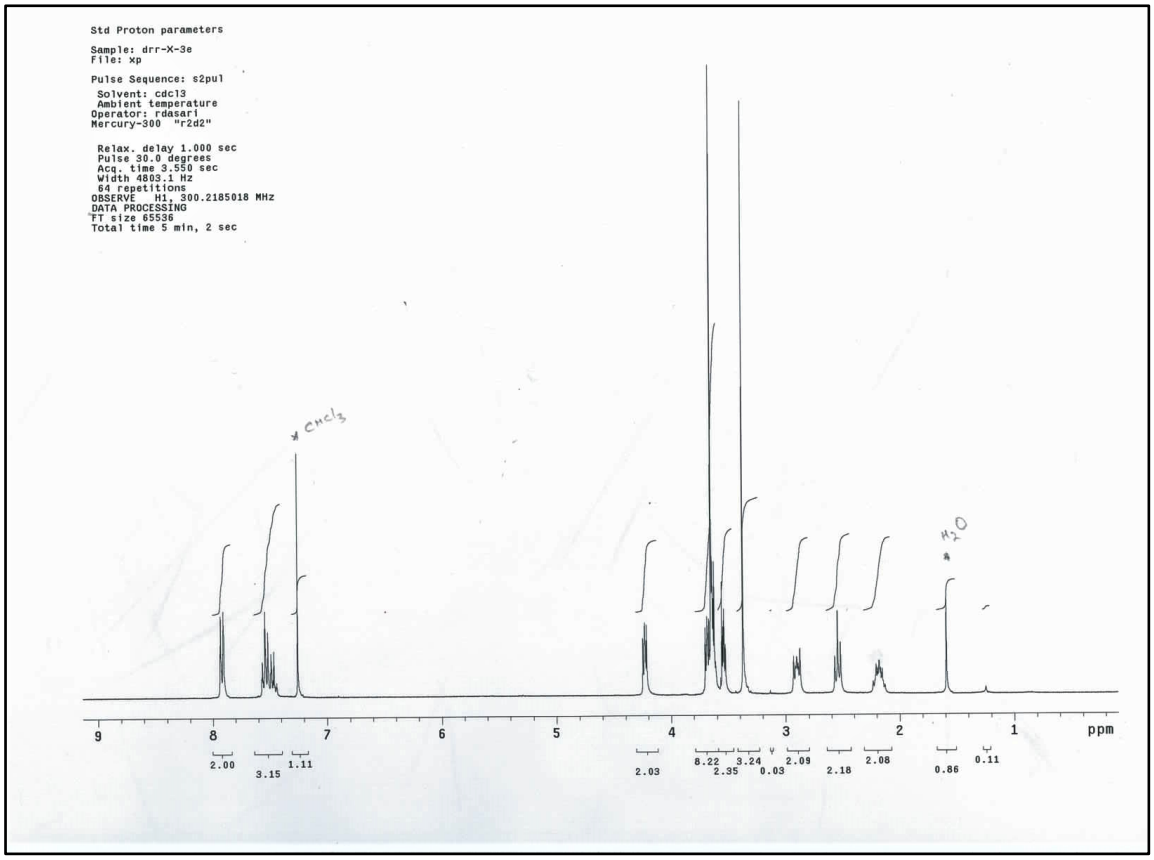

Figure A3.1. ^{1}H NMR spectrum of TEG-PCBM in $CDCl_3$ showing purity of material.

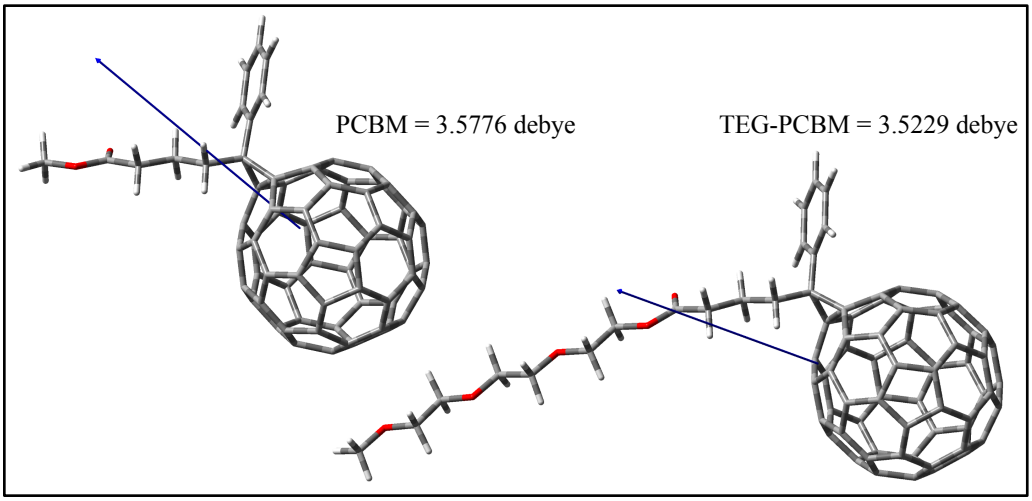

Figure A3.2. Dipole moments of both $PC_{60}BM$ and TEG-PCBM calculated using DFT.

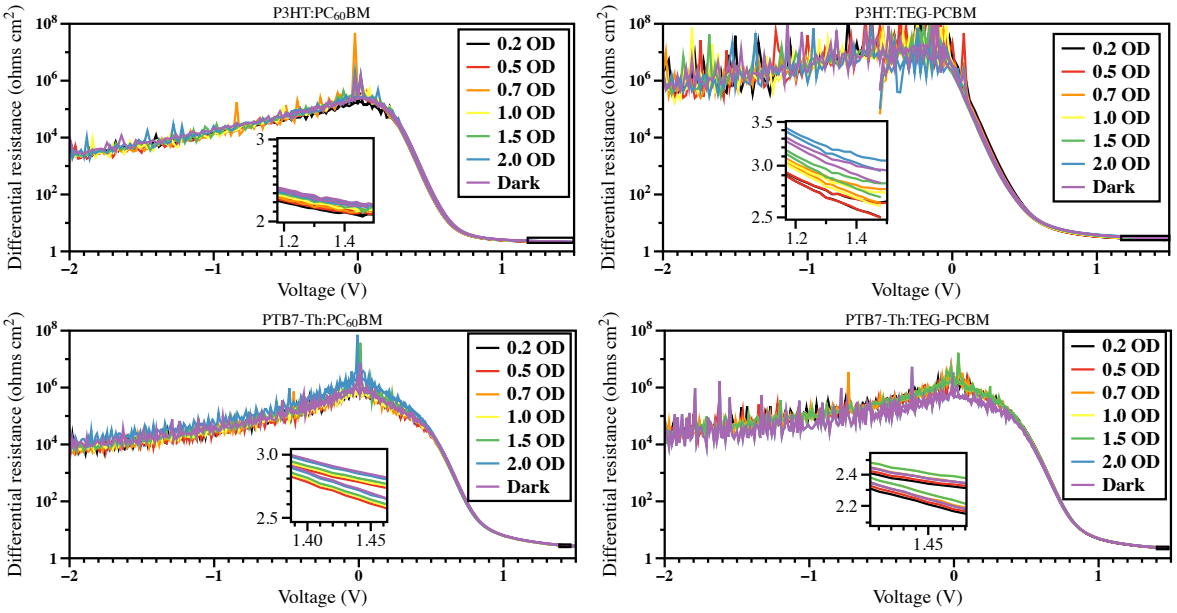

Figure A3.3. Measured differential resistance, $R_{diff} = \Delta V/\Delta J$, to demonstrate high, maintained shunt resistance through testing. Measurement taken in dark after each of labeled light intensities to demonstrate maintained device integrity. Inset shows forward biased saturation AC series resistance, resultant from anode and cathode resistance. Graphs for P3HT:PCBM (upper left), P3HT:TEG-PCBM (upper right), PTB7-Th:PCBM (lower left), PTB7-Th:TEG-PCBM (lower right) show similar and well maintained differential and series resistance throughout testing.

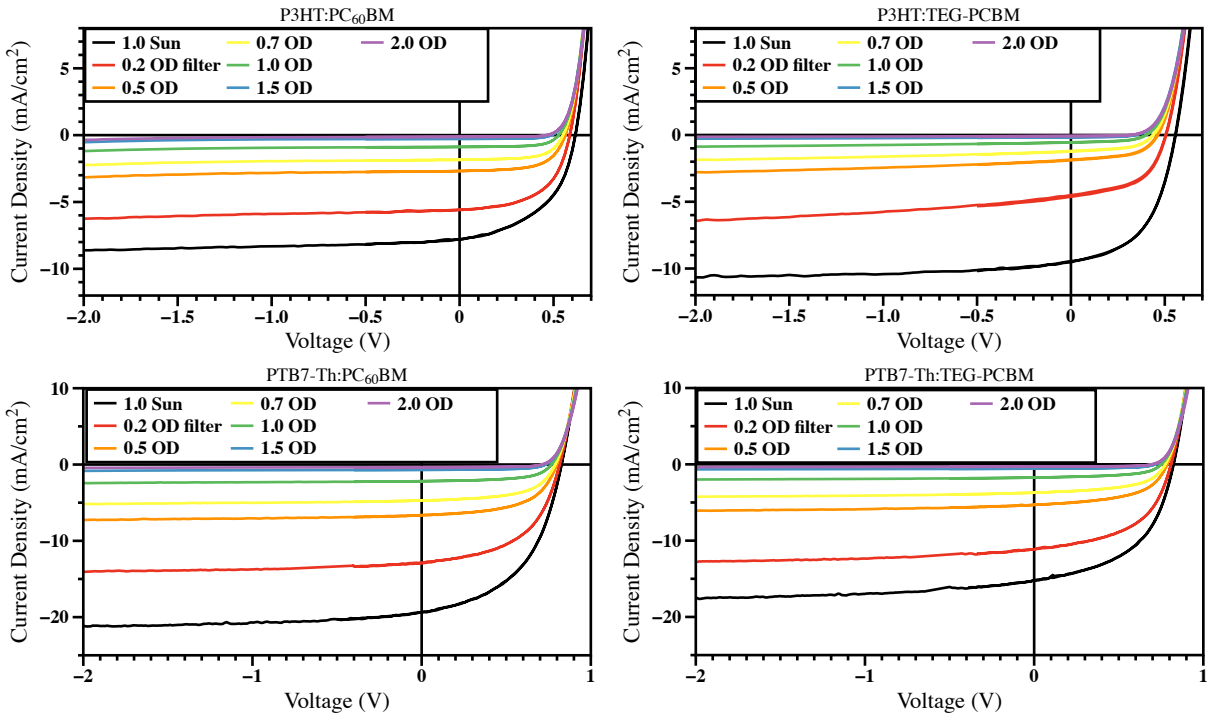

Figure A3.4. Measured *JV* curves to show current response at multiple light intensities. Graphs for P3HT:PCBM (upper left), P3HT:TEG-PCBM (upper right), PTB7-Th:PCBM (lower left), PTB7-Th:TEG-PCBM (lower right) show consistent behavior through several volts and several orders of magnitude of intensity. Please note the changing current scaling on the upper and lower graphs.

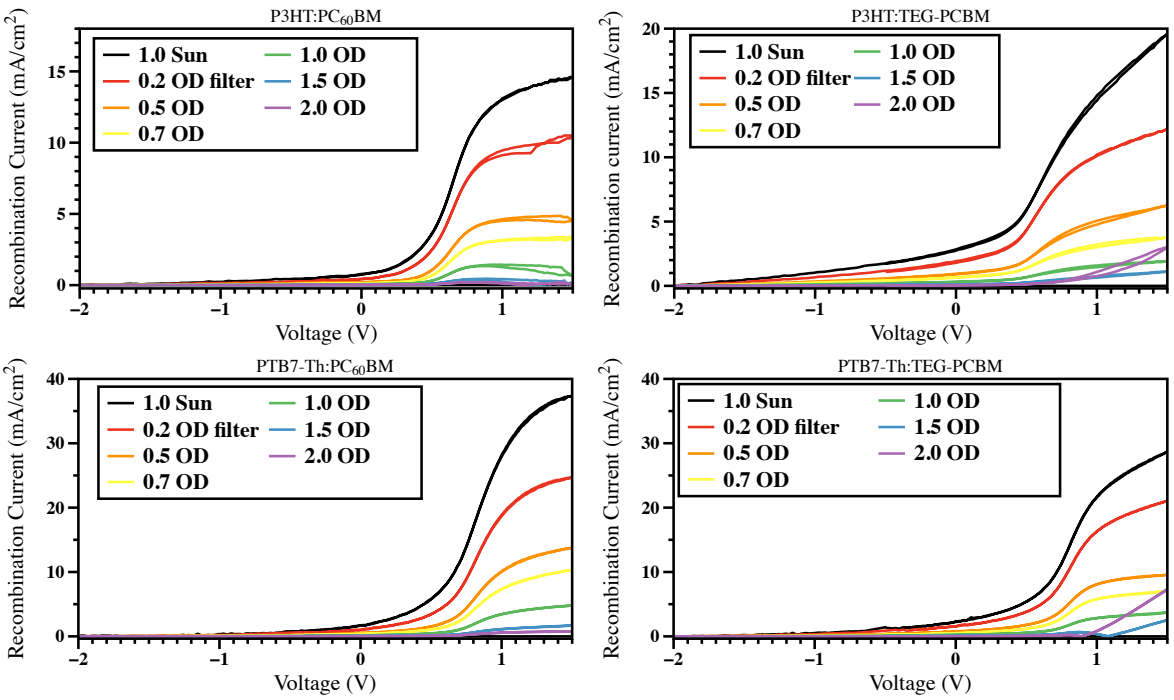

Figure A3.5. Calculated recombination graphs for P3HT:PCBM (upper left), P3HT:TEG-PCBM (upper right), PTB7-Th:PCBM (lower left), PTB7-Th:TEG-PCBM (lower right). Spectra were calculated using measured light (J_L) and dark (J_D) *JV* scans by calculating photocurrent $J_{ph} = J_L - J_D$ and calculating recombination current by subtracting the photocurrent from reversed bias saturation current $J_{rec} = J_{sat} - J_{ph}$ where current is voltage independent. This voltage was found to be -2.0 V for each system.

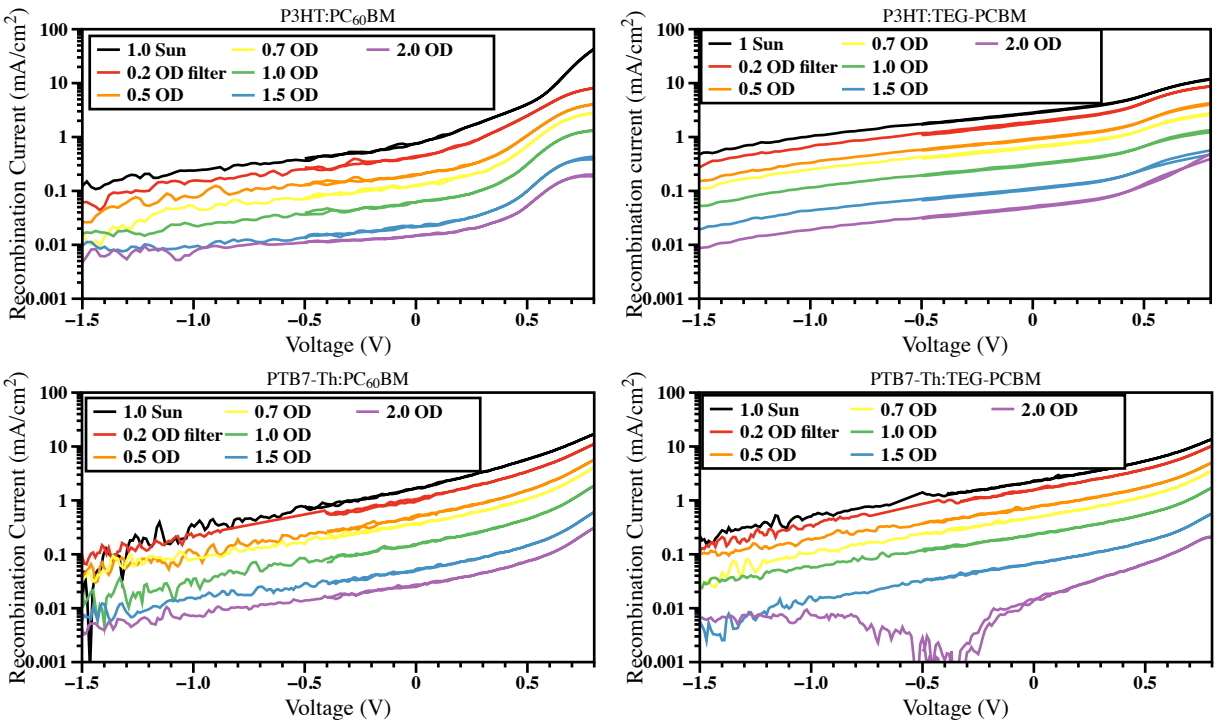

Figure A3.6. Logarithmic scaled calculated recombination graphs for P3HT:PCBM (upper left), P3HT:TEG-PCBM (upper right), PTB7-Th:PCBM (lower left), PTB7-Th:TEG-PCBM (lower right). These graphs show very similar behavior in the low J_{rec} region.

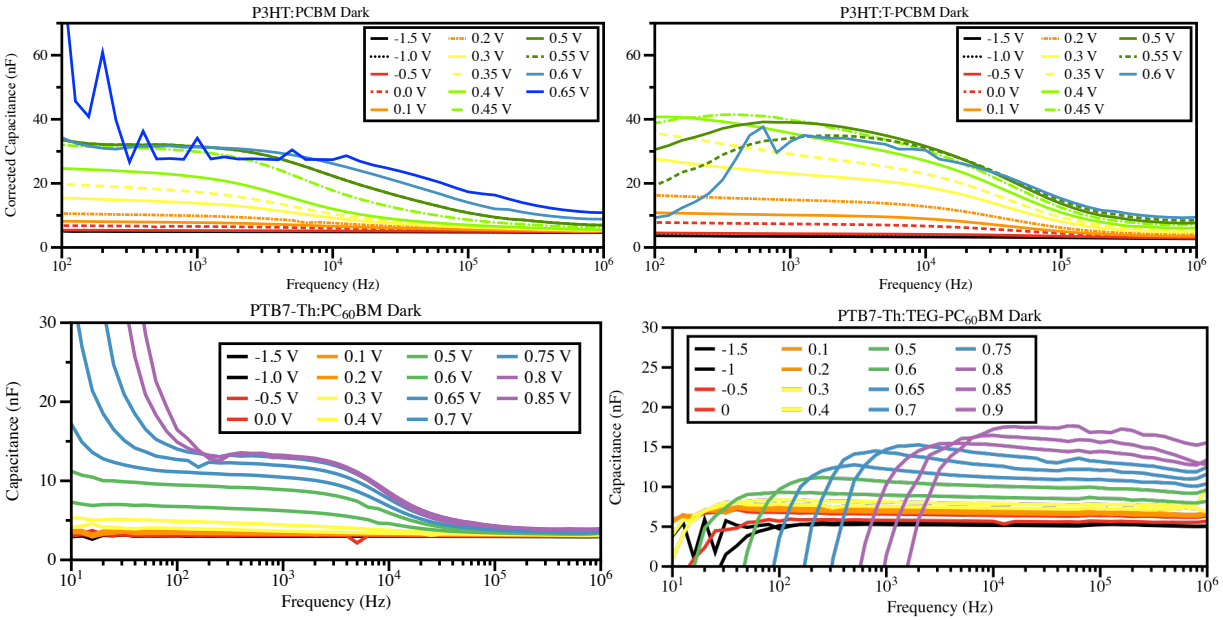

Figure A3.7. Calculated corrected capacitance graphs using **Equation 1** (from chapter 3) in the dark for P3HT:PCBM (upper left), P3HT:TEG-PCBM (upper right), PTB7-Th:PCBM (lower left), PTB7-Th:TEG-PCBM (lower right). Graphs show similar capacitance behavior for each electron donating material for each bias, and similar and expected frequency independent behavior at far reverse bias (-1.5 V). Large capacitance at low/mid frequency range are resultant of injected charge chemical capacitance not relevant in material dielectric constant consideration.

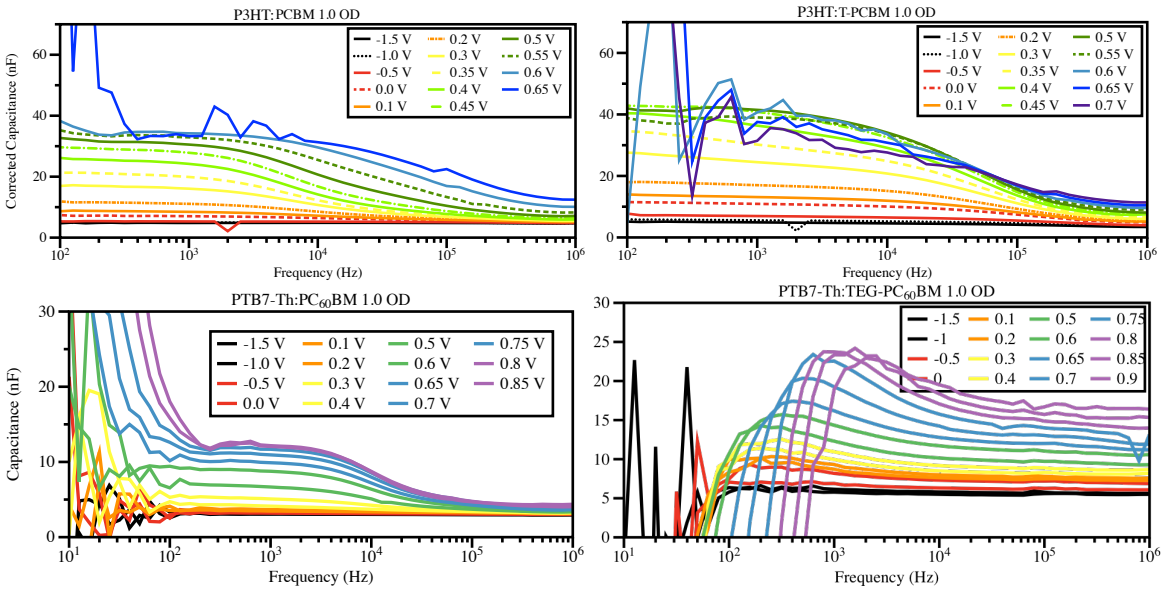

Figure A3.8. Calculated corrected capacitance graphs using **Equation 1** (from chapter 3) at 0.1 OD light intensity for P3HT:PCBM (upper left), P3HT:TEG-PCBM (upper right), PTB7-Th:PCBM (lower left), PTB7-Th:TEG-PCBM (lower right). Graphs beginning to show large low frequency noise resultant from high concentration of charge carrier based chemical capacitance. It may be seen, especially past the max power point, and in the high current PTB7-Th systems.

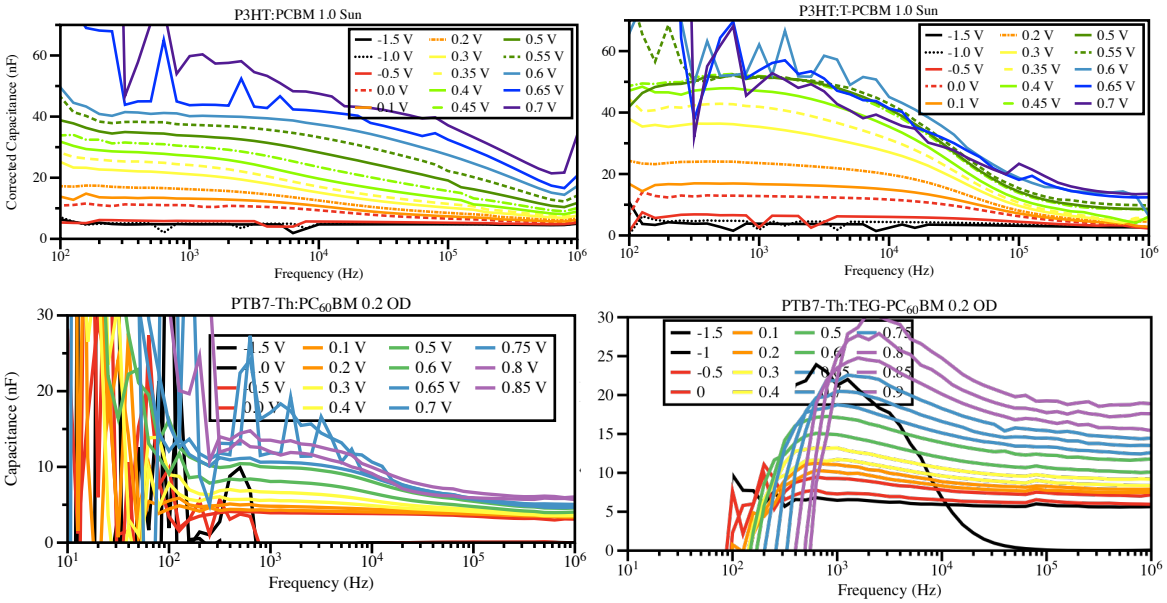

Figure A3.9. Calculated corrected capacitance graphs using **Equation 1** (from chapter 3) at 1.0 sun (0.2 OD for PTB7-Th) for P3HT:PCBM (upper left), P3HT:TEG-PCBM (upper right), PTB7-Th:PCBM (lower left), PTB7-Th:TEG-PCBM (lower right). Additional large low frequency noise observed in forward bias and in the high current PTB7-Th systems. This high capacitance environment prohibits measurement at 1.0 sun light intensity, 0.2 OD is the most intensive before capacitance measures at 0 nF due to high conductivity.